

The University of Maine

DigitalCommons@UMaine

Electronic Theses and Dissertations

Fogler Library

Fall 12-16-2022

Testing and Analysis of Paired, Inflated HIAD Tori

Irja Hepler

University of Maine, irja.hepler@maine.edu

Follow this and additional works at: <https://digitalcommons.library.umaine.edu/etd>

Recommended Citation

Hepler, Irja, "Testing and Analysis of Paired, Inflated HIAD Tori" (2022). *Electronic Theses and Dissertations*. 3740.

<https://digitalcommons.library.umaine.edu/etd/3740>

This Open-Access Thesis is brought to you for free and open access by DigitalCommons@UMaine. It has been accepted for inclusion in Electronic Theses and Dissertations by an authorized administrator of DigitalCommons@UMaine. For more information, please contact um.library.technical.services@maine.edu.

TESTING AND ANALYSIS OF PAIRED, INFLATED HIAD

TORI By

Irja Hepler

B.S. University of Maine, 2020

A THESIS

Submitted in Partial Fulfillment of the

Requirements for the Degree of

Master of Science

(in Civil Engineering)

The Graduate School

The University of Maine

December 2022

Advisory Committee:

William Davids, Professor of Civil Engineering, Advisor

Andrew Young, Assistant Professor of Civil Engineering

Eric Landis, Professor of Civil Engineering

TESTING AND ANALYSIS OF PAIRED, INFLATED HIAD TORI

By Irja Hepler

Thesis Advisor: Dr. William Davids, PE

An Abstract of the Thesis Presented
in Partial Fulfillment of the Requirements for the
Degree of Master of Science
(in Civil Engineering)
December 2022

The Hypersonic Inflatable Aerodynamic Decelerator (HIAD) is a stack of concentric, inflated rings (tori) being developed by NASA for landing spacecraft. This research will build on work previously done at UMaine to understand the structural behavior of the HIAD by examining the response of a system of paired tori. A test fixture previously used to test single tori was analyzed and modified to withstand the estimated forces from testing paired tori. Two single tori of different sizes were tested separately on the fixture at various internal inflation pressures. The tests consisted of displacing the tori equally at 16 discrete points using cables attached to individual actuators. The actuators were synchronized using a modified version of the control code used previously. Noncontact photogrammetry data, as well as the forces in each cable, were collected throughout each test. The photogrammetry data was used to determine the displaced shapes of the specimens. Tori identical to those used in single torus testing were then tested as a paired assembly. A finite element model of the paired tori was developed and verified using data collected from the physical tests.

ACKNOWLEDGEMENTS

I would like to thank the many people who have helped me through my time at UMaine.

Thank you to the NASA HIAD team for sponsoring and collaborating on this research, especially Neil Cheatwood, Keith Johnson, Greg Swanson, Stephen Hughes, and Michael Lindell.

I am especially grateful to my advisor, Bill Davids for his support, guidance and understanding as I worked through the most difficult thing I have ever done. I am extremely excited to continue working with him.

I am also thankful to Andy Young for his invaluable assistance while I was working with his model and for serving on my committee.

I am grateful to Eric Landis for taking time out of his busy schedule to serve on my committee.

I am also thankful to the many people at the Composites Center who helped with my testing including Sam Heathcote, Cody Sheltra, Travis Chappelle, Mike Hunter, Danny Adam and many others.

Finally, I would like to thank my friends and family for their continual support throughout my academic career.

CONTENTS

ACKNOWLEDGEMENTS	iii
LIST OF TABLES	vii
LIST OF FIGURES	viii
CHAPTER 1 INTRODUCTION	1
1.1 Problem Description and Previous Work	1
1.2 Overview and Organization of Thesis	3
CHAPTER 2 TEST FIXTURE MODIFICATIONS	5
2.1 Actuator Location	6
2.2 Pulleys and Mounts.....	7
2.3 Check of Outer Ring Structural Capacity	9
2.4 Additional Hardware.....	10
2.4.1 Proof Testing of Load Cables	11
2.5 Summary.....	12
CHAPTER 3 SINGLE TORUS TESTING	13
3.1 Test Setup and Procedures	13
3.1.1 Specimen and Test Description	13
3.1.2 Data Acquisition and Instrumentation	14
3.1.3 Digital Image Correlation	20
3.1.4 Control	23

3.1.5 DIC Data Post-Processing.....	25
3.2 Results.....	29
3.3 Summary.....	33
CHAPTER 4 PAIRED TORUS TESTING	35
4.1 Loading Method.....	35
4.1.1 Loading Calculation Problem Description.....	36
4.1.2 Loading Calculation Results	37
4.2 Test Setup and Procedures	39
4.2.1 Specimen and Test Description	40
4.2.2 Modifications to Test Setup.....	40
4.2.3 DIC.....	43
4.2.4 Control System Tuning	46
4.3 Test Results.....	48
4.3.1 Control of Test.....	48
4.3.2 PONTOS Data	54
4.4 Summary	70
CHAPTER 5 MODELING OF PAIRED TORUS TESTING.....	71
5.1 Element Properties	71
5.1.1 Torus elements.....	72
5.1.2 Interaction Elements	73

5.1.3 Strap Elements	75
5.1.4 Link elements.....	76
5.1.5 Boundary Elements	76
5.2 Comparison to Paired Tori Testing.....	77
CHAPTER 6 CONCLUSIONS	84
REFERENCES	87
APPENDIX A ACTUATOR CONNECTION CALCULATION	89
APPENDIX B PULLEY MOUNT CALCULATIONS.....	92
APPENDIX C CONTROL CODE	100
APPENDIX D SHEAR CENTER CALCULATION	121
APPENDIX E LOADING CALCULATION.....	127
APPENDIX F PAIRED SPECIMEN DATA	137
BIOGRAPHY OF THE AUTHOR.....	141

LIST OF TABLES

Table 1. New hardware	11
Table 2. Mean and maximum cable load range	53
Table 3. Properties of torus shell	73

LIST OF FIGURES

Figure 1 Photo and renderings of HIAD (Swanson et al 2012 and Young et al 2017a)..... 1

Figure 2. Torus (Clapp, 2017)..... 2

Figure 3. Modified test fixture 5

Figure 4. Original and modified actuator locations 6

Figure 5. Actuator on extension platform 7

Figure 6. Pulley extension..... 8

Figure 7. Loading and boundary conditions of outer ring model 9

Figure 8. Stresses from FEA model of outer ring 10

Figure 9. Testing of crimped wire rope 12

Figure 10. Plan view and cross section of torus (modified from Young, 2017b)..... 13

Figure 11. NI PXIe-1078 with TB 4330 cards (left) and NI PXIe-1082 with TB 4339 cards
(right) 14

Figure 12. Load cable setup 15

Figure 13. Verification of load cell..... 16

Figure 14. Example load cell verification data 16

Figure 15. String pots on outer ring 17

Figure 16. String pot verification..... 18

Figure 17. Examples of string pot and PONTOS dot agreement..... 19

Figure 18. Images from camera calibration 21

Figure 19. Example coded PONTOS dot..... 22

Figure 20. T4 specimen set up 23

Figure 21. Actuator control panel 24

Figure 22. Air pressure regulator and transducer..... 24

Figure 23. Screenshot of PONTOS software	25
Figure 24. Coordinate system used while fitting PONTOS data	27
Figure 25. Displaced shape of T4 (left column) and T5 (right column) at 40x	30
Figure 26. Total applied load vs average radial displacement for single torus specimens.....	31
Figure 27. Radial displacement at final load of single torus specimens	32
Figure 28. Load application via spreader beam concept.....	35
Figure 29. Paired specimen loading problem	37
Figure 30. Paired specimen loading problem results	38
Figure 31. Old (right) and new (left) load cable to strap connections	39
Figure 32. Paired specimen with DIC stickers.....	40
Figure 33. String pot and PONTOS dot displacements during 1/4 in displacement controlled test at 5 psi.....	41
Figure 34. Paired specimen with load saddles	42
Figure 35. Swivel	43
Figure 36. PONTOS dots on paired specimen.....	44
Figure 37. DIC picture showing points used to define coordinate system	45
Figure 38. String pot displacement during displacement controlled test to 3/8 in	46
Figure 39. Difference between string pot reading and target displacement during test to 3/8 in .	47
Figure 40. String pot displacement during displacement controlled testing.....	49
Figure 41. String pot displacement vs cable load	51
Figure 42. Range of cable loads during displacement controlled test	52
Figure 43. Specimen cross section.....	55
Figure 44. Initial radial locations of T4 centroids.....	56

Figure 45. Initial radial locations of T5 centroids.....	56
Figure 46. Initial vertical locations of T4 centroids.....	57
Figure 47. Initial vertical locations of T5 centroids.....	57
Figure 48. Initial distances between corresponding T4 and T5 centroids	58
Figure 49. Initial specimen orientation	59
Figure 50. Radial displacement of T4.....	60
Figure 51. Radial displacement of T5.....	61
Figure 52. Vertical displacement of T4	62
Figure 53. Vertical displacement of the T5	63
Figure 54. Rotation of the T4 cross section	65
Figure 55. Rotation of T5 cross section	66
Figure 56. Change in distance between tori centroids	68
Figure 57. Change in specimen orientation	69
Figure 58. Model.....	72
Figure 59. Illustration of interaction element bending stiffness problem.....	74
Figure 60. Radial displacement of T4, test and model	78
Figure 61. Radial displacement of T5, test and model	78
Figure 62. Vertical displacement of T4, test and model.....	79
Figure 63. Vertical displacement of T5, test and model.....	79
Figure 64. Rotation of T4 cross section, test and model.....	80
Figure 65. Rotation of T5 cross section, test and model.....	81
Figure 66. Change in distance between tori centroids, test and model.....	82
Figure 67. Change in specimen orientation, test and model.....	82

Figure 68. Symbol definitions.....	127
Figure 69. Symbol definitions for the determination of G and H	130

CHAPTER 1 INTRODUCTION

1.1 Problem Description and Previous Work

NASA is making and testing a hypersonic inflatable aerodynamic decelerator (HIAD). The HIAD system is a stack of concentric, inflatable rings (called tori) of increasing diameter strapped together and covered by a heat shield, as shown in Figure 1.

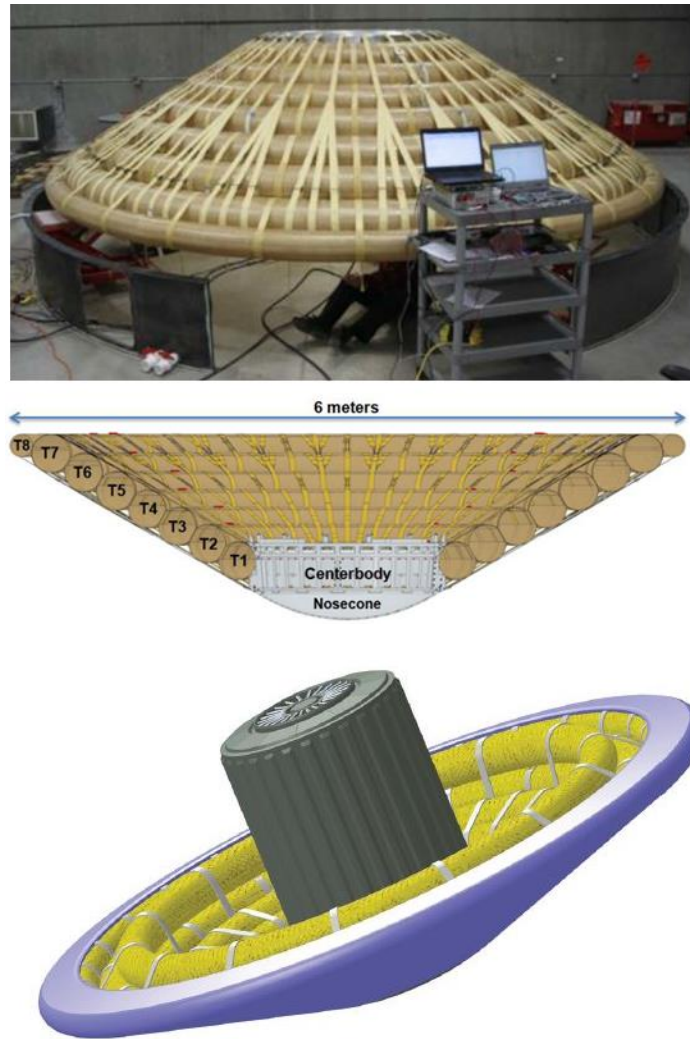


Figure 1 Photo and renderings of HIAD (Swanson et al 2012 and Young et al 2017a)

HIADs are used for decelerating space craft once they reach their destination from hypersonic speeds until a parachute or other conventional deceleration technique can be used. HIADs can be

deflated and packed quite tightly in the spacecraft until they are needed where they are then inflated. This means their inflated diameters can be quite large while their mass is relatively small and so they have the potential to allow heavier payloads to be landed at higher elevations (Young, 2017). The tori that make up the HIAD consist of an outer shell of braided fiber with integral reinforcing cords both of which are high strength and stiffness synthetic fiber (e.g. Technora or Zylon) and an impermeable bladder, as shown in Figure 2.

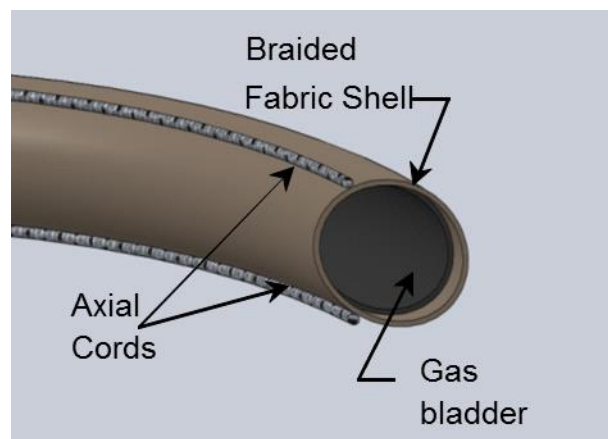


Figure 2. Torus (Clapp, 2017)

The structural mechanics of a HIAD are quite complicated, but testing can be cost prohibitive and complex. Shell based modeling is work and time intensive. To help alleviate this problem, the University of Maine (UMaine) has previously conducted extensive experimental and computational research on HIAD structural behavior. The material properties of the components of the tori were determined through testing tension testing of segments of cord and coupons of bladder and tension-torsion testing of straight segments of the braided shell (Clapp et al 2016a and 2016b). Straight beams with the same size cross section as that of the tori and three reinforcing cords spaced evenly around the circumference of the cross section were tested in 4 point bending (Clapp et al 2016b). These tests were then modeled using both shell elements (Clapp et al 2016b) and beam elements (Young et al 2017a). Individual tori were subsequently

tested under several loading conditions producing both in-plane radial deformation and out-of-plane deformation and modeled using the beam-based finite element model (Young et al 2017b). Finally, pressure tub testing of a full HIAD done by NASA was modeled using the beam-based finite element model (Young et al 2018). For complete literature reviews, see (Whitney 2016 Clapp, 2017, and Young, 2017). To date there has been more work on the testing and modeling of the thermodynamics of the HIAD (Hollis et al 2017, Brune et al 2019, Zhao et al 2022) and a successful flight test of a HIAD (nasa.gov, 12/2022). Though there has been testing on single tori and full HIAD structures, there has not been any testing of paired tori. This is what the current work will focus on.

There were four main goals of this research. One was to test single tori with a loading scheme more closely approximating uniform pressure. This was achieved by increasing the number of load points from the eight used during previous testing (Young 2017b) to sixteen. The second was to test paired tori to better understand torus-torus interaction, or the effect one torus has on the adjacent one. It was also desired to more accurately simulate torus-torus and torus-strap interactions using the model developed by Young (2017, 2017a, 2017b, 2018). Finally, modeling of the paired testing would further validate the model using a new test case.

1.2 Overview and Organization of Thesis

This thesis details the testing and modeling of a set of paired tori. The objective of this research was to test a set of paired tori, to continue to validate the model developed by Young et al (2017a, 2017b and 2018) and to better understand the effect adjacent tori have on a given torus.

The thesis is organized as follows:

Chapter 2 discusses the modifications made to the test fixture detailed by Young et al (2017b) in order to withstand the forces required to load a set of paired tori.

Chapter 3 discusses the testing of two single tori each identical in size and construction to the one of the two tori making up the paired specimen.

Chapter 4 details the testing of the paired specimen and compares the results to those from the single torus testing.

Chapter 5 discusses modeling the paired specimen test and includes a comparison to the results from Chapter 4.

Finally, Chapter 6 includes a summary and recommendations for future work.

CHAPTER 2 TEST FIXTURE MODIFICATIONS

In order to test the paired tori, the test fixture from (Young et al 2017b) was modified. Both the concept and the finished fixture are shown in Figure 3 below.

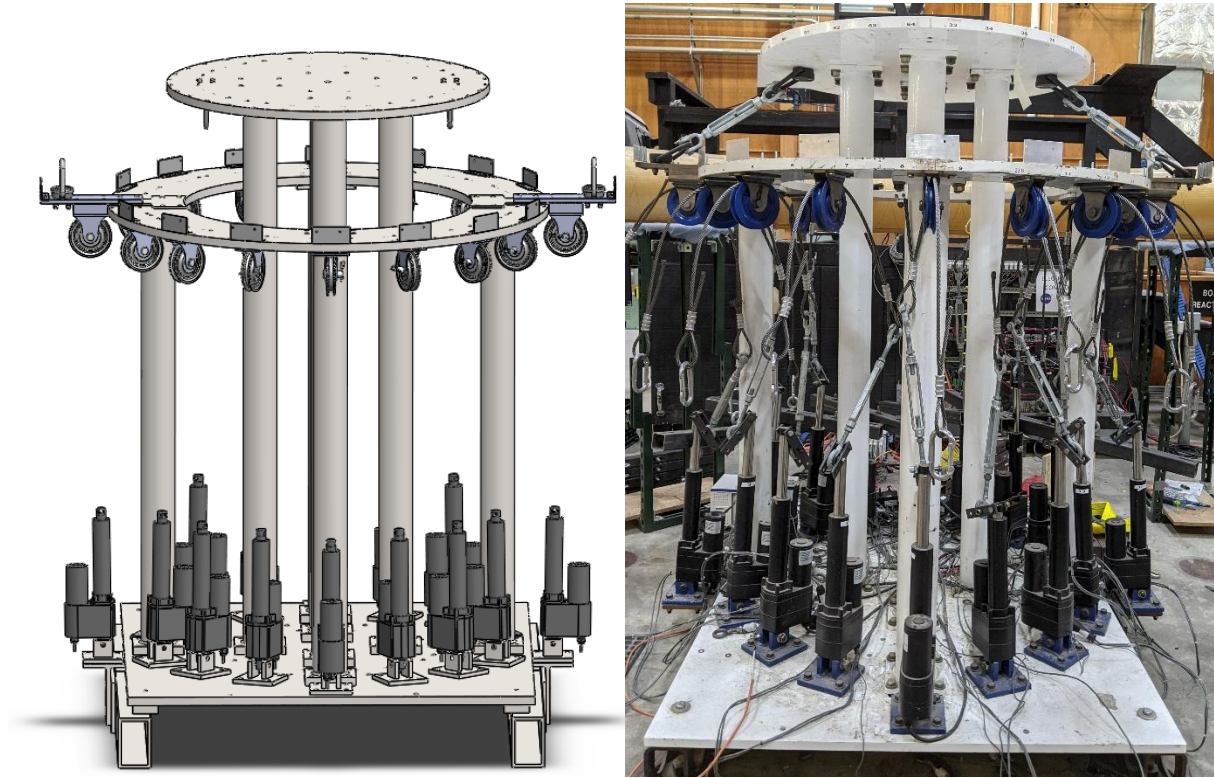


Figure 3. Modified test fixture

The test fixture consists of two steel plates, one circular and one ring shaped, referred to in this paper as the upper plate and outer ring, respectively. The plates are supported by steel columns which connect to a base plate that is attached to reaction beams bolted to the floor. Sixteen actuators are bolted to the base plate. Wire cable is connected from the actuators, routed through pulleys on the outer ring and then connected to the specimen. For the new testing, it was decided that sixteen pull points would be used. Since the fixture had previously only been used to test single tori, many of its components had to be checked, replaced, or redesigned in order to ensure

they could withstand the increased loads. The actuator capacity of 2000 lbs was used for design and calculating factors of safety.

2.1 Actuator Location

One aspect of the fixture that required modification was the location of the actuators. The original and new actuator configurations are shown below in Figure 4.

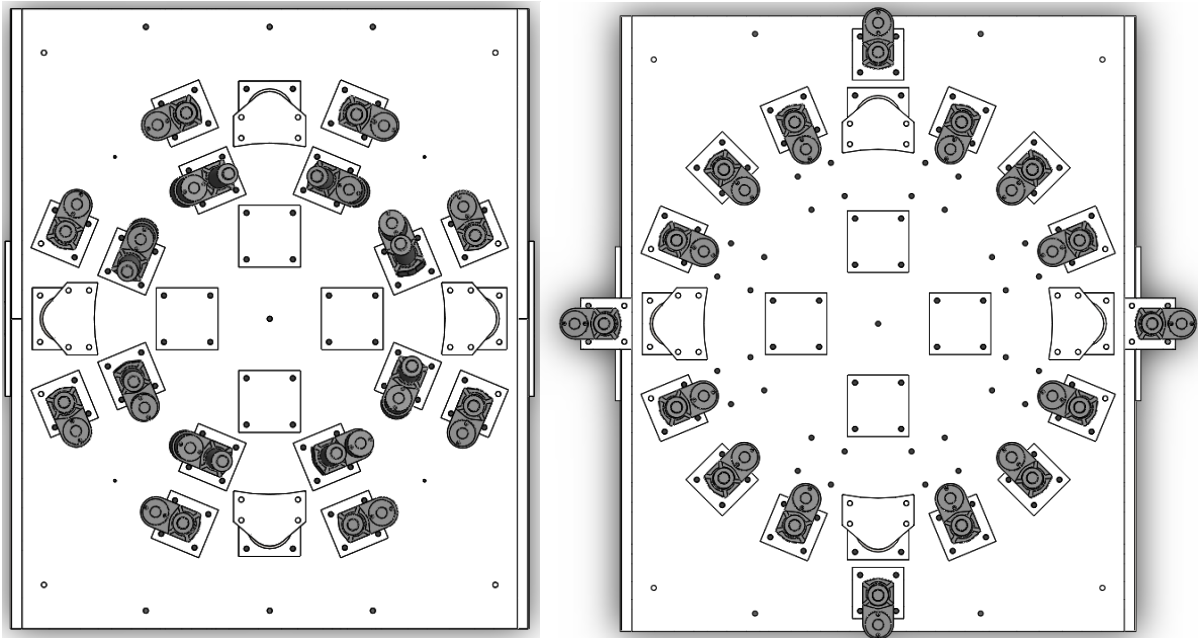


Figure 4. Original and modified actuator locations

Because of the position of the support columns, only 14 actuators could fit on the base plate, 12 at a constant distance to the center of the baseplate and 2 shifted to the outside of the columns.

New holes were cut into the base plate for the six actuators that were moved. To attach the remaining two actuators, two extension platforms were fabricated and bolted into the existing pattern on the reaction beams, shown in Figure 5. They were analyzed as an indeterminate structure and have a factor of safety of 1.39.



Figure 5. Actuator on extension platform

All actuators were connected to either the baseplate or the extension platforms using the original actuator mounts. The calculations for the design of the extension platforms, along with a check of the actuator mounts can be found in 0. Although it is not ideal to have actuators at varying distances radially from the center of the baseplate, the actuators are mounted in such a way so that they can rotate freely in this direction and the orientation of all cable forces was accounted for during calculations.

2.2 Pulleys and Mounts

In addition to the actuators, the pulleys and the pulley locations had to be modified. The original pulley mounts were not strong enough, so new pulley mounts were designed. The pulley mount baseplate was designed with a factor of safety of 1.55 in bending. The full calculations can be found in APPENDIX B. The mounts were cut from 36 ksi steel with a waterjet and then sent to UMaine's Advanced Manufacturing Center for welding. New holes were cut into the outer ring to attach the pulleys so that they were aligned with the actuators. Two pulley mounts did not fit

because they interfered with the bolts and gusset plates connecting the two halves of the outer ring together. These mounts were attached to extension plates that were bolted into existing holes (see Figure 6).

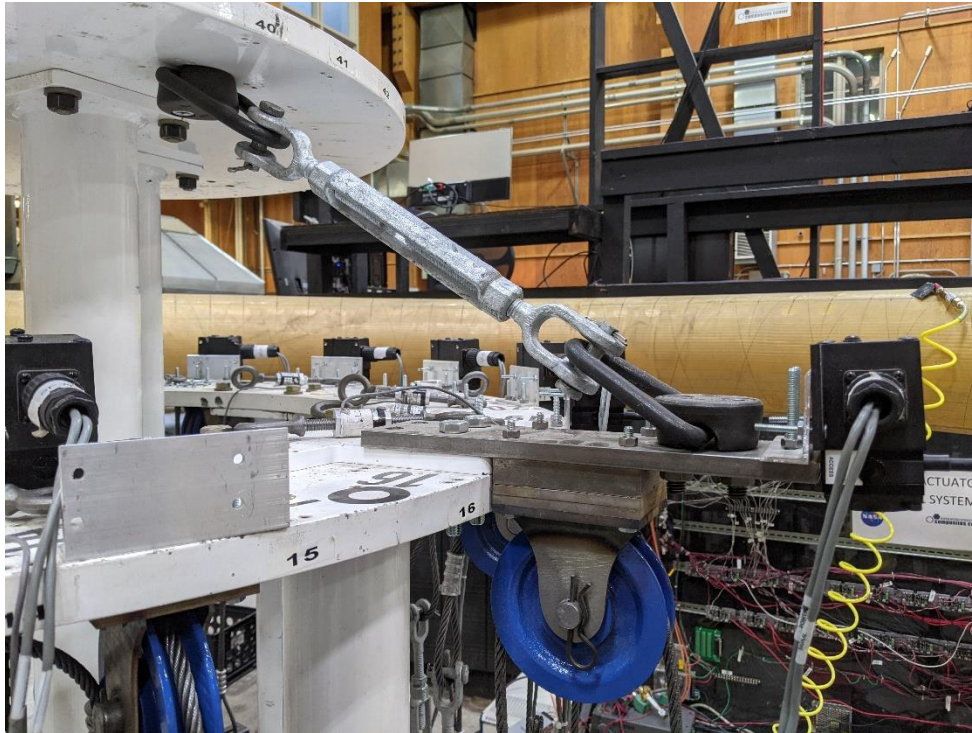


Figure 6. Pulley extension

Because the extension plates alone have insufficient bending strength, they were supported by a turnbuckle connected by hoist rings to the upper plate of the fixture. The plates and hoist-ring system was analyzed as an indeterminate structure and was designed as a beam in bending. The bending factor of safety is estimated to be 1.45. The turnbuckles were purchased from McMaster-Carr and sized assuming they carried the full actuator capacity. See APPENDIX B for the full calculations.

2.3 Check of Outer Ring Structural Capacity

A stress analysis of the outer ring was conducted using the commercial finite element software ABAQUS. One half of the ring was modeled as linearly elastic steel using 8-noded reduced integration shell elements. The plate was discretized using a structured mesh with a target element size of 0.06 in. Point loads with magnitudes corresponding to the full actuator capacity of 2000 lbs were applied at the centers of the bolts holes where the pulley mounts are connected. The plate was supported along three radial lines, at both ends and in the middle, corresponding to locations of the midlines of the support columns. The ends were pinned, and the middle was supported vertically. The loading and boundary conditions are shown in Figure 7, and the resulting maximum principal stresses at the top of the plate are shown in Figure 8.

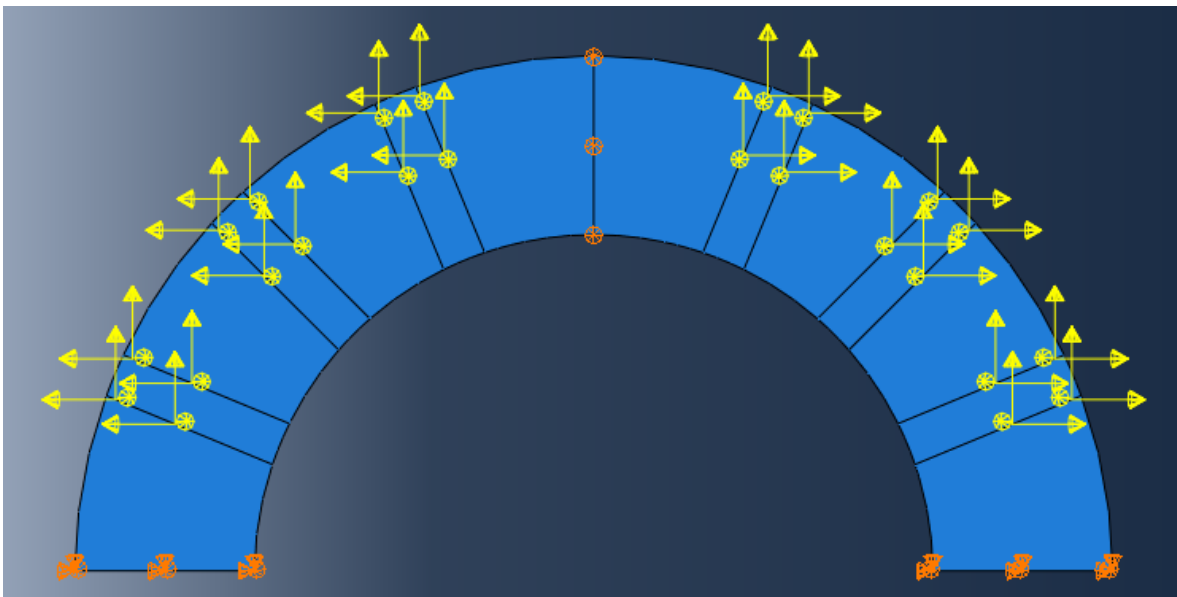


Figure 7. Loading and boundary conditions of outer ring model

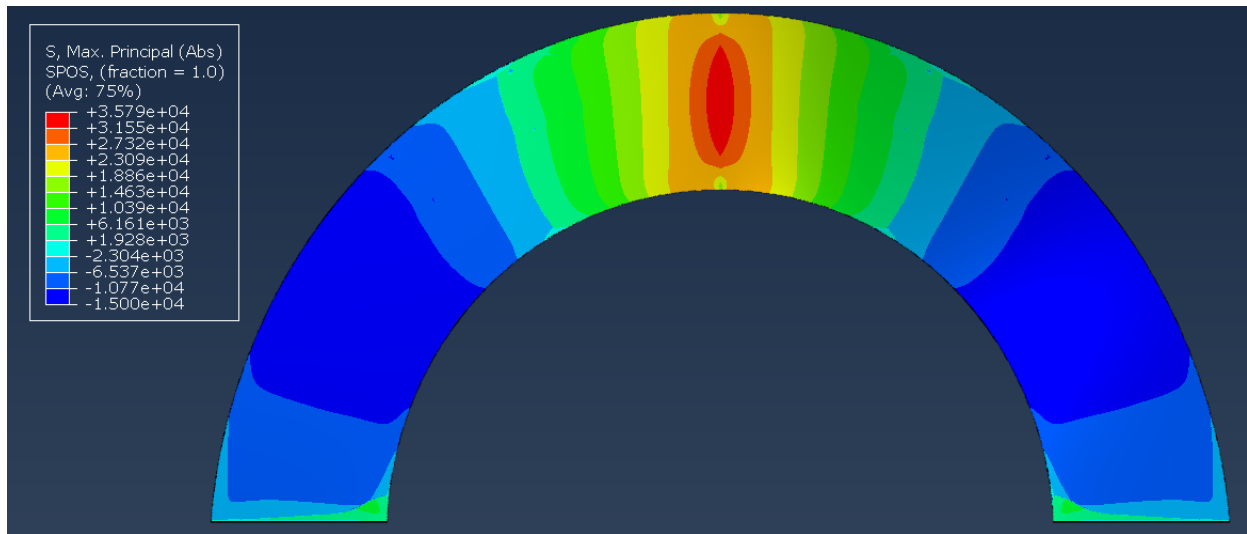


Figure 8. Stresses from FEA model of outer ring

The maximum stress is 35.8 ksi, which gives a factor of safety of 1.01 against yielding assuming the ring is made from 36 ksi steel. However, this is still sufficiently conservative for several reasons. First, the loads used were the actuator capacity, but the actual predicted maximum cable load from preliminary modeling is 1500 lbs (Throckmorton, 2019). Using the predicted maximum loads, the factor of safety is 1.34. Further, these loads are most likely conservative because the model assumes a torus with no geometric imperfections, and geometric imperfections will reduce capacity and thus required actuator forces. Finally, it is unlikely that all sixteen load points will be at the maximum load at the same time. Given these considerations and the difficulty and cost associated with strengthening the outer ring, it was not modified.

2.4 Additional Hardware

To resist the increased load, some of the hardware for the test fixture had to be replaced. All the new hardware was purchased from McMaster-Carr. See Table 1 for a summary of the replacements and the new hardware for the pulley extensions. See APPENDIX B for more details.

Table 1. New hardware

	Catalog #	Capacity (lbs)	Required Strength (lbs)
5/16" wire cable	3441T66	2100	2000
Compression sleeves	3896T7	2100	2000
Turnbuckles	3000T54	2200	2000
2" wide loading straps	9073T632	4800	1000
Pulleys	3168T43	3000	2920
Clevis pins	98340A180	-----	-----
Cotter Pins	92375A510	-----	-----
Gr. 5 1/4" dia. bolts (pulley mounts)	92865A552	*	*
Hoist rings	29505T23	5000	3500
Turnbuckles (pulley extensions)	3001T57	3500	3500
*See APPENDIX B			

2.4.1 Proof Testing of Load Cables

The loading cables were created by crimping both ends of pieces of wire rope. The critical detail in the cable is the crimp, which is created manually using a special tool. To ensure adequate safety, the crimped assembly was proof tested to the maximum actuator force of 2000 lbs using a hydraulic actuator with an inline load cell, as shown in Figure 9. To provide a reasonable sample, four crimp specimens were fabricated in the lab and tested, and all carried the applied load of 2000 lbs with no apparent damage.



Figure 9. Testing of crimped wire rope

2.5 Summary

The test fixture discussed by Young, (2017a) was modified to accommodate paired torus testing using sixteen load points. The actuators were moved, and extensions were attached where needed. The pulleys, their mounts and the wire rope were all replaced with stronger versions. The outer ring of the test fixture was checked. Single torus testing utilizing the modified test rig is described in the next chapter.

CHAPTER 3 SINGLE TORUS TESTING

3.1 Test Setup and Procedures

3.1.1 Specimen and Test Description

The two specimens tested were identical except for major radius, where one was 10" larger than the other. The smaller one was called a T4 and the larger, T5. They had a 71 deg braid with two integral reinforcing cords on the inner half of the cross section at +/- 60 deg from horizontal.

Figure 10 shows a plan view and a cross section of a torus, with the major and minor radii labeled. It also shows the cylindrical coordinate system referenced throughout this paper. The Z-direction is coming out of the page.

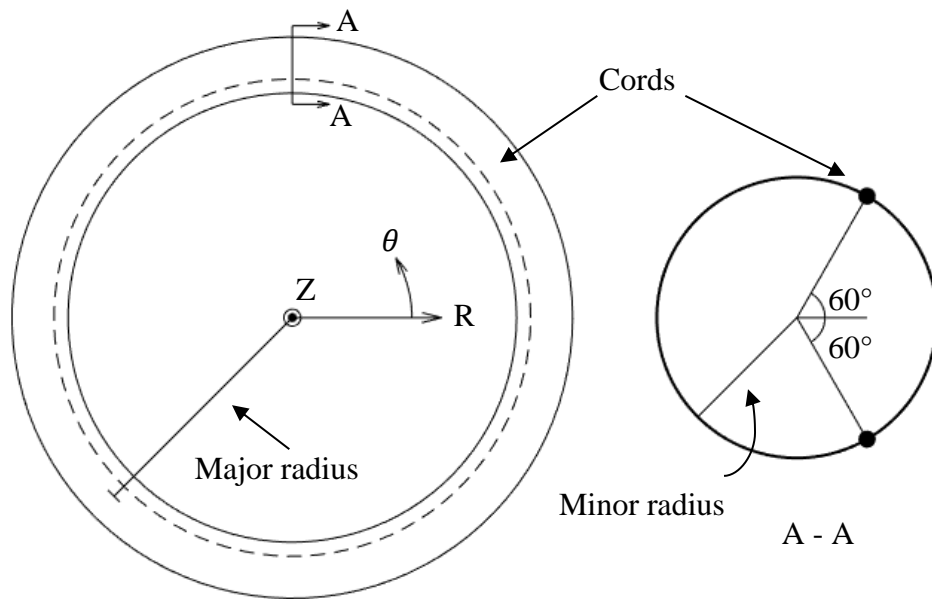


Figure 10. Plan view and cross section of torus (modified from Young, 2017b)

The specimens were tested at three internal pressures 10, 15 and 20 psi. These pressures bound the expected operating pressure for a HIAD device, which is between 15 and 20 psi. Six tests were run at each pressure, in two groups of three. Each test consisted of a load controlled phase where the cables were preloaded to 30 lbs each and followed by a displacement controlled phase where the cables were loaded such that the string pots displaced 1/4 inch. During testing, the

pressure was regulated to +/- 0.1 psi. The control code ran at 10 Hz, because this was the quickest the system could control the actuators. The data acquisition ran at 1000 Hz. The cameras were triggered once a second but not all triggers resulted in a picture. Roughly 80% of the photos triggered were acquired.

3.1.2 Data Acquisition and Instrumentation

The data acquisition system consists of two National Instruments PXI modules, NI PXIe-1078 and NI PXIe-1082. Sixteen load cells were wired into National Instruments TB 4330 cards which were then connected into the 1078 module. In addition, 16 string potentiometers were wired to National Instruments TB 4339B cards which were connected to the 1082 module. The actuators and pressure transducer were also connected to this module; both are discussed later. The string pots and pressure transducer were powered using a Keithley 2220G-30-1 power supply. The two modules and their corresponding cards are shown in Figure 11.



Figure 11. NI PXIe-1078 with TB 4330 cards (left) and NI PXIe-1082 with TB 4339 cards (right)

In addition, photogrammetry data was collected using two JAI BM-500CL cameras with 2456x2050 resolution. They were controlled by a National Instruments PCIe-1430 Camera Link frame grabber.

3.1.2.1 Load Cells

16 Transducer Techniques TLL-1K load cells were used to measure load in the sixteen load cables. The load cells had 1000 lbs capacity and were connected between the load cable and a 2in wide polyester load strap, as shown in Figure 12. Before the load cells could be used, their accuracy was verified using an electro-mechanical load frame with in-line load cell, shown in Figure 13. An example set of verification data and the corresponding best fit line are shown in Figure 14.



Figure 12. Load cable setup



Figure 13. Verification of load cell

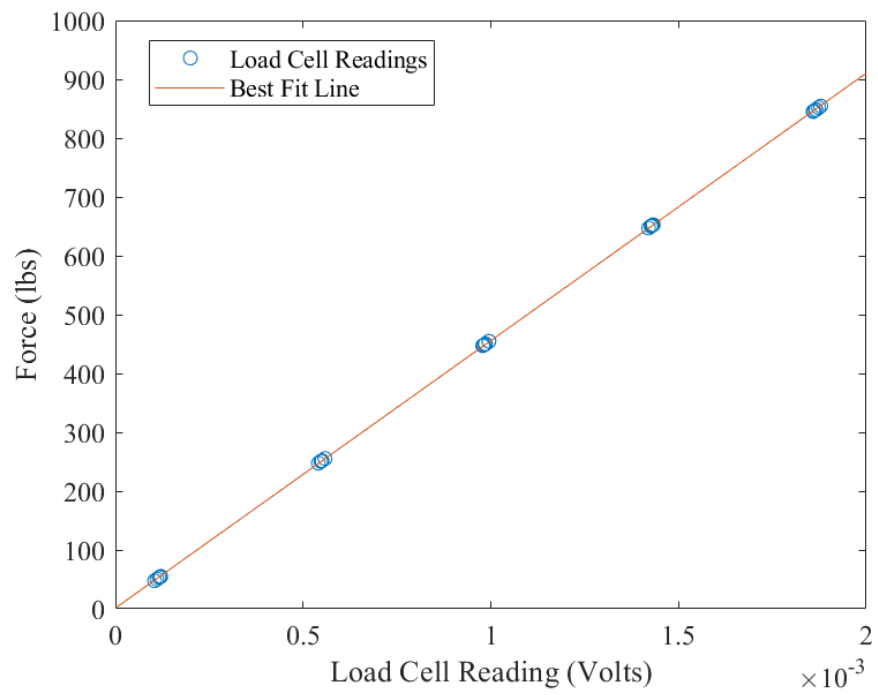


Figure 14. Example load cell verification data

3.1.2.2 String Potentiometers

Sixteen Celesco PT1A-10 string potentiometers (string pots) were used to measure real-time displacement of load cables, and these displacements were then be used to control the actuators. The string pots have a maximum extension of 10 inches and were mounted to the outer ring directly above the front of the pulleys as can be seen in Figure 15. For the pulleys on extension plates, the string pots were attached at the end of the plate.

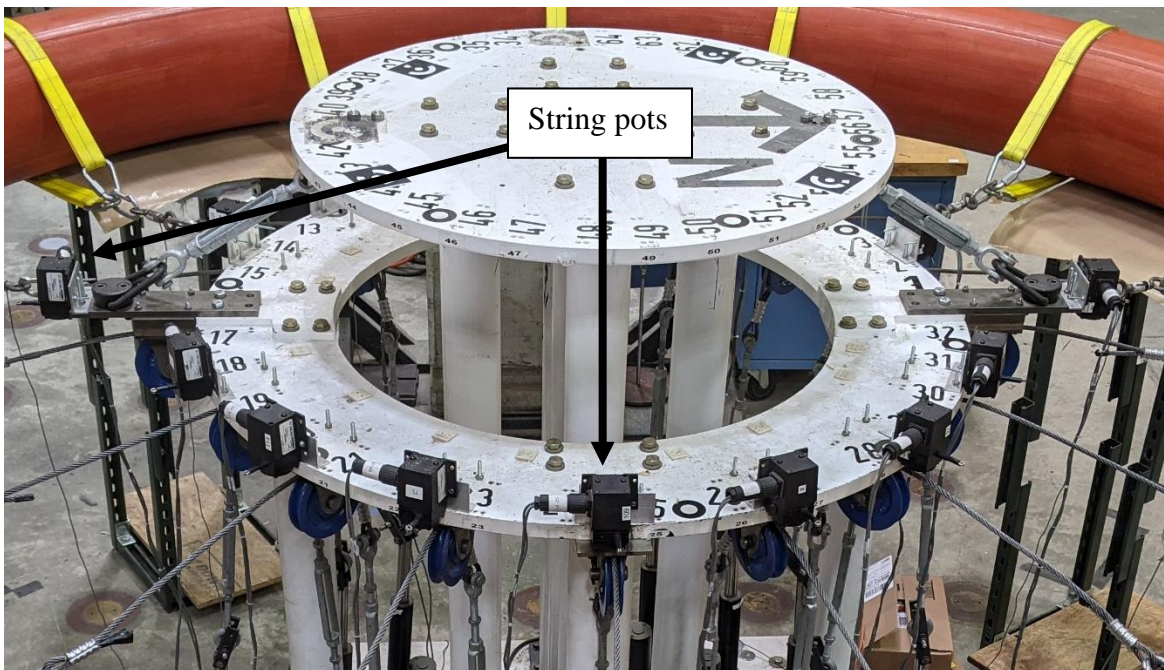


Figure 15. String pots on outer ring

The string pots were verified using a steel plate with three calibrated distances of 3, 5 and 7 inches. The string pot verification rig is shown in Figure 16.

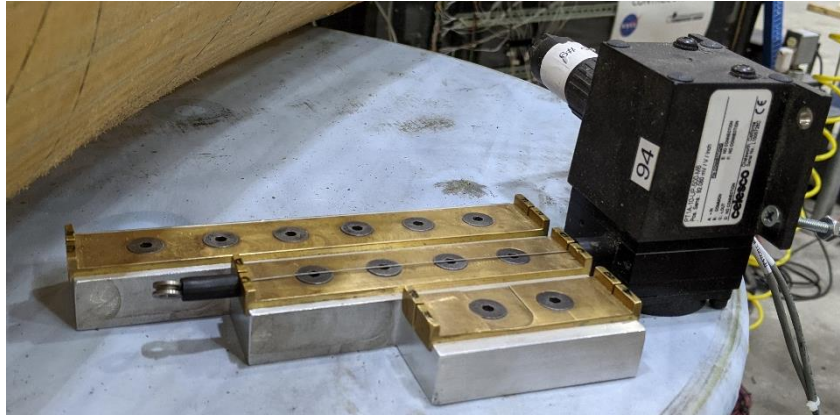


Figure 16. String pot verification

Initially, the string pots were connected to the load cables using monofilament line. Preliminary testing showed poor agreement between the DIC data and the string pot displacements. The string pot setup was modified so that the string pots were more directly measuring torus displacement near the load straps. Large hose clamps were attached to the torus close to the load straps and cushioned with strips of neoprene. The monofilament lines connected to the string pot strings was tied to the screws on the hose clamps. The hose clamps were rotated so that string pot strings were level. Once the hose clamps were added, the string pots and radial PONTOS displacement agreed quite well. Figure 17 shows two examples of the agreement from a test of a T4 at 15 psi.

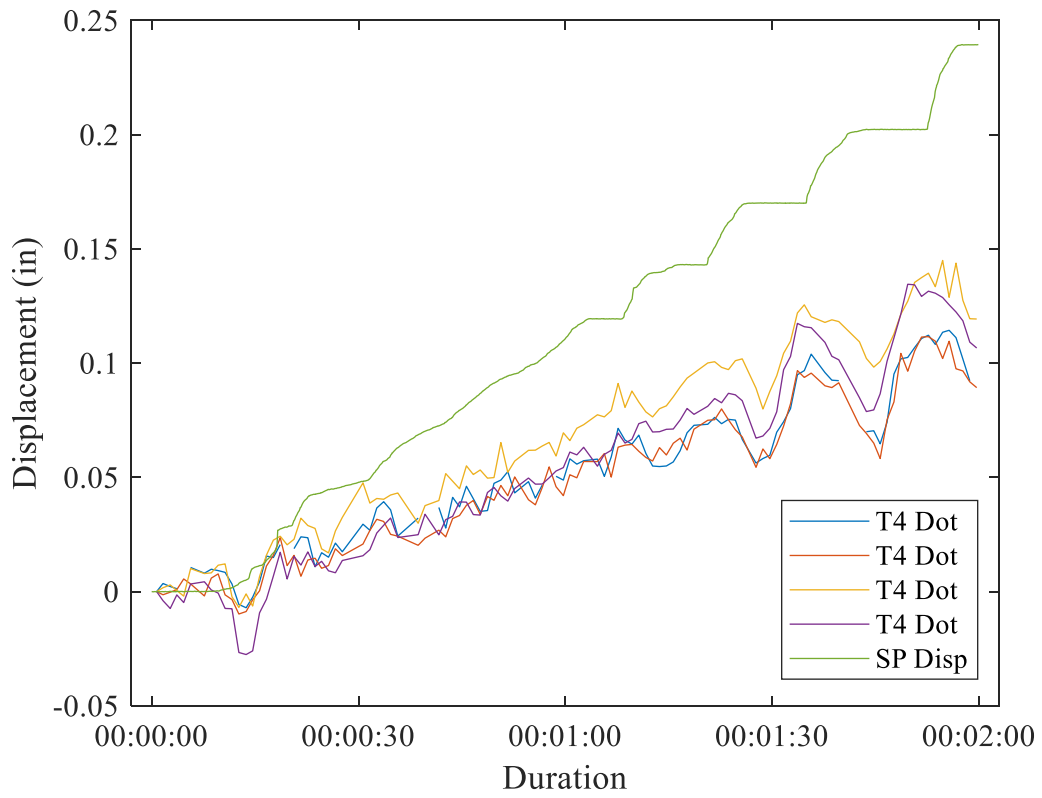
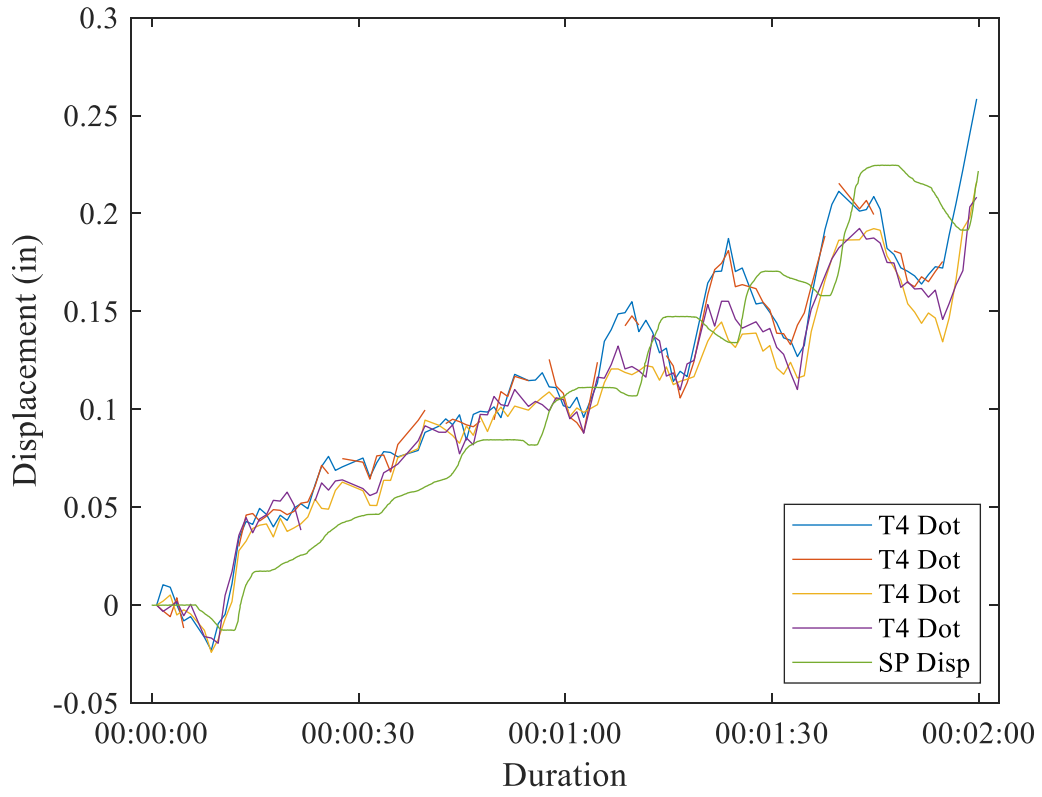


Figure 17. Examples of string pot and PONTOS dot agreement

3.1.3 Digital Image Correlation

Digital image correlation (DIC) was used to track the movements of the tori. DIC is a noncontact method for tracking displacements where a set of calibrated stereo cameras take pictures of a specimen with targets during a test. Those images are then post-processed so that the displacement of the targets are known in each time step. For this testing, the software used was PONTOS.

3.1.3.1 Equipment and Triggering

The DIC system consisted of two JAI BM 500-CL machine vision cameras controlled by a National Instruments PCIe-1430 Camera Link frame grabber. During previous testing detailed by Whitney, (2016), the cameras were triggered using National Instruments Labview software. A MATLAB script communicated with Labview via ActiveX. To reduce lag in the data acquisition, the MATLAB script was modified to communicate to the cameras directly using the Image Acquisition Toolbox. After taking some preliminary images, it was determined that the lag between the two cameras was still too large and that hardware triggering was required. New camera cables with 12pin Hirose connectors that had the ability to both power and trigger the cameras were made and installed. The cameras were triggered by a NI cDAQ 9191 digital output card.

3.1.3.2 Calibration and Camera Stand Modification

The camera stand detailed in Whitney, (2016) was used for the current testing. During the first attempt at calibration, it was determined that the cameras could not capture the entire volume of the T5 torus. The cameras' stand was extended so the cameras were further from the specimen. After this, an extended calibration was successfully completed. Due to the large tori major diameters, an extended calibration is required to enable the cameras to track the full torus. This

involves combining calibration images from five different positions, one on each of the four torus stands and one on top of the fixture. See Figure 18 for example calibration images from both cameras.



Figure 18. Images from camera calibration

3.1.3.3 Target Application

PONTOS targets, also called dots or points, are white circles surrounded by a thick, black border. For the current testing, special targets called coded points were used. Coded points have an additional white barcode outside the black border. This allows the PONTOS software to uniquely identify each dot at each time step. An example dot is shown in Figure 19.

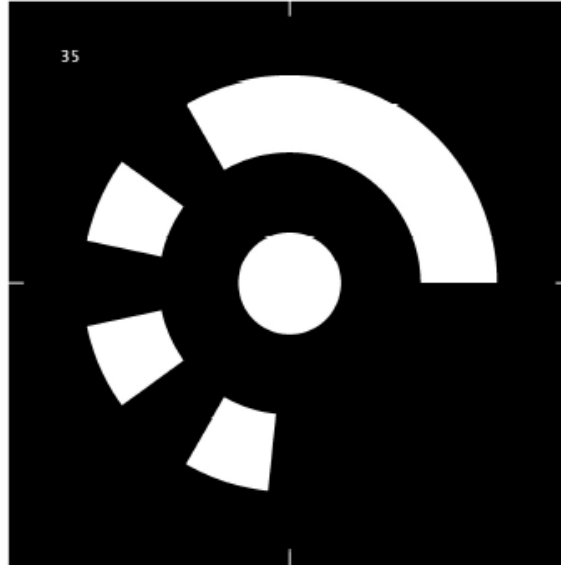


Figure 19. Example coded PONTOS dot

PONTOS most easily tracks points that are planar and parallel to the camera bar. Since the tori are curved, this limited where the PONTOS dots could be placed. Also, it was desired to use the PONTOS data to fit the torus cross sections. Since the cross section is a circle, ideally there would be at least three points around the minor circumference. It was decided that three rows of points would be used. The points were printed on sticker paper and then glued to the torus using silicone, which is also the material used to coat the torus during fabrication. Dots were also adhered to the loading straps and the test fixture as shown in Figure 20. The hose clamps discussed in 3.1.2.2 can also be seen.

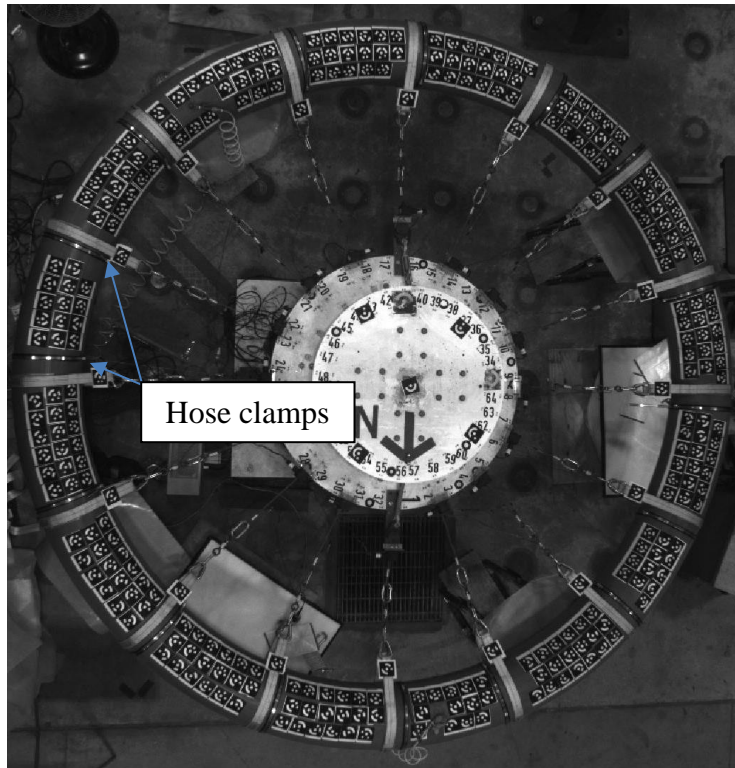


Figure 20. T4 specimen set up

3.1.4 Control

Both the actuators and the air pressure of the specimen were controlled using National Instruments hardware and MATLAB. A copy of the control code can be found in APPENDIX C.

3.1.4.1 Actuators

To load the specimens, 16 screw jack actuators from Progressive Automations (PA-17-6-2000) were used. They have a maximum load of 2000 lbs and a maximum loading rate of 0.3 in/sec. The actuators were powered using two 100A Power Max PM3-100-12 power supplies connected through Cytron technologies MD10C H-bridge cards. The actuators will be controlled using NI PXIe 6612 cards and a PID controller written in MATLAB using the Data Acquisition toolbox (Whitney 2016). The actuator control panel can be seen in Figure 21.

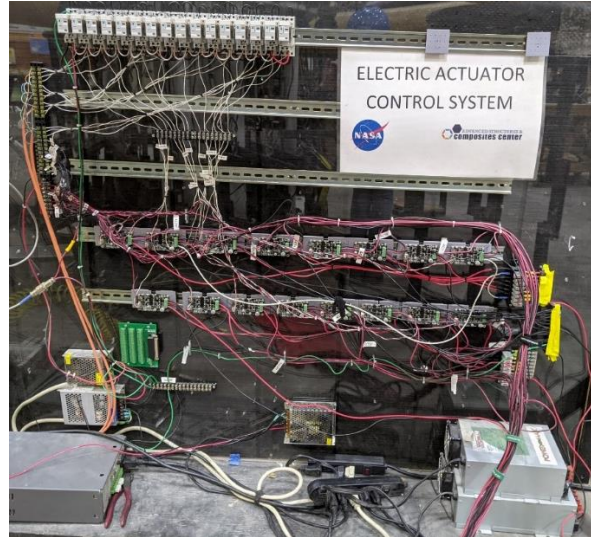


Figure 21. Actuator control panel

Ideally the actuators would be run entirely in load control but they react too slowly for this to be feasible at high loads. Instead each test was split into two phases, a preload phase run in load control using the load cell readings and a second phase run in displacement control using the string pots.

3.1.4.2 Air Pressure

The air pressure of a torus is controlled using a regulator consisting of two red hat solenoids and a Serta transducer, both of which are pictured below in Figure 22. The regulator is controlled using a NI cDAQ 9191 digital output card.



Figure 22. Air pressure regulator and transducer

3.1.5 DIC Data Post-Processing

In order to get useful data, the DIC data must be processed. The following procedure is similar to what was done previously by Clapp, 2017. First, the images are pre-processed by masking so that only the specimen, load cables and test stand are visible. The unwanted pixels are changed to a constant value. Then the modified images are imported to the PONTOS software where the DIC targets are identified. Because the pictures are of a large area, the PONTOS software incorrectly identifies some points. The software ignores the areas greyed-out in the previous step so the number of undesirable points is reduced. See Figure 23 for an example PONTOS project.

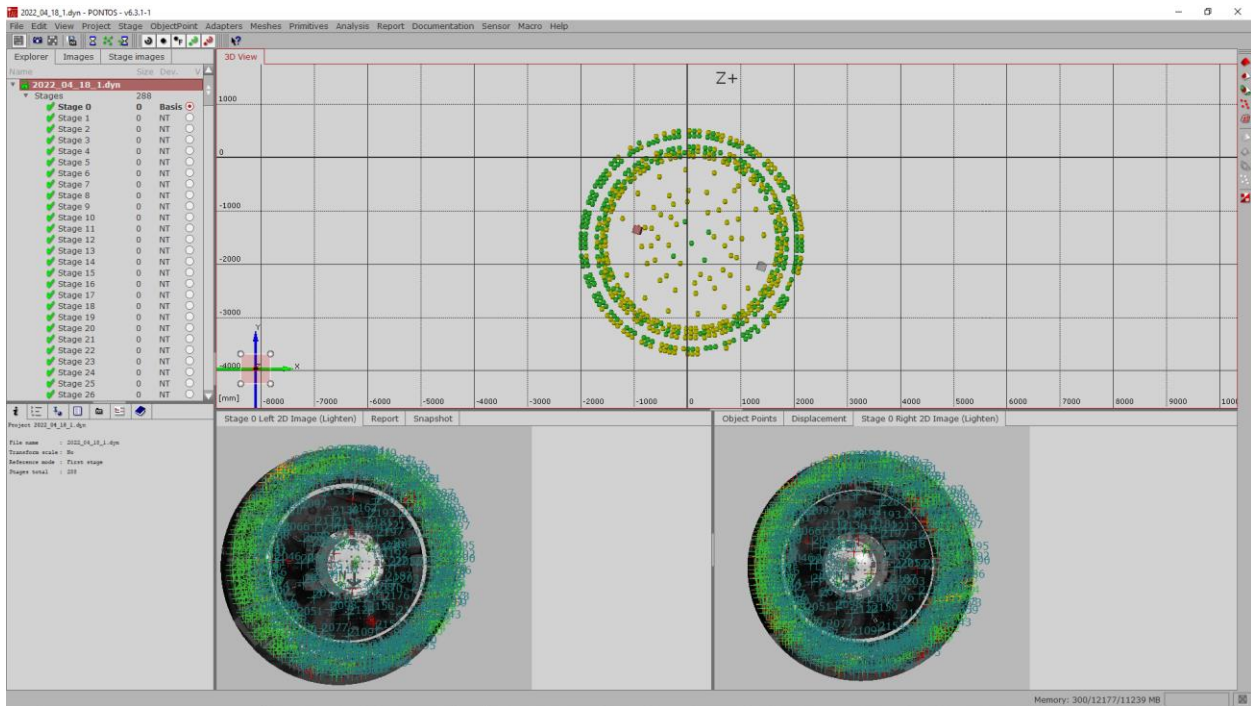


Figure 23. Screenshot of PONTOS software

The exported PONTOS data was then transferred to MATLAB where the bad points were removed, and the remaining data was used to calculate the centroids of the cross sections of each torus throughout the test. Fitting the centroids allows the displacements of the PONTOS dots to be converted to translations of the centroids and rotations about the torus cross section. The

centroids are determined by fitting sections of DIC data to a perfect torus, similar to Clapp, 2017. During the testing detailed by Whitney, 2016, the PONTOS dots were placed in very specific locations on the torus, which made determining which points were correctly identified relatively simple. In the current testing, this was not the case and so it was not as clear which points were correctly identified. In addition to this, the cameras were further away from the specimens and calibrated for a larger volume to accommodate the T5. This increased the errors in the PONTOS data especially in the case of the T5 because dots farther from the center of the volume are less readily identified by the PONTOS software. Through examination of the dots on the test fixture, which should not move, it was estimated that the errors were less than 0.05 inches. However, the test fixture dots are at the center of the volume and are therefore the easiest for PONTOS to identify.

The coordinate system used during processing (shown in Figure 24) is cylindrical with the origin at the location of a PONTOS dot placed at the center of the upper plate of the test fixture. The r - θ plane at $z = 0$ is defined as the top of the upper plate of the test fixture and was determined by fitting a plane through the PONTOS dot at the origin and two additional dots on the upper plate.

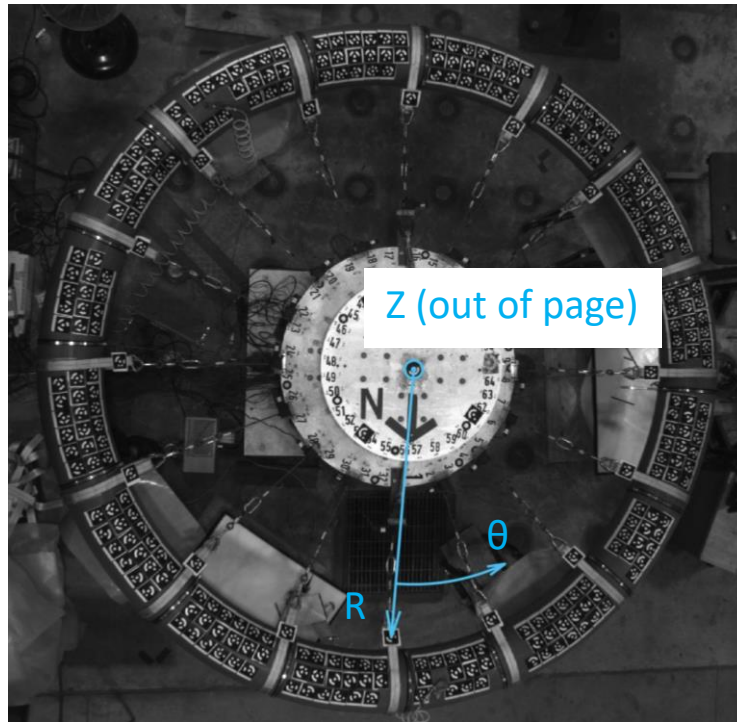


Figure 24. Coordinate system used while fitting PONTOS data

The coordinate system was defined in the first timestep and then propagated throughout the rest of the stages. This is different than Clapp, 2017, who fit the coordinate system at each timestep. This change was made so the error in the dots on the stand, as discussed above, did not add additional variation into the measurements of the PONTOS dots on the specimens.

Once the data is transformed into the correct coordinate system, it is sorted by tangential location and then broken up into overlapping sections. Each section is centered on a given PONTOS dot and includes the n closest on either side. For the current testing, $n = 4$. For reference, this means that adjacent sections are shifted by one dot. For example, if there is a set of 10 dots there is two centroids, one fitted using dots 1-9 centered at dot 5 and the second fitted using dots 2-10 centered at dot 6. Each group of dots is translated and rotated to best fit a horizontal torus centered around the origin. The major radius and height of the torus is also fitted, giving a total of 6 fitting parameters also including the two rotations and two translations. The error is

calculated as the difference between each dots' minor radius and the nominal minor radius of 6.7 inches. After the fit, the tangential location of the centroid is set as the tangential location of the central PONTOS dot of the group. Then, the new centroid is transformed back to the original coordinate system to get its coordinates.

Because of the errors in the PONTOS data discussed previously, a few modifications were made to the fitting procedure described above. First, each torus was split into the 16 segments between the load straps. Centroids were only fit within each segment and not between two segments.

Also, if any points had an error over a set threshold while fitting a given centroid, the point with the largest error was thrown out and the current centroid was refit. This process was repeated until all the points had an error under the tolerance, set at 0.1 inches for the single specimens.

This process still did not catch all the bad points and so during post processing, centroids with displacements that were outliers at a given time step were thrown out. An outlier was defined as a point with more than twice the interquartile range (IQR) less than the first quartile or more than the third quartile, where the IQR is the difference between the first and third quartiles. The two times multiplier of the IQR was chosen by trial and error while post processing the data. It would have been better to improve the fitting code so that it did not fit bad points instead of removing bad centroids after the fact but this was not feasible within the scope of the current project.

In some plots, displacements are averaged over the whole torus. To obtain these averages, the torus was split into the 16 sections between the load straps. The displacement values in each section were averaged and then these were averaged again to get the average for the torus. This method grossly simplified the response of the torus and points in sections that have few points have a larger effect on the final mean displacement. However, each section has the same effect

on the final mean, which is desirable. This would not be the case if a simple average of the displacements was used because some sections have significantly more points than others.

3.2 Results

The results of the single torus testing are shown below. Figure 25 shows example displaced shapes of the T4 on the left and the T5 on the right for all three specimen pressures. There is some tangential movement of the centroids, especially in the T5 at 10 and 15 psi. This is possibly caused by imperfections in load strap orientation. Figure 26 shows total applied load vs the radial displacements of the centroids averaged over the whole torus as described in 3.1.5 . Figure 27 shows the radial displacement of all centroids at final load, as a function of tangential location. These plots show the variation in radial displacements at a given time step. Radial displacement in towards the center of the torus is taken as positive.

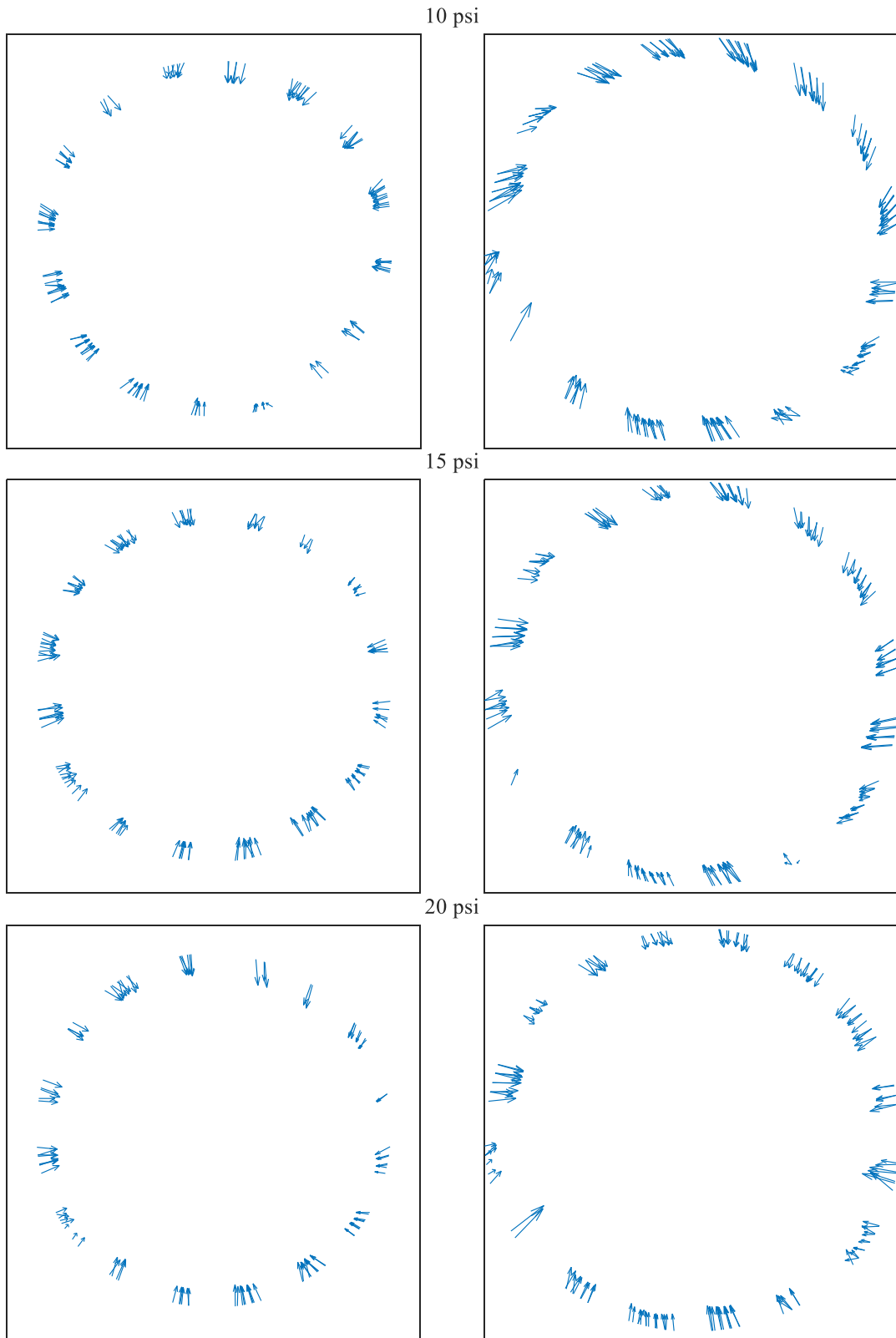


Figure 25. Displaced shape of T4 (left column) and T5 (right column) at 40x

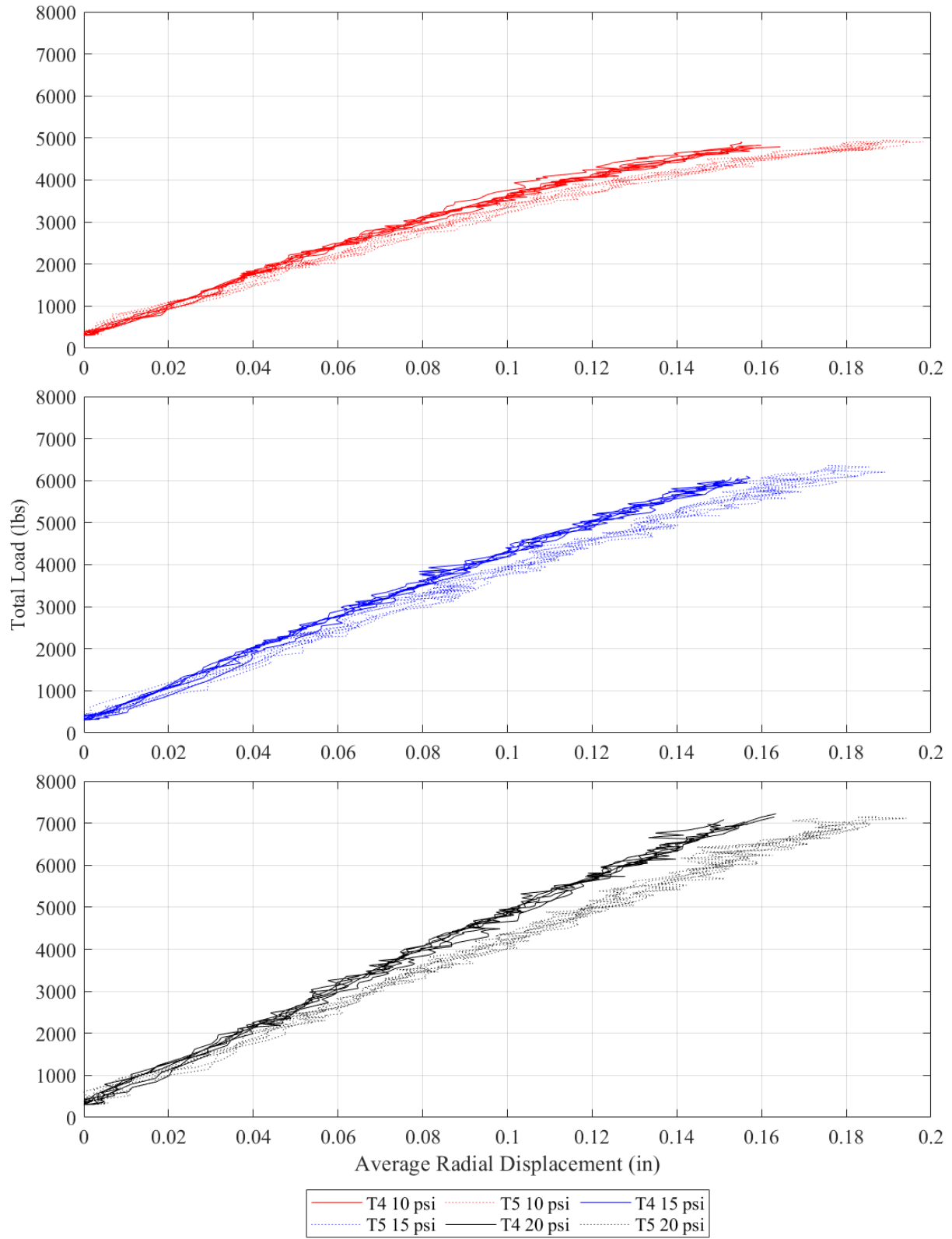


Figure 26. Total applied load vs average radial displacement for single torus specimens

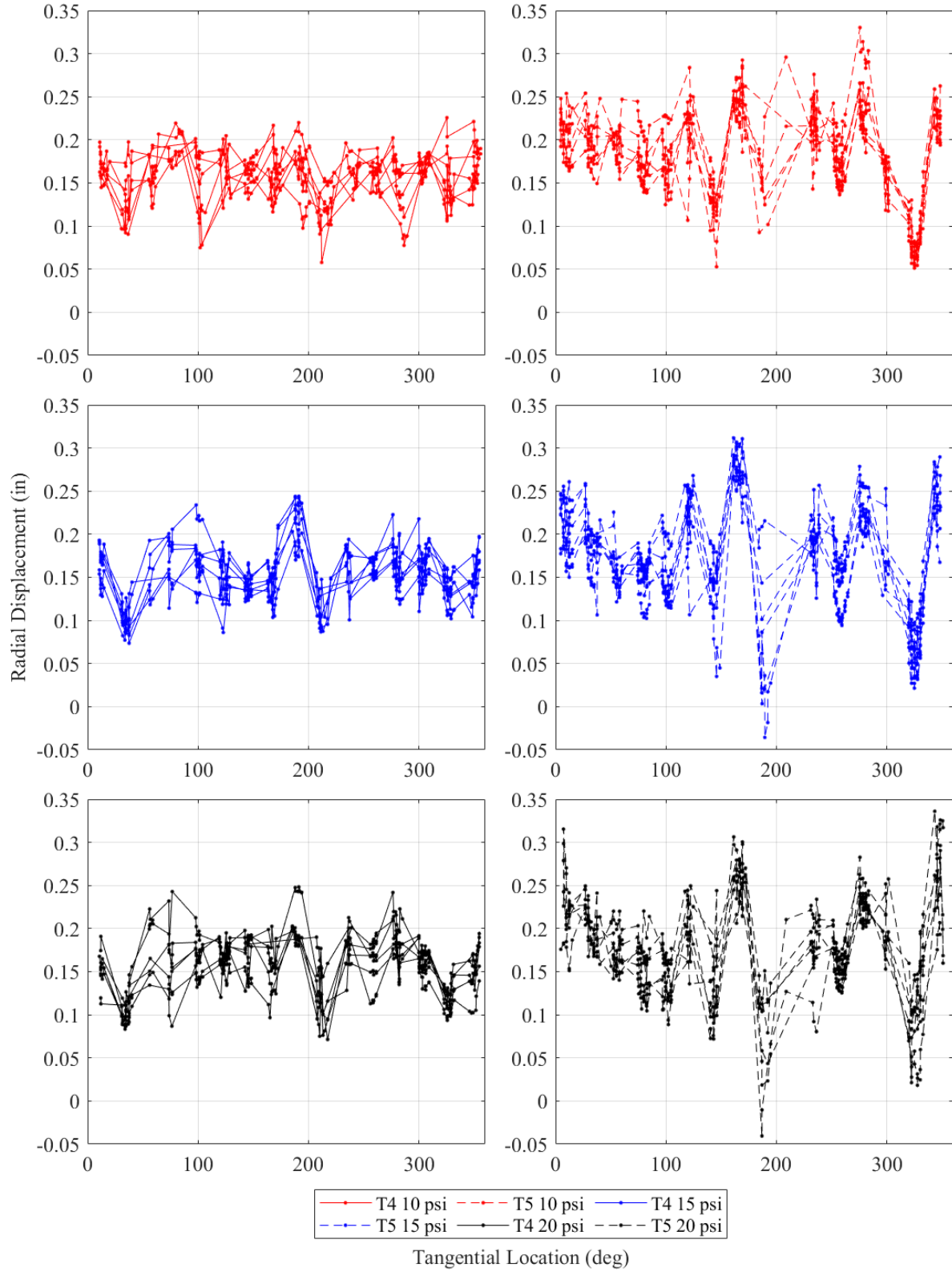


Figure 27. Radial displacement at final load of single torus specimens

Figure 26 shows the average radial displacement of the torus centroids versus the total applied load for all 36 tests. Because of its smaller major radius, the T4 is stiffer than the T5. At an average radial displacement of 0.15 inches, the T4 was 8.2%, 8.1% and 15% stronger at internal specimen pressures of 10, 15 and 20 psi, respectively. Increased internal specimen pressure also decreased the displacement at a given load, as expected. For the T4, at an average radial displacement of 0.15 inches, increasing the internal specimen pressure from 10 to 15 psi increased the total load by 26% and increasing the pressure from 15 to 20 psi increased the load another 16%. The load carried by the T5 at the same average radial displacement increased by 27% and 9% for the same increases in specimen pressure.

Whitney, (2016) also performed single torus testing of a T4 but with 8 pull points. At a change of average radius of 0.09 inches, the T4 held roughly 2410, 2660 and 2840 lbs at 10, 15 and 20 psi, respectively. This is less than the roughly 3380, 3990 and 4500 lbs held by the T4 at the same change in average radial displacement and specimen pressures during the current testing. This was as expected because increasing the number of load points means the loading is closer to uniform and local effects at the straps are less impactful. However, this comparison is imperfect because Whitney calculated average radius differently, by interpolating values at every 1 degree around the whole major circumference instead of only within the segments between the load straps that had data, like done in this research.

3.3 Summary

Testing of single tori was set up and two tori of different sizes were tested in displacement control. The test was controlled using a PID controlled built in MATLAB and data from the 16 string pots and load cells active during the test. Photogrammetry data was also collected to track movement of the specimen and this data was then used to determine the centroids of the

specimen cross sections by fitting. The testing results showed clear internal specimen pressure dependence and also showed that increasing the number of load points increased the total load a specimen could carry, as expected. In the next chapter, similar testing on a specimen consisting of a set of paired tori is discussed.

CHAPTER 4 PAIRED TORUS TESTING

4.1 Loading Method

Originally, the paired specimen was going to be loaded through the shear center via a spreader beam to eliminate applied torque. The shear center was verified to be at the tangent point as the calculations in APPENDIX D detail. The spreader beam concept and shear center are illustrated in Figure 28.

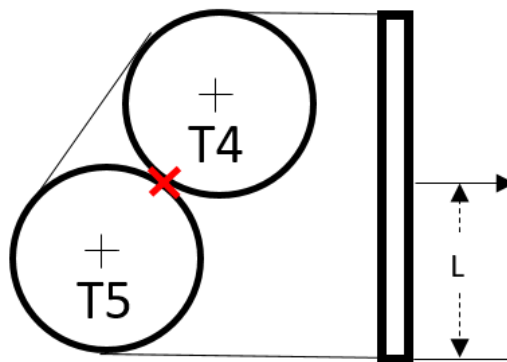


Figure 28. Load application via spreader beam concept

However, it was determined that there was not enough space between the outer ring of the test fixture and the inside of the torus to fit the spreader beam. It was then decided that the ends of the load straps would be hooked together and connected to the load cables, like during testing of the single specimens. With this method, the best height of the specimen had to be determined because it influenced the loading. Ideally, the specimen would be loaded horizontally through the shear center so that the net force was in the radial direction. However, as explained in the next section, this was not possible because the geometry of the cross section would not allow the strap to be in equilibrium. This meant that there would be a net vertical reaction on the specimen and/or applied torque due to not loading through the shear center.

4.1.1 Loading Calculation Problem Description

To choose a height for the torus stands, angle of twist of the specimen cross section and the vertical reaction on the torus stands were desired. This meant the applied forces on the torus needed to be determined. To do this, a system of three equations was developed and then solved using MATLAB. The first two were the sum of the forces in the x (horizontal) and y (vertical) directions, with self-weight neglected. The third was that the length of the loading strap is 78 inches. The system is defined below in Equation 1. Here r_{tor} is the minor radius of a torus. See Figure 29 for other variable definitions. A full derivation is in APPENDIX E.

$$\sum f_x = \left(\frac{A_x - D_x}{\sqrt{(A_x - D_x)^2 + (A_y - D_y)^2}} + \frac{B_x - D_x}{\sqrt{(B_x - D_x)^2 + (B_y - D_y)^2}} \right) \dots \quad \text{Equation 1}$$

$$* F + \frac{L - D_x}{\sqrt{(L - D_x)^2 + (-\Delta h - D_y)^2}} * P = 0$$

$$\sum f_y = \left(\frac{A_y - D_y}{\sqrt{(A_x - D_x)^2 + (A_y - D_y)^2}} + \frac{B_y - D_y}{\sqrt{(B_x - D_x)^2 + (B_y - D_y)^2}} \right) \dots$$

$$* F + \frac{-\Delta h - D_y}{\sqrt{(L - D_x)^2 + (-\Delta h - D_y)^2}} * P = 0$$

$$L_{strap} = \sqrt{(A_x - D_x)^2 + (A_y - D_y)^2} + \sqrt{(B_x - D_x)^2 + (B_y - D_y)^2} \dots$$

$$+ 2 * r_{tor} + r_{tor} * (2\pi + \theta_2 - \theta_1) = 78 \text{ in}$$

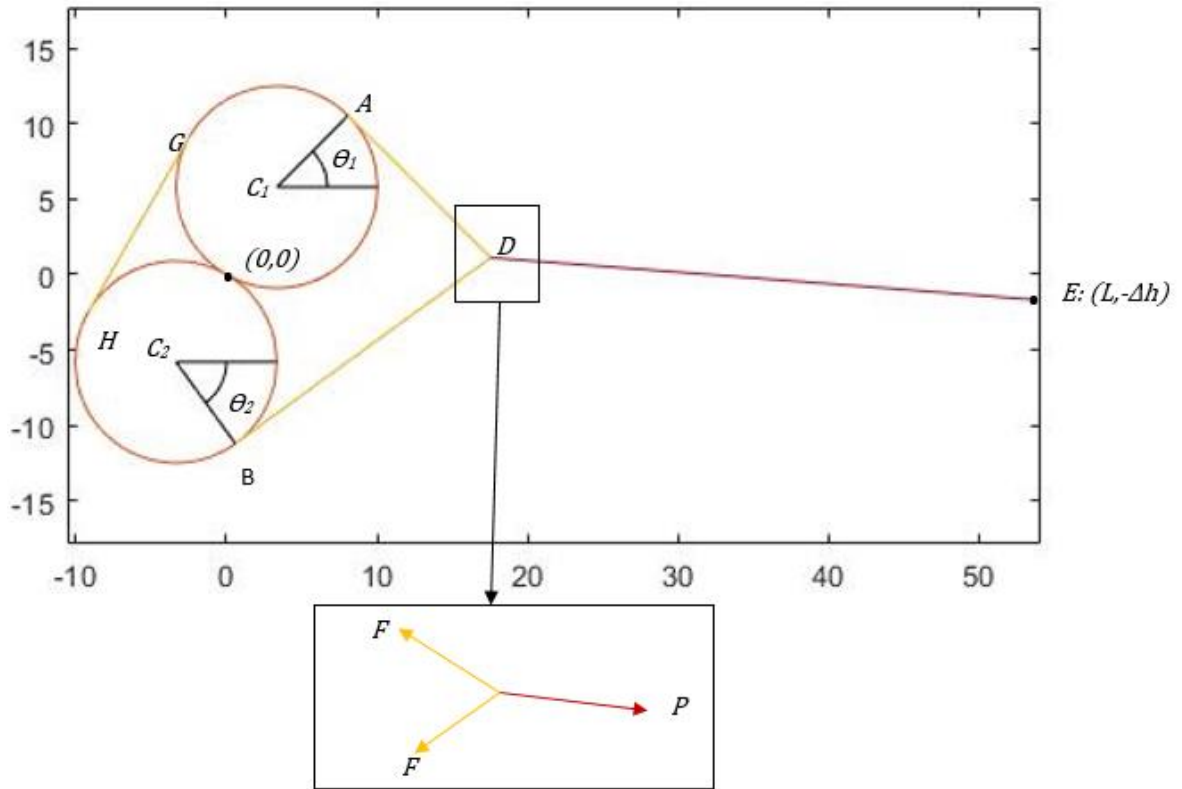


Figure 29. Paired specimen loading problem

The system can then be solved for the force in the load cable, P . From this, the reaction on a torus stand and the angle of twist of the torus cross section can be determined. After a few preliminary runs, the equations were solved and R and φ calculated for Δh ranging from -3 inches to 9 inches. This range was chosen so that the stand reactions did not act downwards on the torus. This is because in reality the specimen is not connected to the stands so they cannot provide a negative reaction.

4.1.2 Loading Calculation Results

The results normalized by the force in a load cable are below in Figure 30.

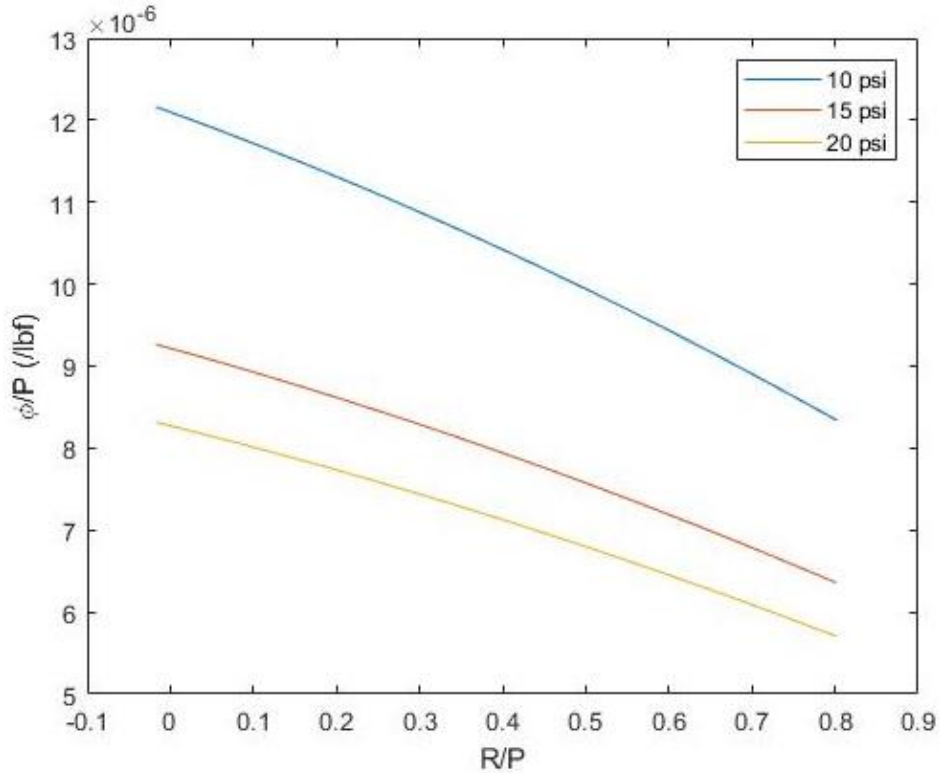


Figure 30. Paired specimen loading problem results

As can be seen in Figure 30, the angle of twist is negligibly small. Because of actuator limits, the cable load can be no larger than 2000 lbs. This means the maximum angle of twist is 0.026 rad. Based on this analysis, it was decided that the torus stands would be set such that the orientation of the cable load is close to horizontal.

Once a height was chosen, the torus stands were positioned. During preliminary testing, it was observed that the specimen was lifting off the stands. This implies that point *D* (see Figure 29 above) was lower than predicted, most likely because the effect of self weight is nonnegligible at small loads. The torus stands were then positioned higher such that the specimen remained in contact with them.

During preliminary testing, the load straps were switched for wider load saddles, discussed later in section 4.2.2.2. The load cable to strap connection also had to be modified, so that both strap

ends connected to one triangular link instead of each end connecting to separate links, as shown in Figure 31.



Figure 31. Old (right) and new (left) load cable to strap connections

As a result, the calculation described above was no longer completely representative of the actual test set up. Further, the calculation could not be easily modified to simulate the new set up. However, since the geometry did not change significantly and the results of the calculation showed that rotations were small, this was not pursued further.

4.2 Test Setup and Procedures

This section describes the setup and execution of the paired specimen testing. This includes modifications of the test setup from single torus testing, a discussion of the application of digital image correlation to paired testing and control of the paired specimen test. Aspects of the test setup and procedure that remained unchanged from the single-torus testing detailed in Chapter 3 are not detailed here.

4.2.1 Specimen and Test Description

The specimen consists of two tori with the same construction as for the single specimens (see section 3.1.1). One torus is a T4 and the other is a T5. They are strapped together with sixteen evenly spaced 2 inch wide straps called pairing loops. An image of the specimen set up on the test rig is shown in Figure 32. The pairing loops are the brown and red straps.

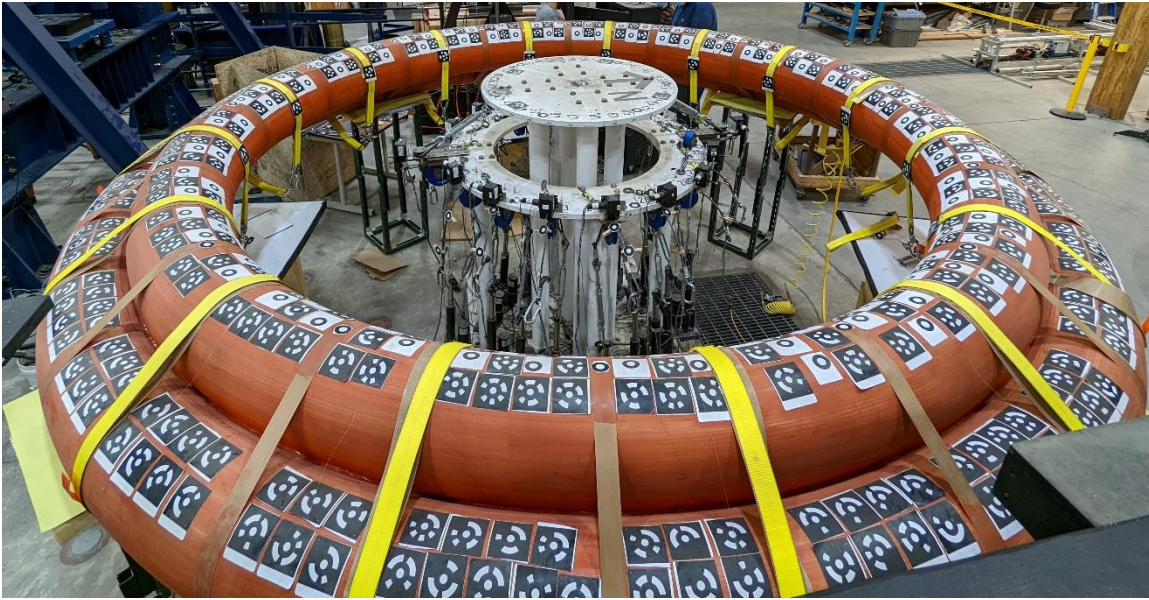


Figure 32. Paired specimen with DIC stickers

The test procedure was similar to that of the single torus tests. First, the cables were preloaded to 35 lbs each and then the string pots were displaced 3/8 inch. The test was run twice at each of three pressures (10, 15 and 20 psi). Like the single testing, the pressure was regulated to ± 0.1 psi. The control code and the data acquisition ran at 10 times a second and the cameras were triggered once a second.

4.2.2 Modifications to Test Setup

The setup of the string pots and loading cables had to be modified to accommodate the paired specimen as described in this section.

4.2.2.1 String pots

With the paired specimen, there was no space to put a hose clamp around a single torus. This meant the string pots had to be attached to the specimen in a new way. For each string pot, a piece of monofilament line was placed around the specimen cross section and both ends were tied to one side of a barrel swivel. A second piece of line was tied to the other side of the barrel swivel and to the end of the string pot string.

During preliminary testing, agreement between their readings and the DIC data was checked. It was determined that string pot readings did not agree well with the DIC data at small displacements. See Figure 33 for an example.

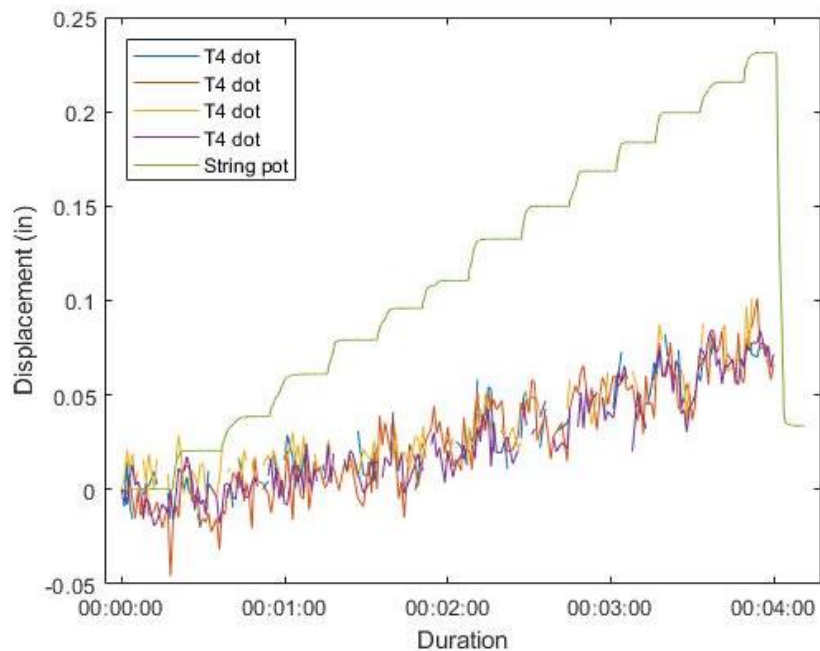


Figure 33. String pot and PONTOS dot displacements during 1/4 in displacement controlled test at 5 psi. With the current string pot setup, this disagreement is unavoidable; the two tori rotate as they are loaded and this rotation affects the string pot readings. Also, while it is desirable, agreement between the two data sets is not strictly necessary. The string pot readings are used only to

control the test and the goal of the test is to load the specimen with sufficiently large and uniform loads in the cables, which was achieved as detailed later.

4.2.2.2 Load Cells, Straps and Cables

Originally, the same 2 in load straps used during single torus testing were used for paired testing. However, it was determined that at high loads the load straps locally compressed into the tori significantly. To better distribute the load and alleviate this, the straps were replaced with 6 in wide woven fabric saddles, shown in Figure 34. The saddles were positioned so they were halfway between 2 pairing loops. To make sure all of the load cables started at the same height, before each test their locations were measured from a piece of aluminum square tube attached to the upper plate of the test fixture, which is shown in Figure 34.

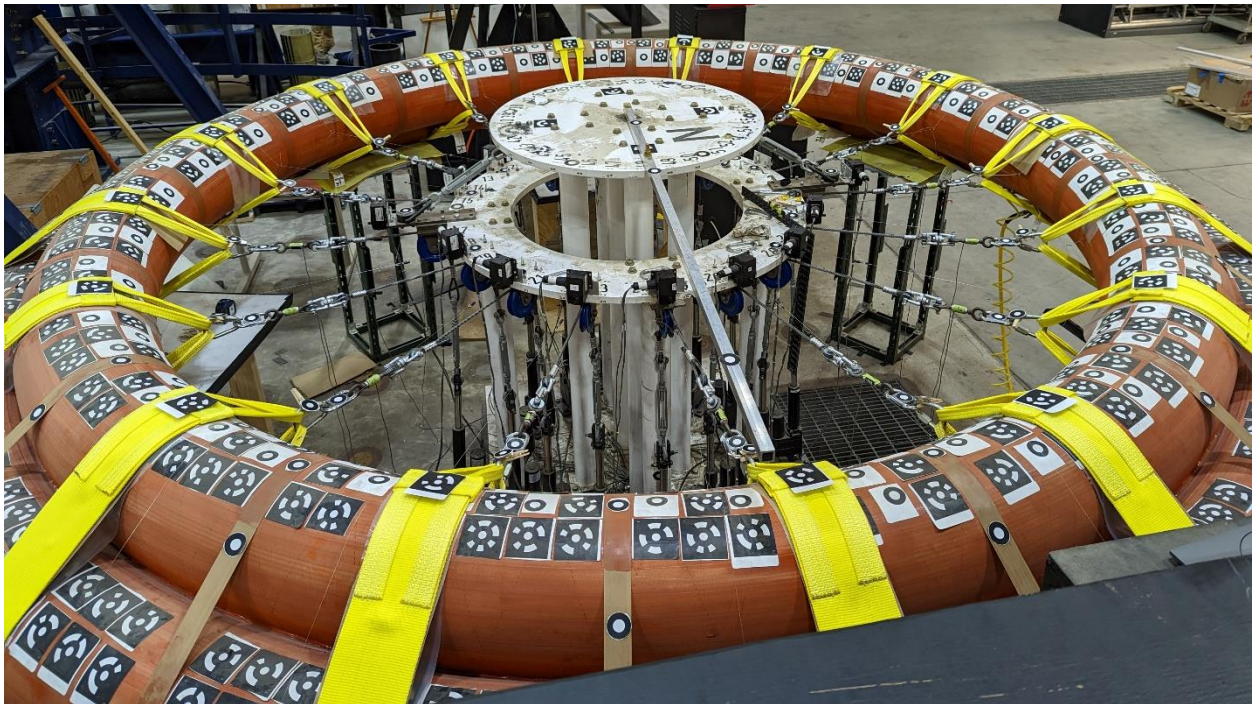


Figure 34. Paired specimen with load saddles

The 1000 lb capacity load cells were replaced with 2000 lb capacity ones. It was also discovered that some of the load cables are twisting and unscrewing the eyebolts fastened to the load cells so

2000 lbs capacity swivels (see Figure 35) were obtained and Loctite was applied to the load cell eyebolts.



Figure 35. Swivel

4.2.3 DIC

When testing the single tori, DIC targets called coded PONTOS dots were used. Coded dots are special because they have a bar code so that the PONTOS software can more accurately track each dot throughout time. However, only 430 unique coded points exist and more could fit on the paired specimen. Also with the paired specimen, the T4 (top) torus blocked the cameras' view of the T5 torus. Since the T5 has a larger major radius, the software has a more difficult time tracking points on it. Taking all of these things into account, 2 rows of coded dots were applied to the T5. Three rows of dots were applied to the T4 consisting of alternating coded and uncoded points. Dots were also added to the pairing loops and load cables. This is shown in Figure 36. It can also be seen in Figure 32, above.

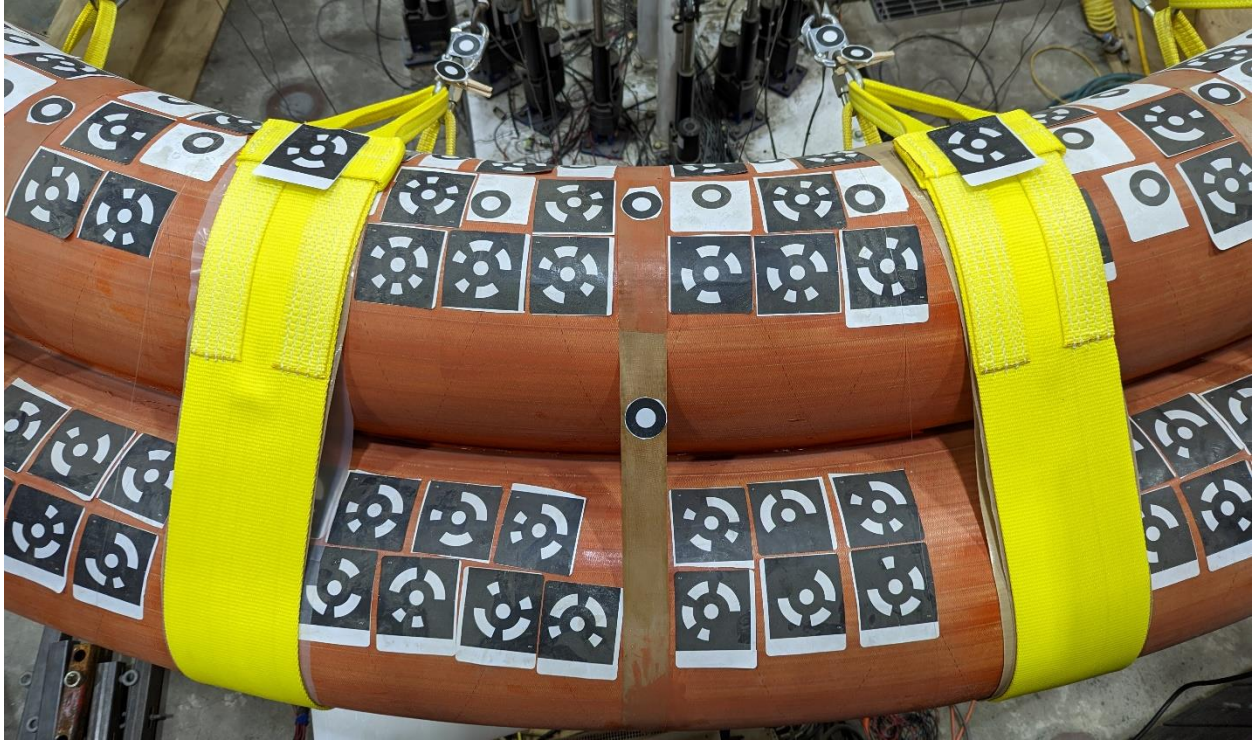


Figure 36. PONTOS dots on paired specimen

At first, the number of DIC targets identified by the PONTOS software was too low. To remedy this, the bar the cameras sit on was rotated 5 degrees such that the cameras were at different heights compared to the specimen. This helped to some extent, and another 70 DIC targets were identified by the software. However, the number of dots identified was still not consistent. It was determined that since the two tori in the specimen are at different heights, PONTOS is very sensitive to the exposure settings on the cameras. There must be a balance between getting enough light for PONTOS to identify the dots on the T5 without overexposing the dots on the T4. The correct amount of light was determined using trial and error.

The DIC data was processed and fit using a similar procedure as that for the single tori (see 3.1.5), with a couple of modifications. The error tolerance for acceptable points during fitting was 0.15 inches. Also, because of the aluminum square tube discussed in 4.2.2.2, the DIC target used for the origin of the coordinate system was blocked. Instead, 4 targets were placed in a cross

shape centered at the center of the upper plate, as shown in Figure 37. The centroid of these points was used as the origin. Like for the single tori testing, the $r-\theta$ plane was defined by fitting a plane through three points on the upper plate.

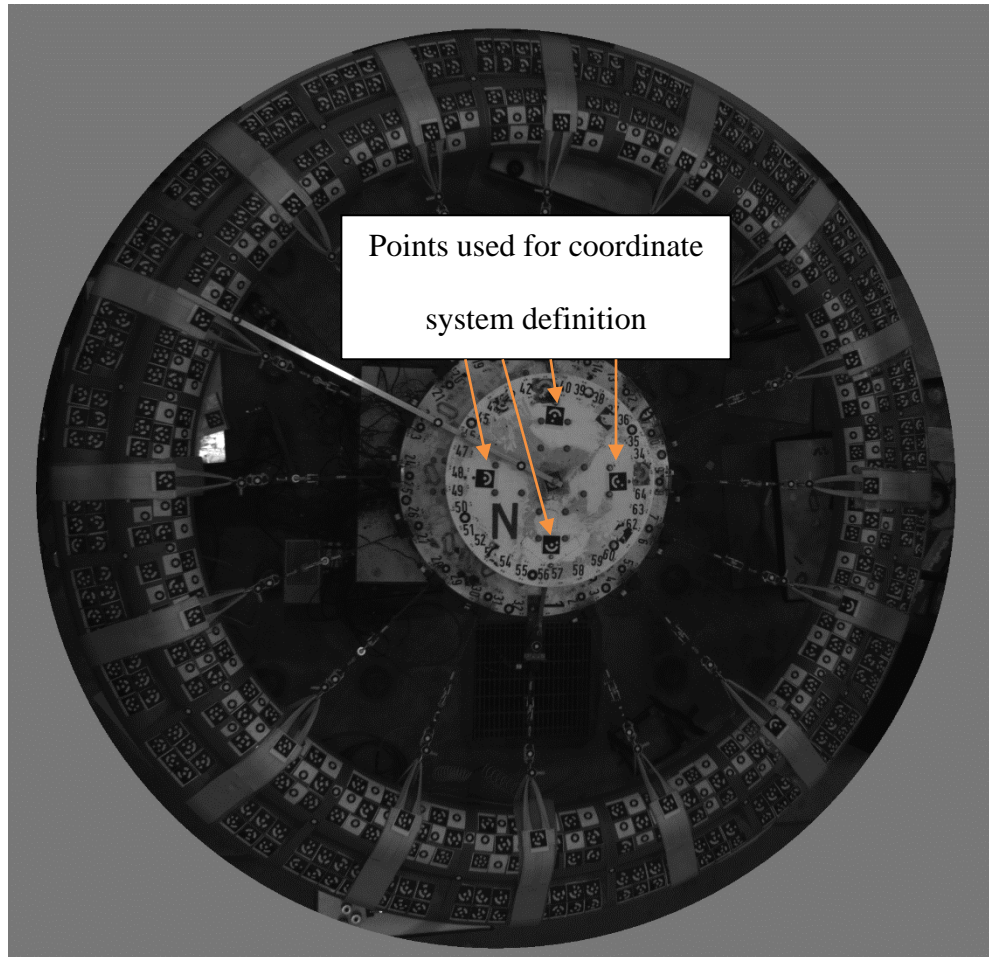


Figure 37. DIC picture showing points used to define coordinate system

The distance between the centroids and the specimen orientation (as defined in Figure 43), were calculated using the PONTOS data. Since this required a centroid of the T4 and the T5 at the same tangential location, missing centroids were interpolated, but only within each segment between two load straps.

4.2.4 Control System Tuning

During preliminary testing, there were issues with stability of the control system (not the specimen). This instability was evidenced by fluctuations in string pot displacements as shown in Figure 38 and Figure 39.

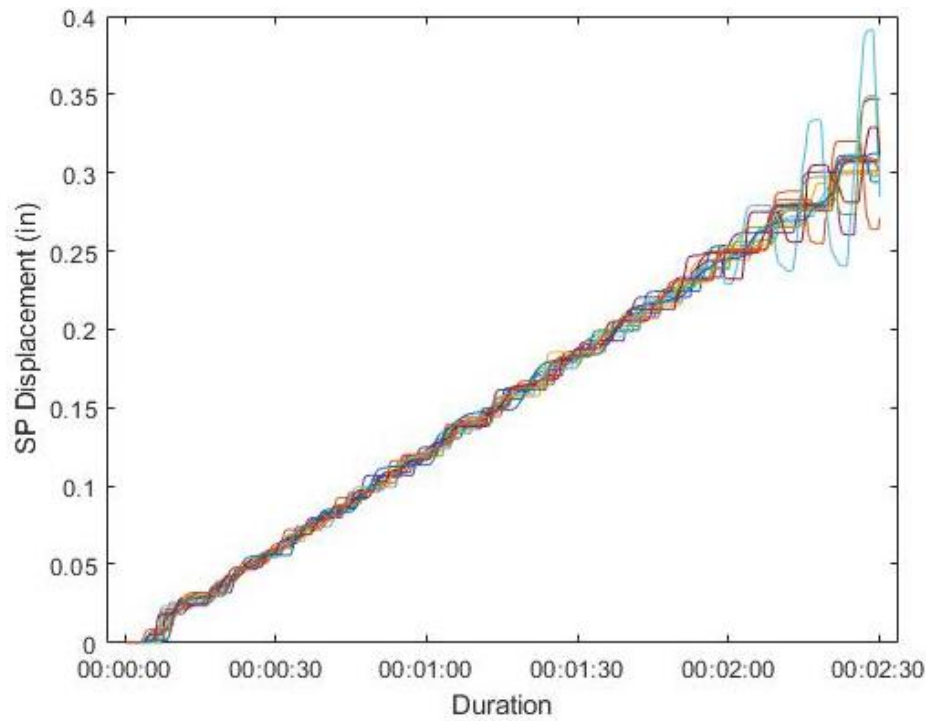


Figure 38. String pot displacement during displacement controlled test to 3/8 in

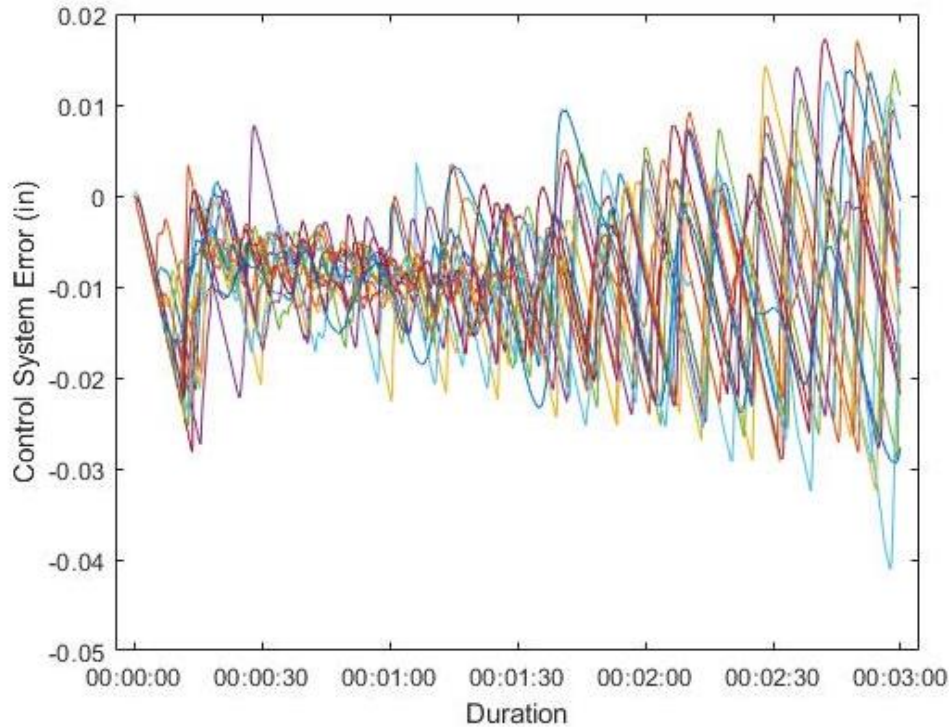


Figure 39. Difference between string pot reading and target displacement during test to 3/8 in

Instability during the load controlled preload phase was fixed by keeping the preload low, at 35 lbs/cable. To remedy instability during the displacement-controlled phase, the PID parameters of the control system had to be changed. See Whitney, (2016) for an in-depth explanation of the control algorithm. A basic PID controller has three parameters proportional, integral and derivative. The proportional parameter defines how the system reacts to the current error. The integral parameter defines how the system reacts to past errors (integral of error vs time curve over a set time interval) and the derivative parameter defines the rate at which the system reacts to the error predicted (slope of error vs time curve). With a basic PID controller, these parameters are constant but the control algorithm developed by Whitney (2016) uses load scaling which means P, I and D vary with the load in the cables. Originally, P decreased and I increased as load increased. At high loads, the integral parameter dominated which meant that errors had to accumulate to a certain level before the system reacted. Sometimes this meant the system

overreacted and went unstable. The load scaling of the proportional parameter was changed such that it slightly increased with increasing load instead of decreasing. This made the control system more responsive and stable.

4.3 Test Results

4.3.1 Control of Test

Ideally, the whole test would be run in load control but most of the test is run in displacement control. This is because the actuators do not respond quickly enough for load control to be stable. The aim of the testing is to simulate uniform pressure, so displacement control is acceptable provided the forces in the cables are close to equivalent. The goal of the displacement-controlled portion of the test was to linearly increase the string pot displacements from 0 to 3/8 inches. This was achieved, as shown by the actual displacements in Figure 40.

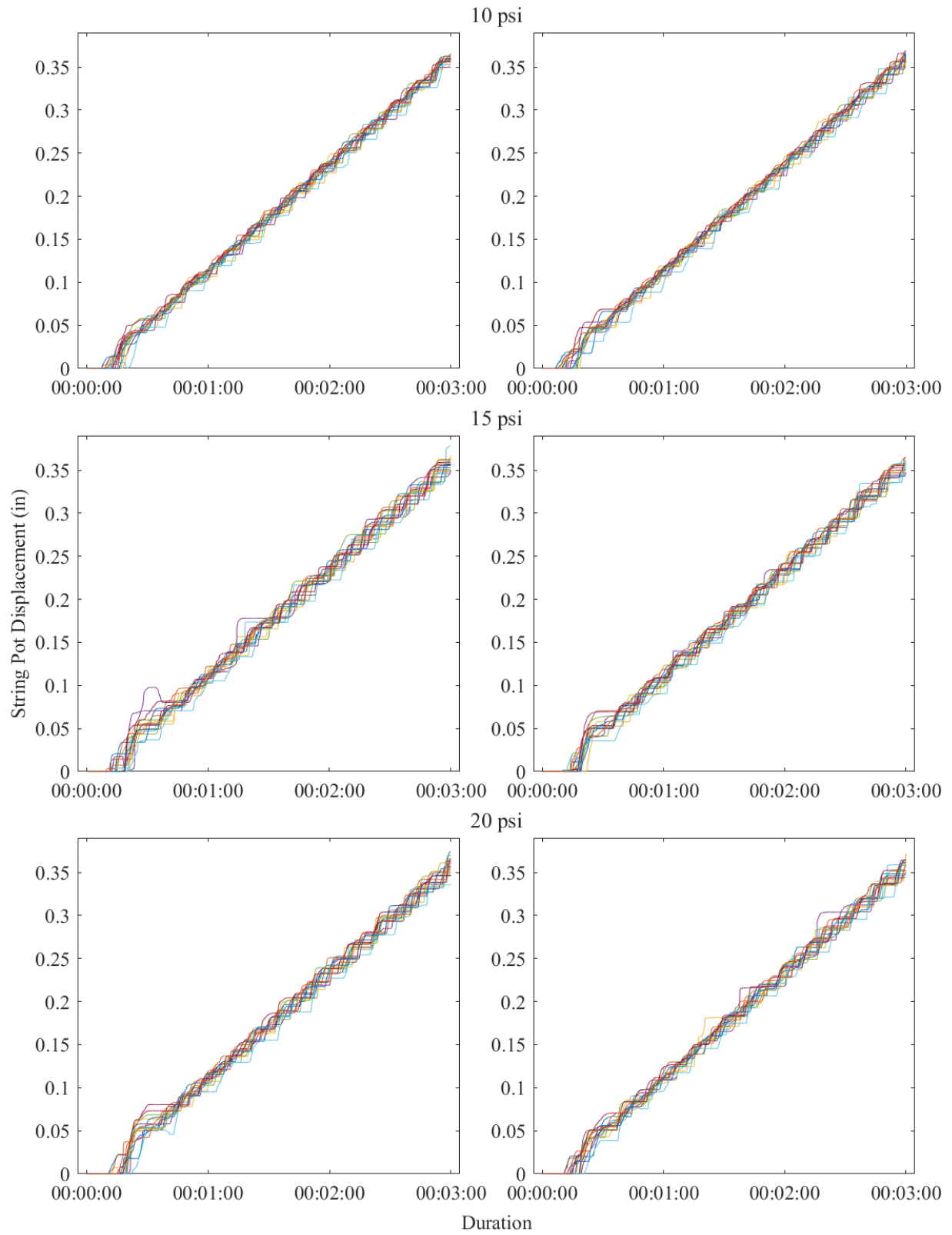


Figure 40. String pot displacement during displacement controlled testing

It should be noted that the string pot displacements are not perfectly linear and had a tendency to stay constant for some time, quickly increase and then repeat. This is a short coming of the control system, which cannot be finely tuned. This could be due to the fact that the actuators can be run at a maximum of 10 Hz, which is relatively slow for a control system. However, preliminary testing indicated that the effect of this behavior on the test was small enough to be acceptable.

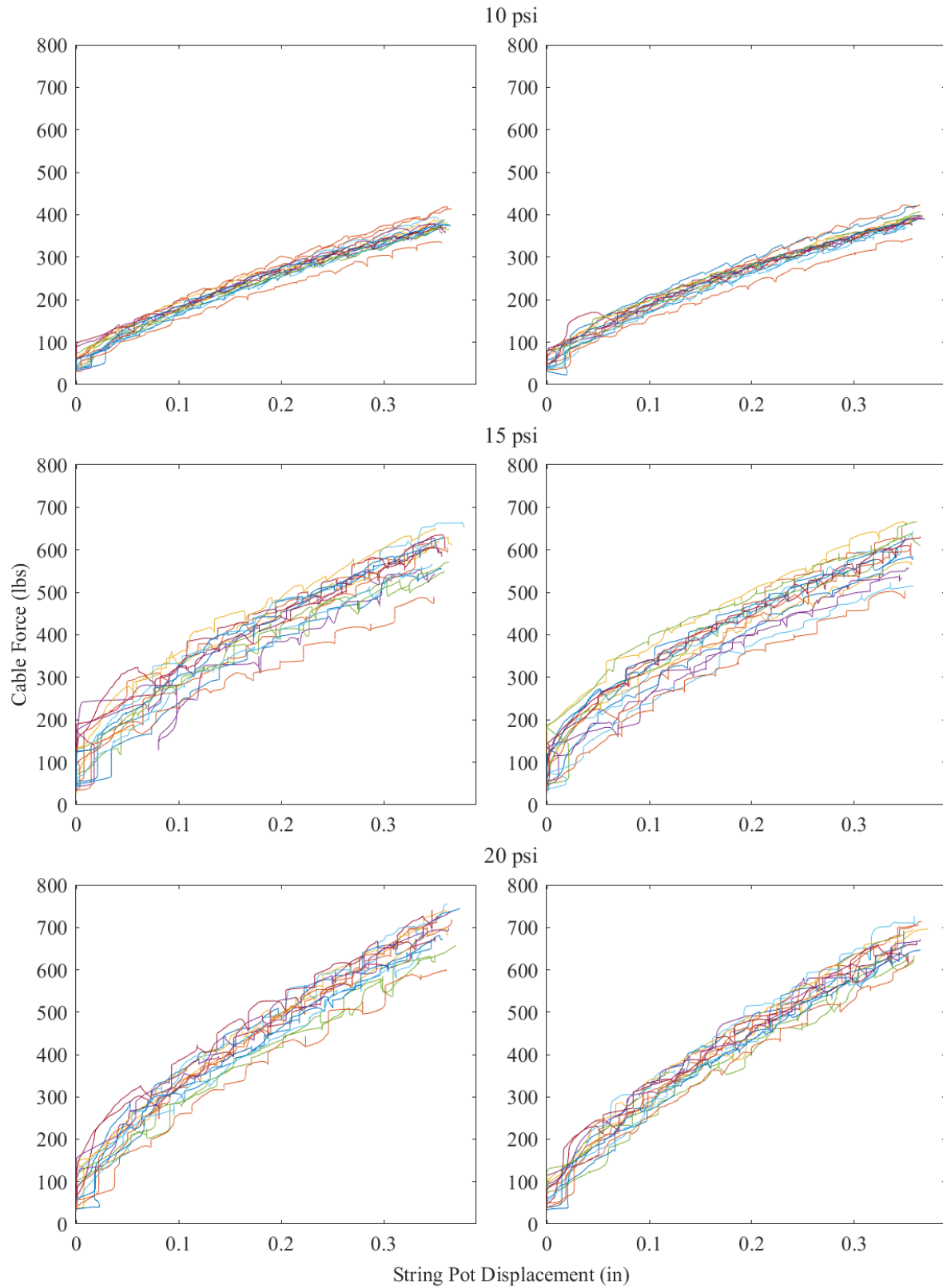


Figure 41. String pot displacement vs cable load

The load vs displacement relationships for each load cable string pot pair for all six tests are shown in Figure 41. Variations in string pot displacements during a single test could be a result of multiple sources including imperfections of the specimen geometry, variations in load cable and string pot orientation, or low cable preload. Because of issues of stability of the load control, the specimen could only be preloaded to 35 lbs/cable this load was not high enough to remove all of the slack from the cables or engage all of the string pots. As a result, the string pots engaged at a range of loads at the beginning of the displacement controlled phase and this variation stayed present for the remainder of the test. More information on the variation in cable loads is below in Figure 42 and Table 2.

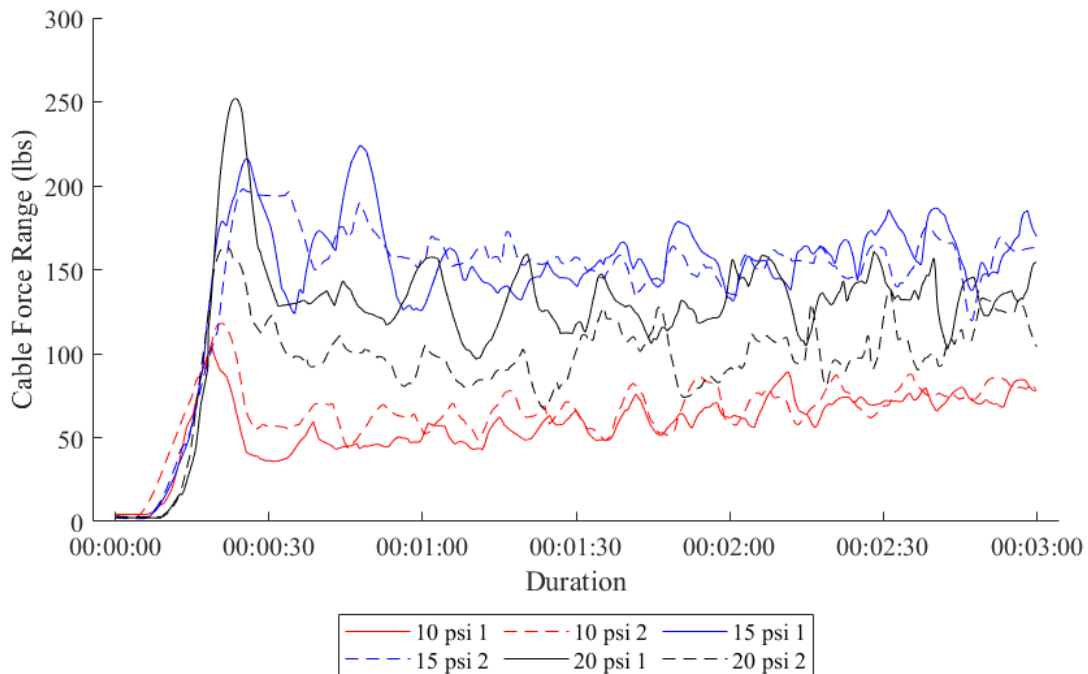


Figure 42. Range of cable loads during displacement controlled test

Table 2. Mean and maximum cable load range

Pressure (psi)	Test number	Mean cable load range (lbs)	Maximum cable load range (lbs)	Sum of all cable loads (lbs)
10	1	35	104	6040
10	2	39	118	6140
15	1	86	224	9470
15	2	85	198	9500
20	1	73	252	11020
20	2	56	164	10600

Table 2 and Figure 42 give more information on the variation in cables loads for all six tests. For many of the tests, the maximum variation occurred at the beginning. This is because the preload was so low that some (but not all) of the string pots had not engaged yet. This meant the load in the corresponding cables increased rapidly at the beginning of the displacement controlled phase, sometimes so quickly that it over shot and then decreased again. The two 10 psi tests have similar variations, but the 15 and 20 psi tests are less similar. This is because the quality of the control was also dependent on the computer used to run it. It was observed in some tests that the computer lagged more than others which negatively affected the control. Despite these issues, it was determined that the variation in cable loads was small enough for the purposes of this testing.

One important observation is the clear increase in load with pressure for the same test protocol. The results in Table 2 show that on average, the total applied load corresponding to the maximum string pot displacement increased by 56% as pressure was increased from 10 to 15 psi, and grew another 14% as pressure was increased from 15 psi to 20 psi. These results agree qualitatively with expectations of increasing stiffness and capacity with increasing inflation pressure. For comparison, the single torus tests showed increases in capacity of about 27% and 15% for these same pressure differences and a string pot control displacement of 1/4 inch (see

Chapter 3). However, the single torus tests were run to larger specimen displacements for the smaller string pot control displacement, which makes comparison of peak loads between single and paired tori impossible.

4.3.2 PONTOS Data

Information about the initial configuration of the specimen and its displacements during testing was obtained from the PONTOS data and are discussed below. The DIC system is capturing its maximum possible volume because the specimen is so large. This means the PONTOS data is imperfect, as discussed in 3.1.5 . These tests are small displacement tests and so some displacements are close or within the error threshold of roughly 0.05 inches. This contributes to some of the variability seen in the following plots. In addition to this, the T5 only had two rows of PONTOS dots on it because that was all that was visible by the cameras. The centroids used in the following plots were calculated by fitting the cross section of the torus to a circle with a radius of 6.7 inches. Ideally, this fit would use points in at least 3 locations around the cross section but in the case of the T5 this was not possible.

Shown below in Figure 43 is a rendering of the specimen cross section with some terminology and the sign conventions of displacements used in this chapter. The distance between the centroids of the two tori at a given tangential location is called the distance between the centroids. The angle that the line through both centroids makes with the horizontal is called the specimen orientation. Positive radial displacements are inwards towards the center of the specimen and positive vertical displacements are upwards. Positive cross section rotations and change in specimen orientation are counterclockwise in the picture shown (ie with the cross section of the T4 to the right of the T5).

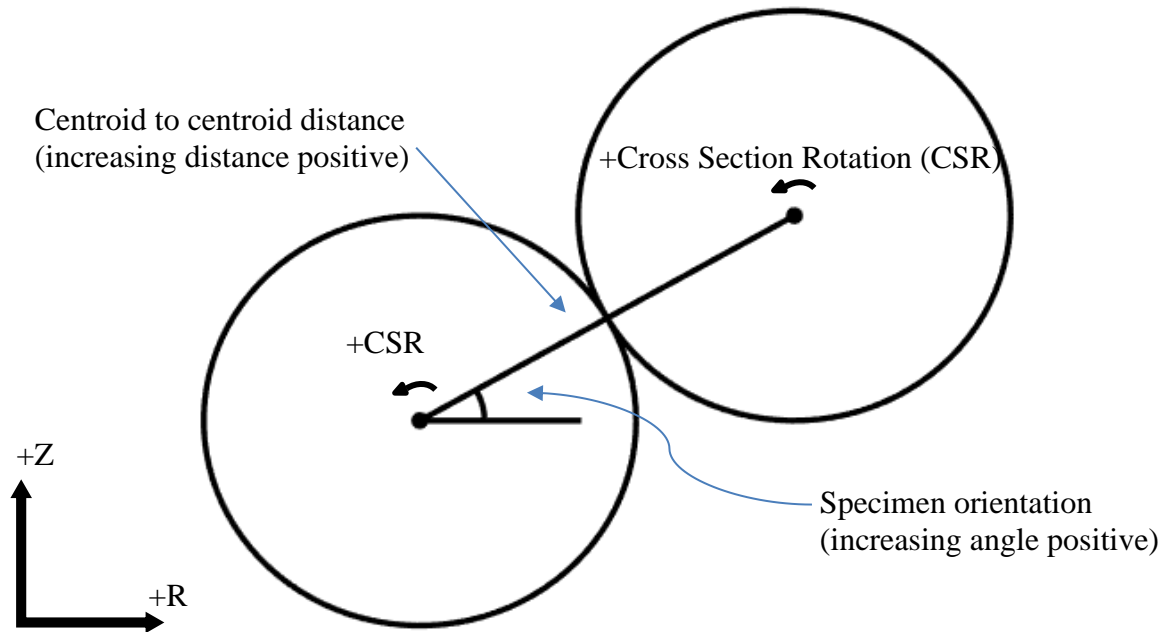


Figure 43. Specimen cross section

4.3.2.1 Initial Shape

The nominal specimen consists of two perfectly circular and horizontal tori with a specimen orientation of 30 degrees. The tori radii and heights in the actual specimen are not constant and also vary with pressure as can be seen in the figures below.

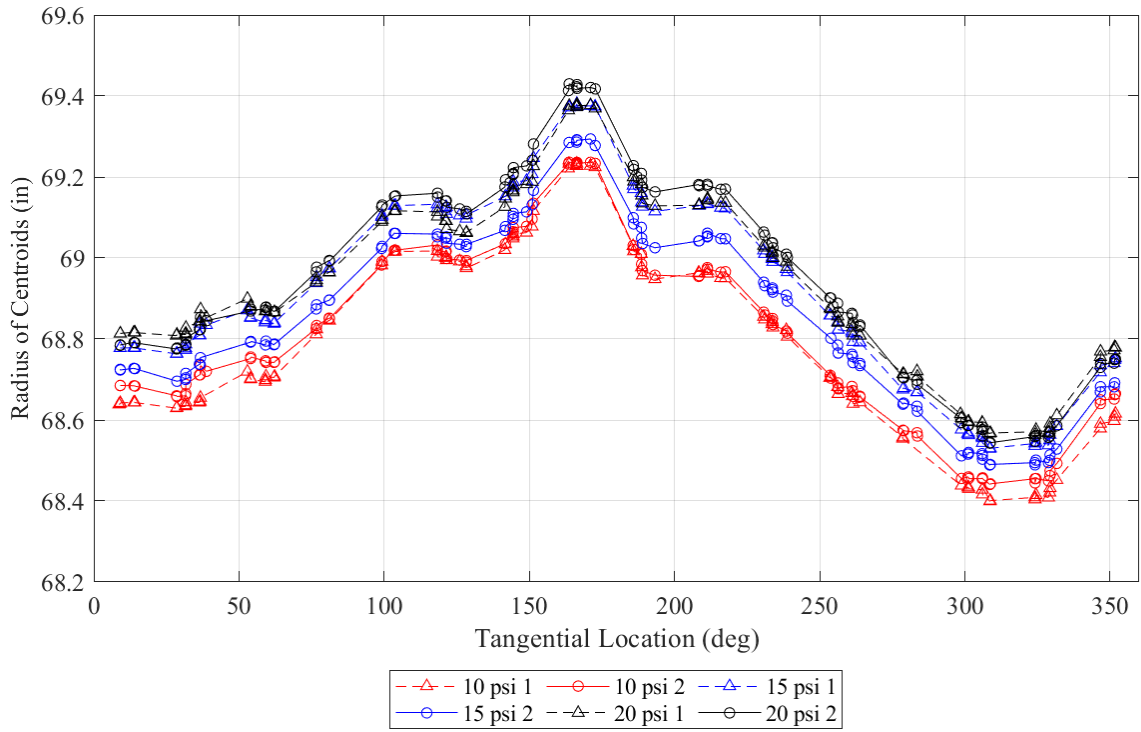


Figure 44. Initial radial locations of T4 centroids

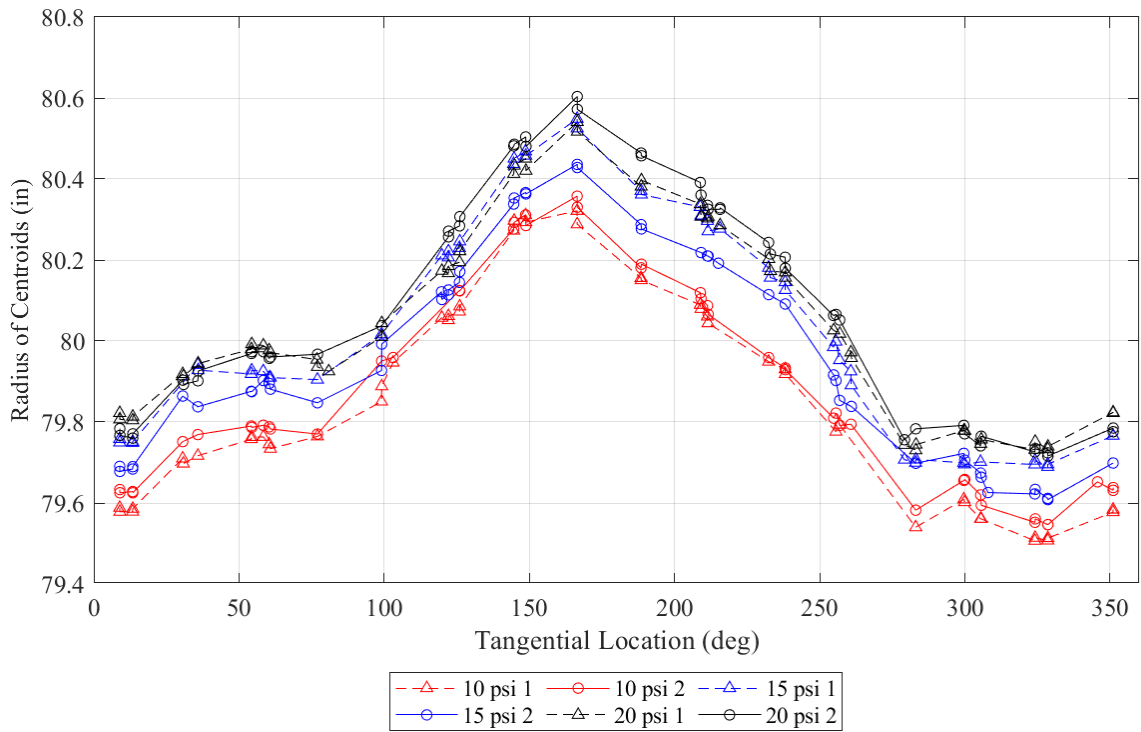


Figure 45. Initial radial locations of T5 centroids

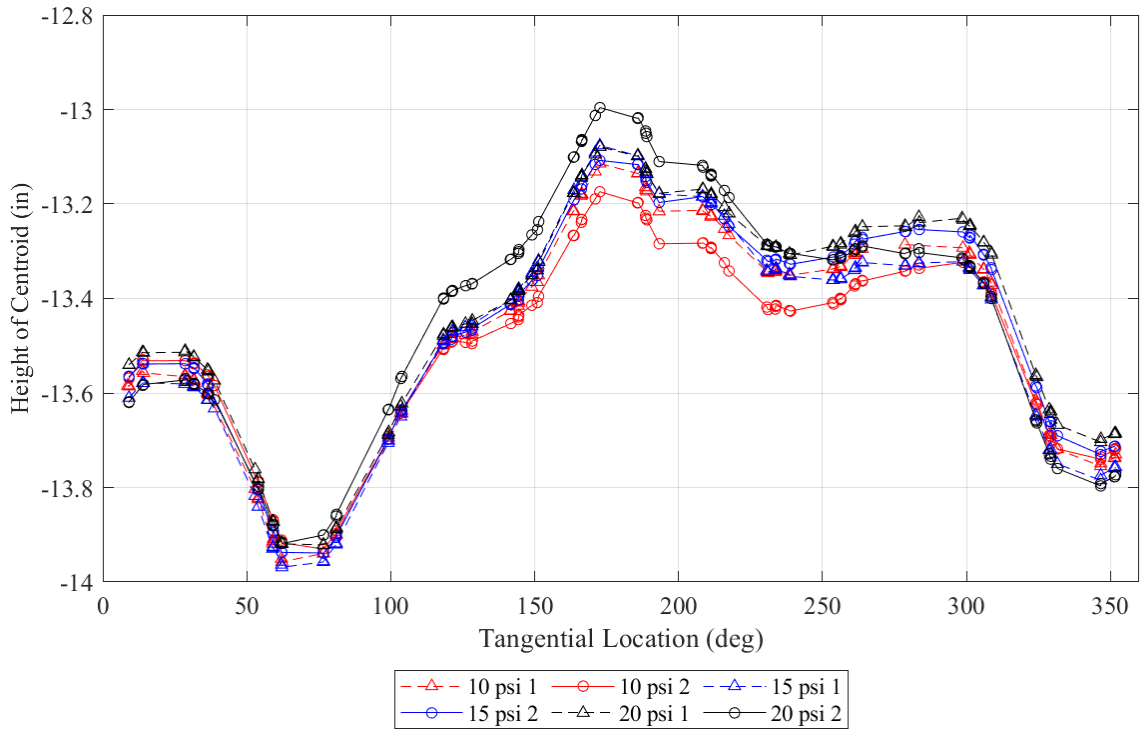


Figure 46. Initial vertical locations of T4 centroids

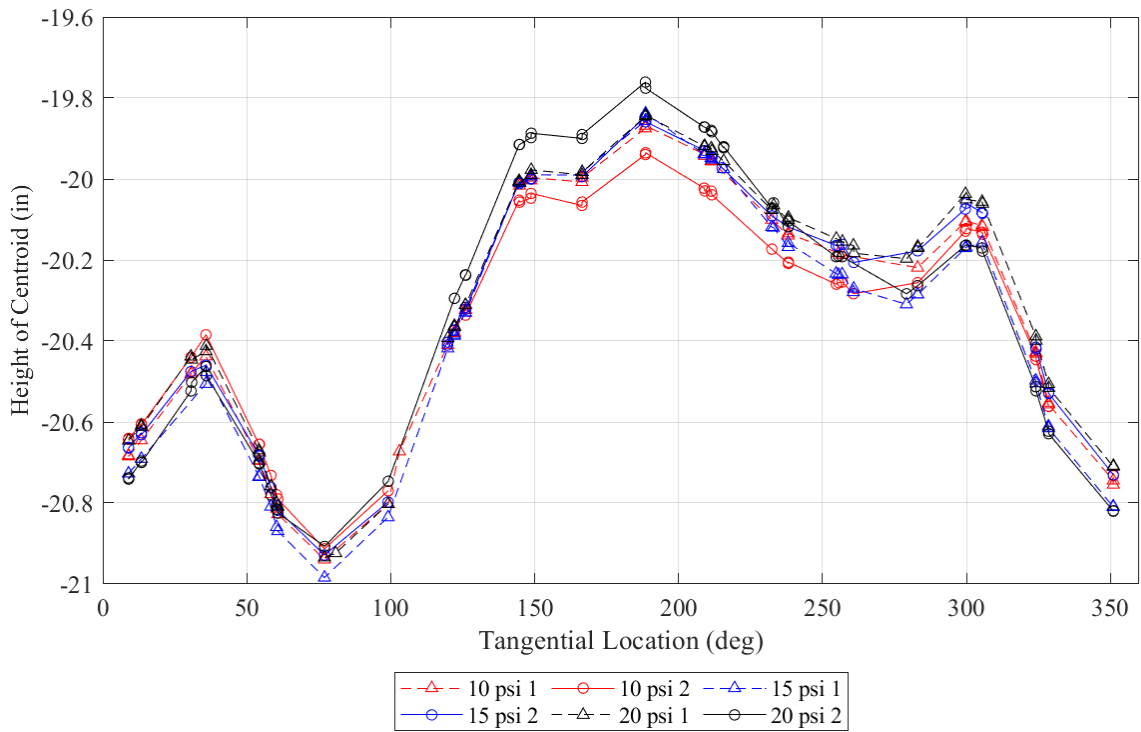


Figure 47. Initial vertical locations of T5 centroids

Figure 44 - Figure 47 above show the starting radial and vertical locations of the T4 and T5. The radius and height for the T4 and T5 vary with respect to tangential location in similar ways, by about an inch. This makes sense because they are strapped together. Tori with geometric imperfections are not as strong as those whose centroids lie on a horizontal circle but because these tori are paired together this may not have much of an effect.

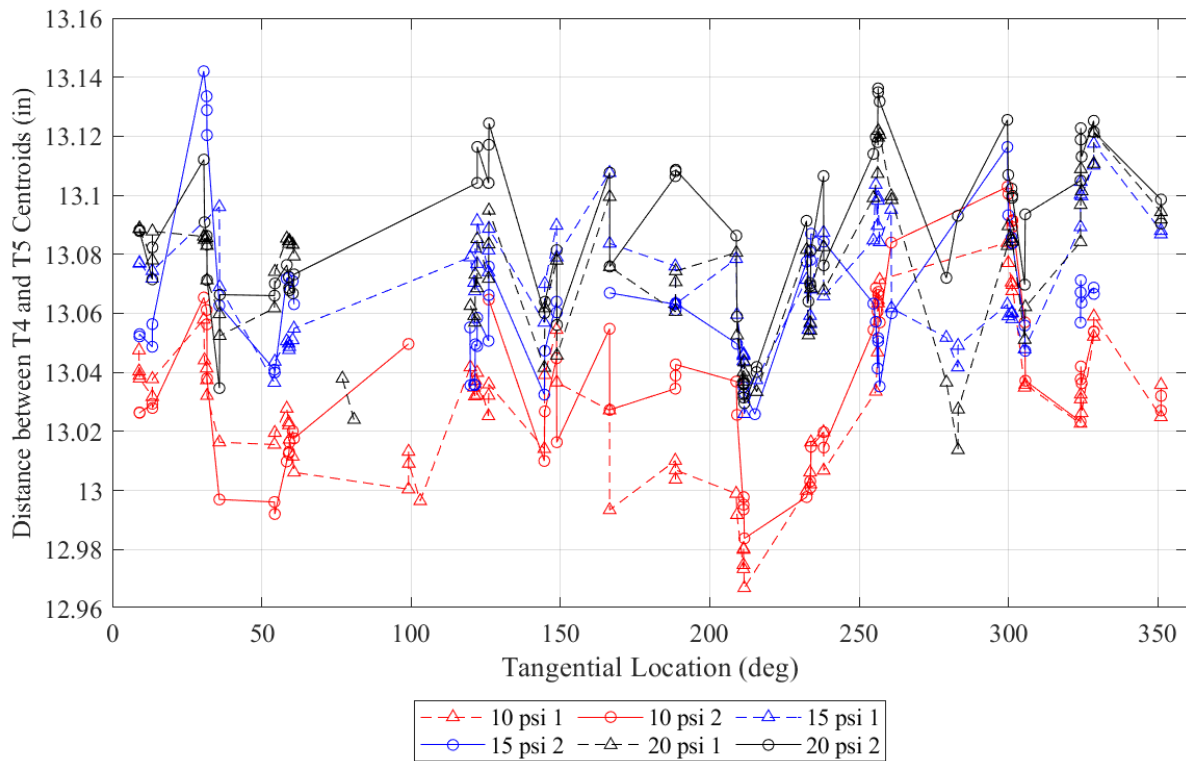


Figure 48. Initial distances between corresponding T4 and T5 centroids

Figure 48 shows that there is not much variation of the distance between the tori centroids with respect to tangential location or pressure. This suggests the pairing loops holding the tori together keep them in a constant position relative to each other. The average centroid distance is 13.06 inches. The minor radii of the uncompressed torus cross sections are 6.7 inches, which means to just barely be in contact with each other the centroid distance must be 13.4 inches. This suggests the tori are not compressed together significantly.

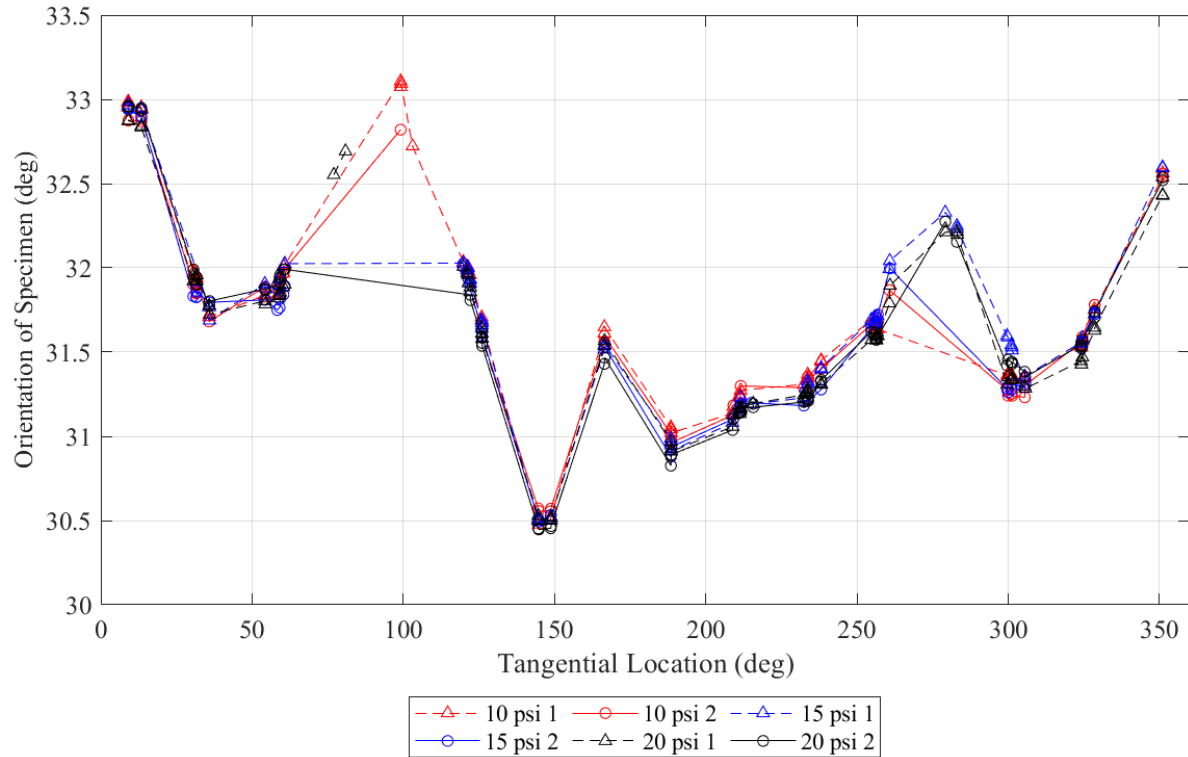


Figure 49. Initial specimen orientation

Figure 49 shows the variation in specimen orientation with respect to tangential location. This plot suggests specimen orientation does not vary with pressure, likely because the pairing loops fix the specimen orientation. The variation with respect to tangential location is most likely a result of variations in the individual tori geometry.

4.3.2.2 Displacement of Specimen

Figure 50 through Figure 57 show average displacements versus total applied load. The averages were calculated by the method described in 3.1.5 . Underneath each plot of torus averages, the section averages at final load are shown. Breaks in the lines of these plots mean there was no centroid data for a section. Raw centroid data at final load are shown in APPENDIX F.

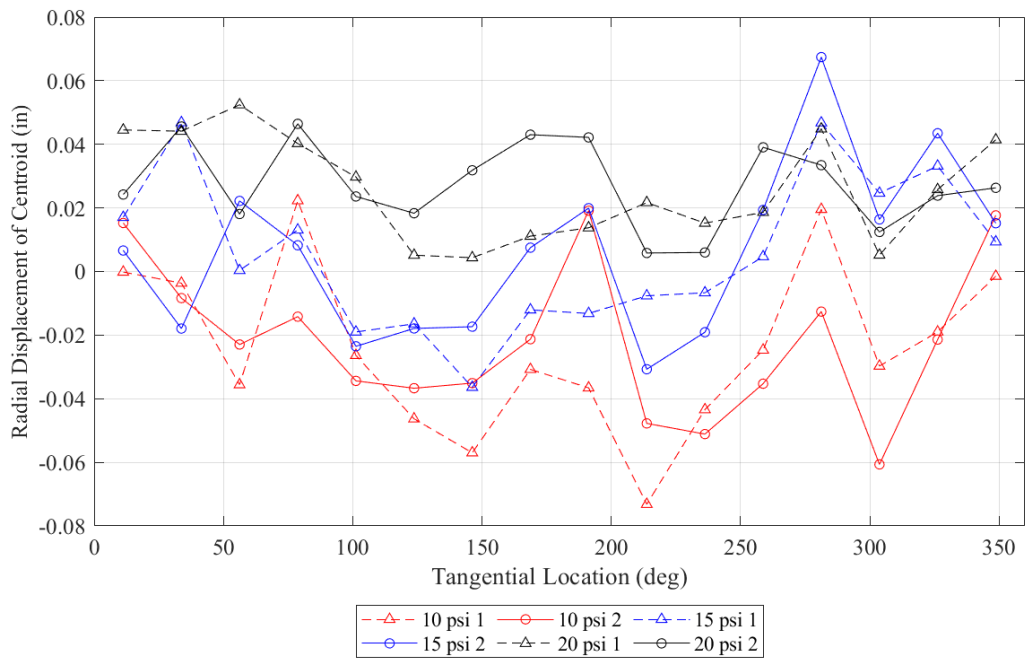
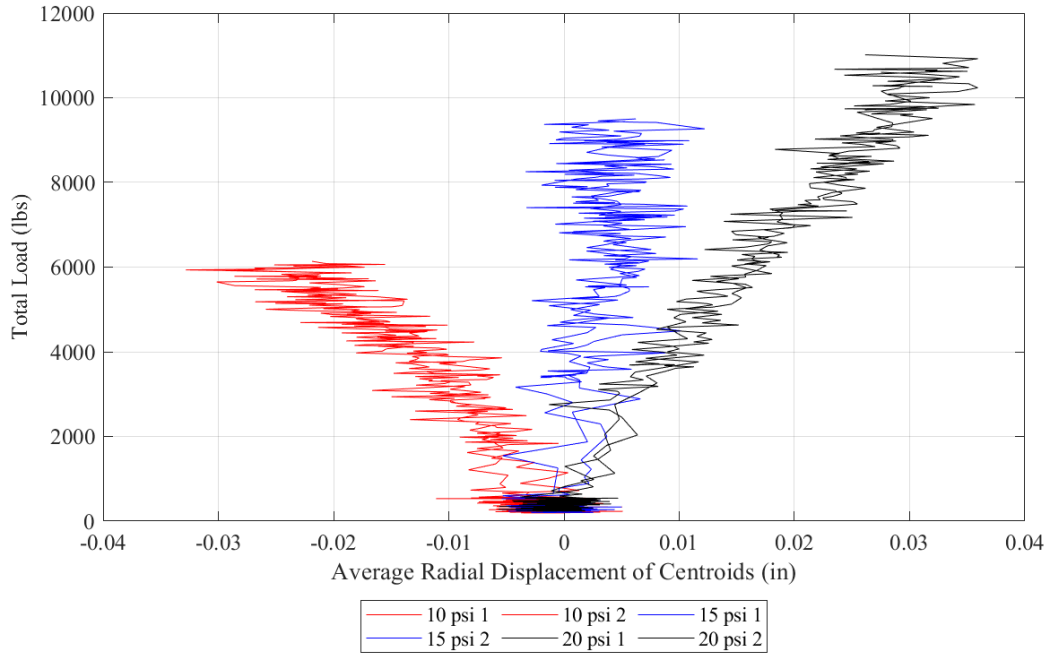


Figure 50. Radial displacement of T4

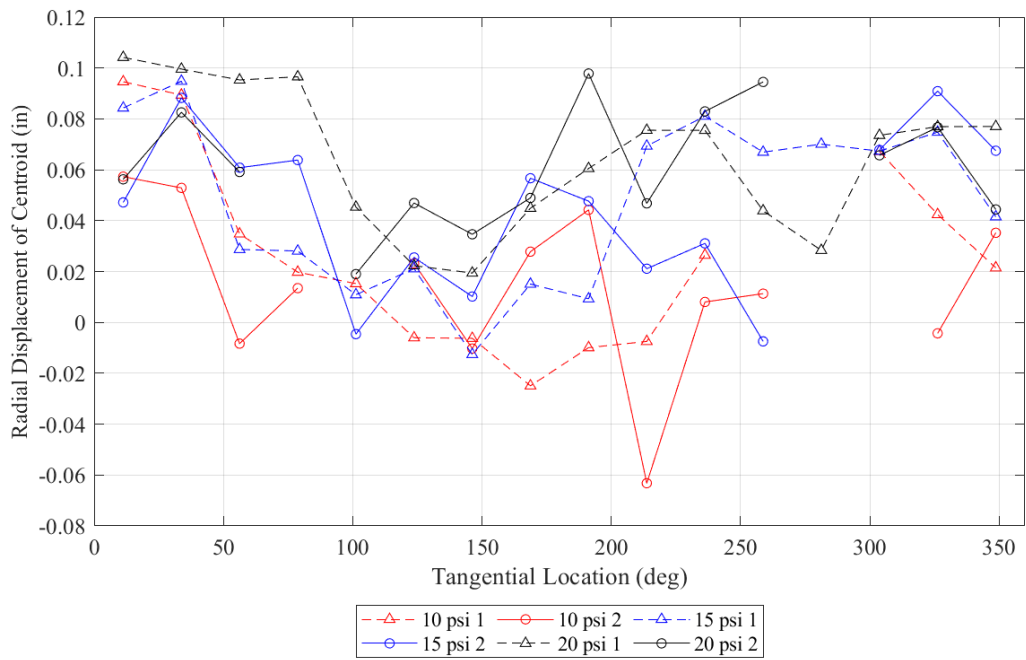
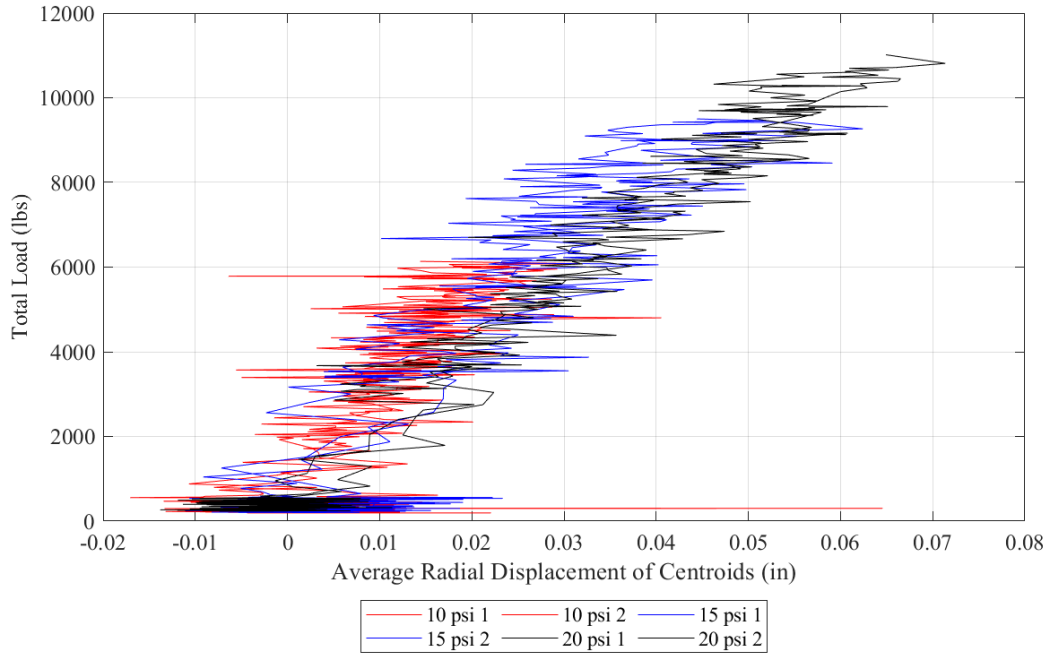


Figure 51. Radial displacement of T5

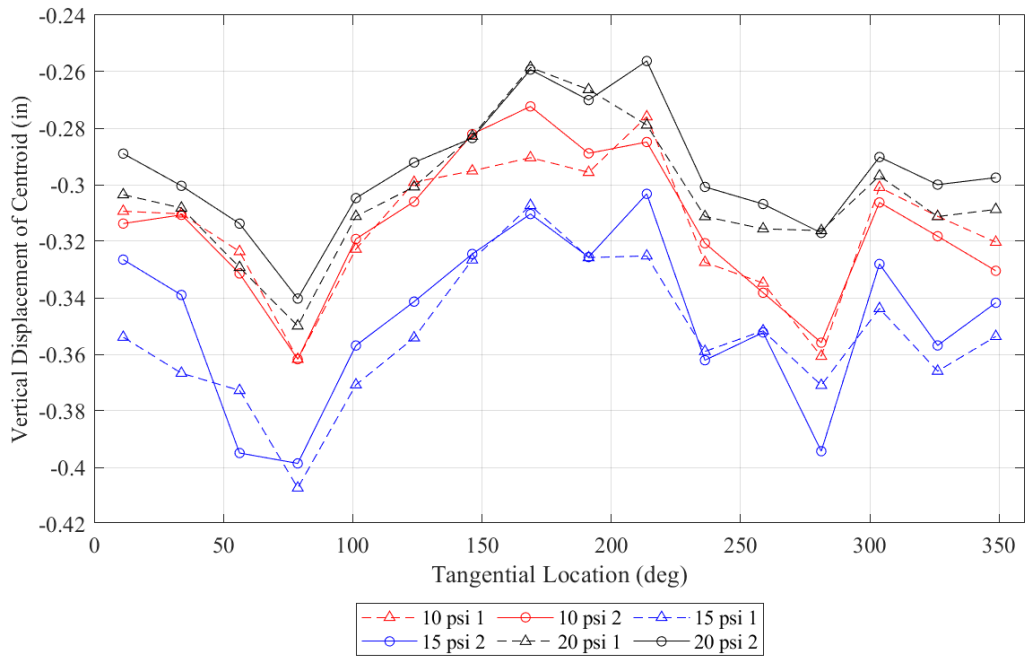
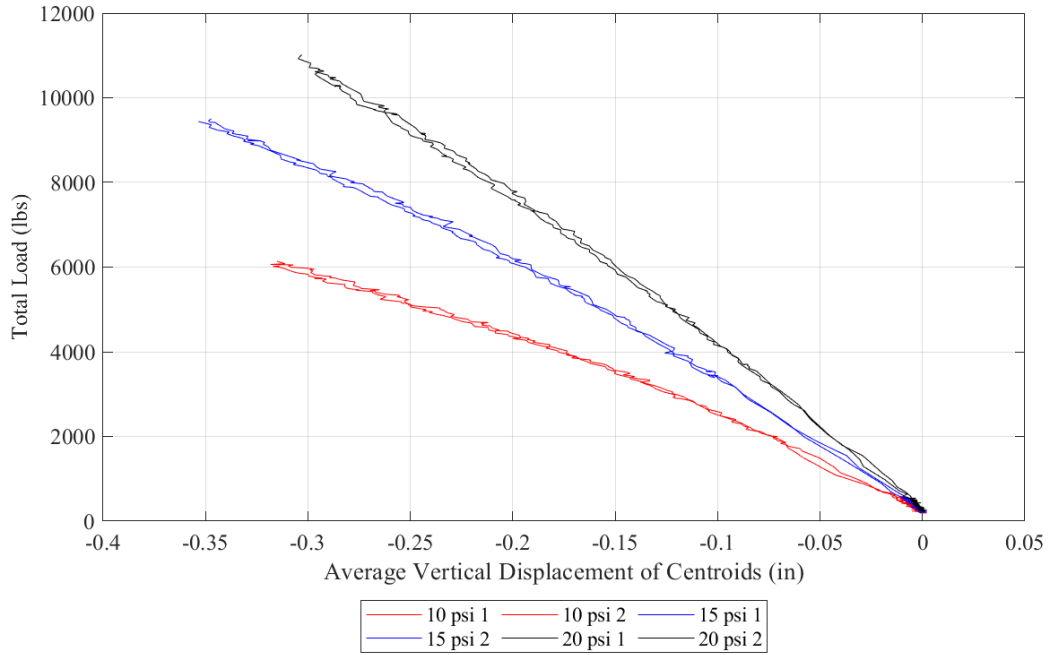


Figure 52. Vertical displacement of T4

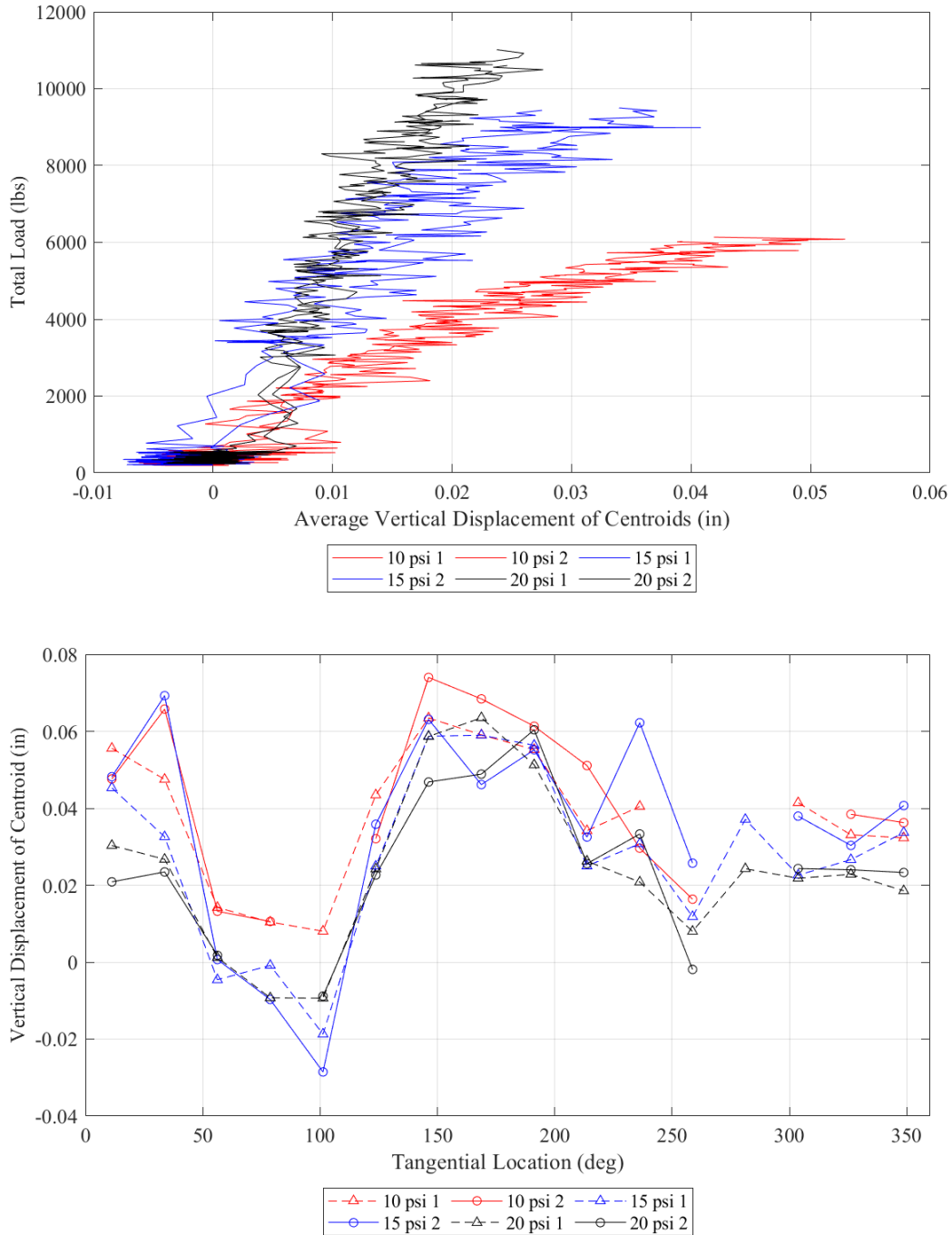


Figure 53. Vertical displacement of the T5

As can be seen in Figure 50 and Figure 51 depicting radial displacement, neither torus compresses much radially, indicating a high degree of stiffness. Based on the 20 psi test, the T5 moved radially inward only about 0.07 inches for a total applied load of 11,000 lbs, and the T4

moved inward even less. This implies a radial stiffness measure of 11,000 lb/0.07 inches = 157,000 lb/inch. In contrast, when subjected to 16 load points, the individual T4 and T5 exhibited radial stiffness of about 45,300 lb/inch and 39,700 lb/inch, respectively. Clearly, the sum of the stiffnesses of the individual T4 and T5 are much less than the total stiffness of the paired tori. This indicates that the paired T4 and T5 are much more structurally efficient, and that the pairing loops are effective at connecting the two tori.

At 10 psi, the T4 displaces outwards, despite the load strap pulling the opposite direction. Though the displacements are small enough that the error in the PONTOS data could have an effect, considering where the load strap contacts the T4, it is also possible that the force resultants from the load straps on the upper torus are outwards radially. This means that the T4 is compressing into the T5 more radially at lower pressures, which suggests it is also possibly restraining the T5 more in the radial direction. This could help explain why there is very little pressure dependence of the radial displacement of the T5; though it gets stiffer with increasing internal pressure, it is also potentially supported less by the T4.

As shown in Figure 52, the T4 displaces downwards significantly. Correspondingly, Figure 53 suggests that T5 moves slightly upwards, although displacement is small enough that the error in the PONTOS data could have a significant impact. It is also possible that the force resultants from the load straps on the T5 are slightly upwards. Taken together, these results indicate that the T4 is being pulled inward and is rotating down over the T5.

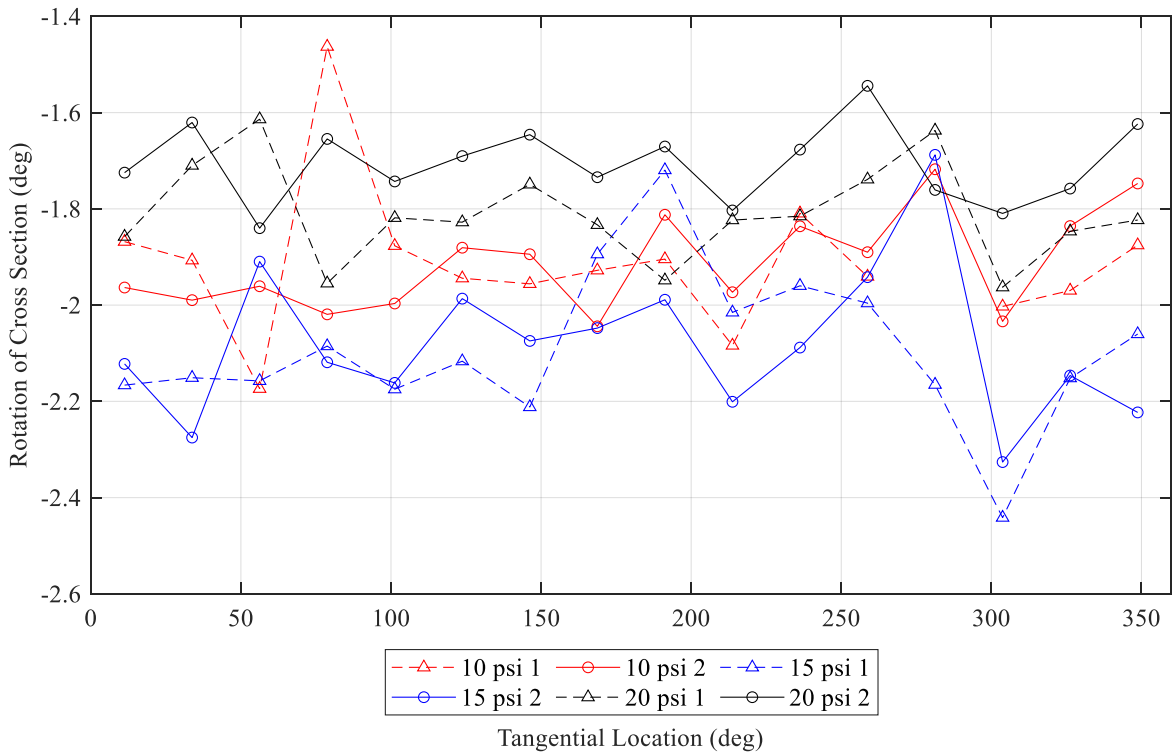
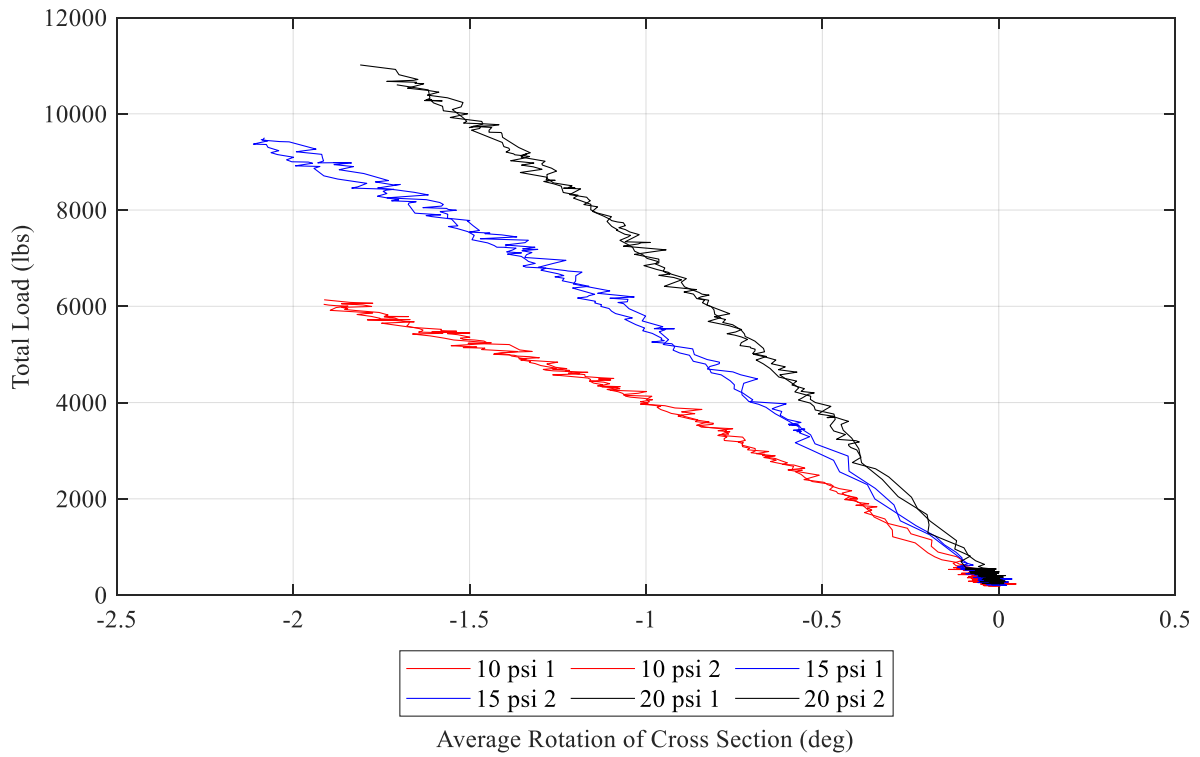


Figure 54. Rotation of the T4 cross section

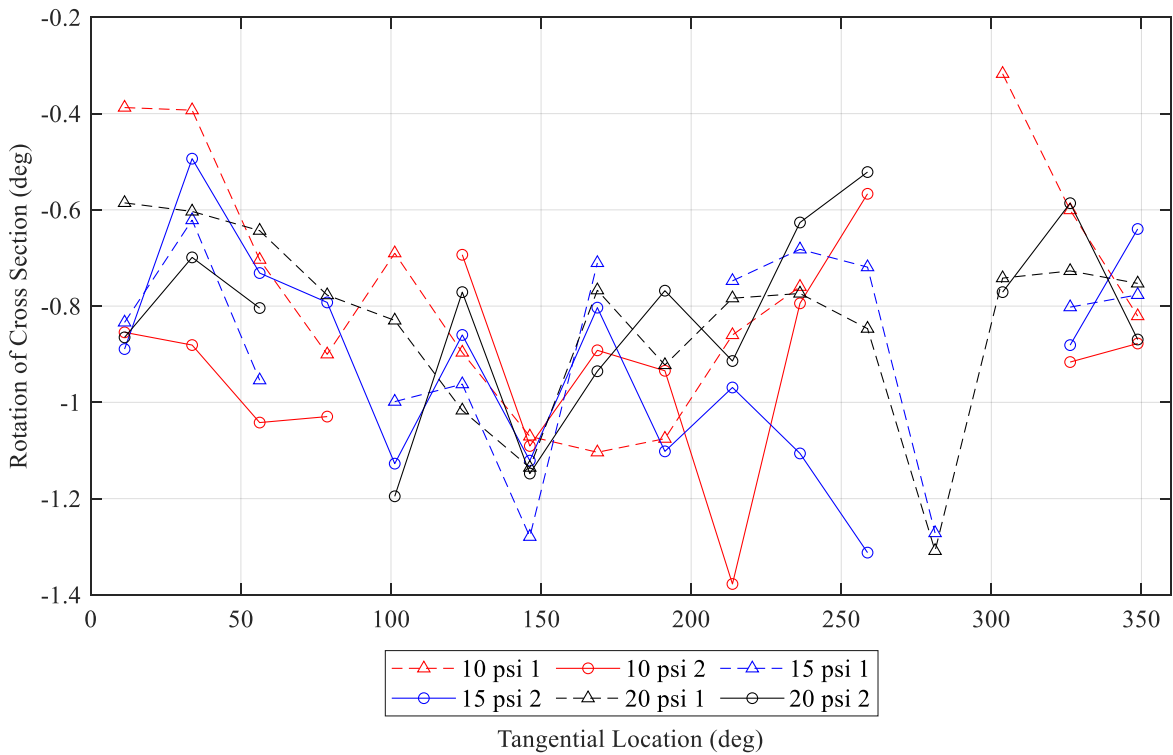
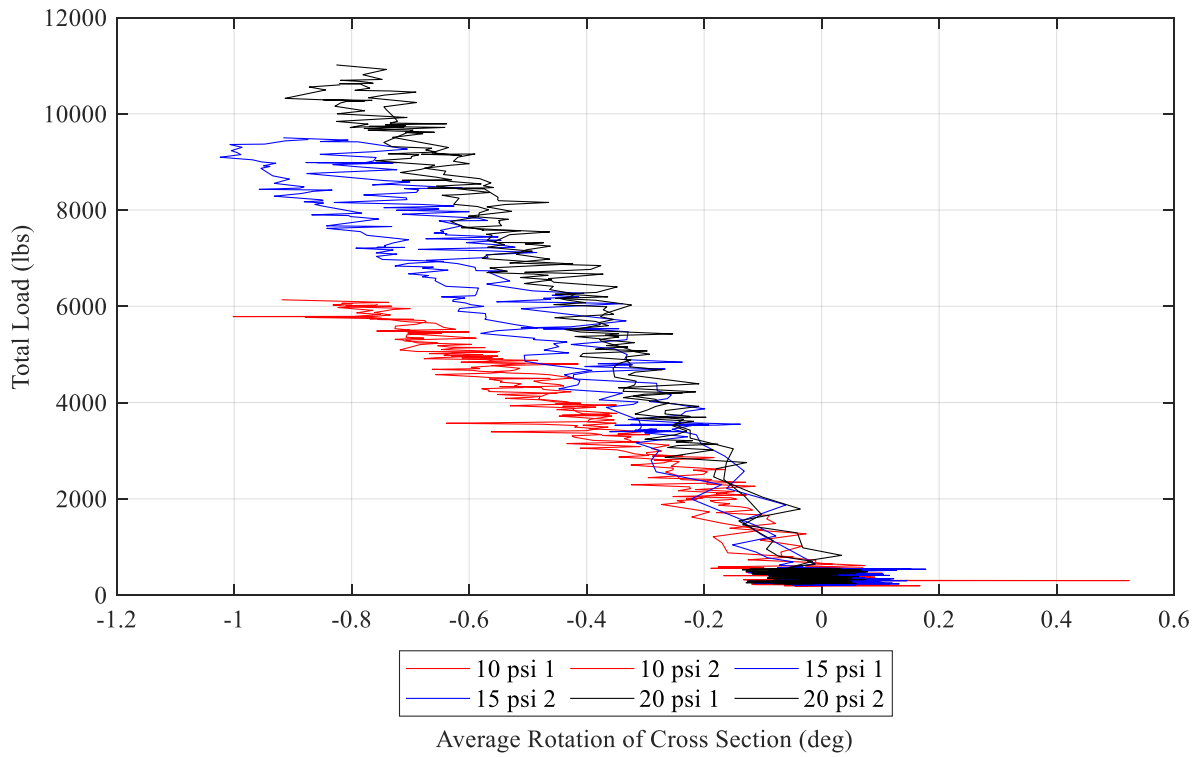


Figure 55. Rotation of T5 cross section

As can be seen in Figure 54 and Figure 55, both tori rotate about their centroids, and the rotation of the T4 is about twice that of the T5. This rotation could be caused by unintended friction between the load saddles and the specimen, which could produce differential loads in the strap ends and the transfer of torque from the saddles to the tori. Another possible explanation is that the load straps deform the cross section of the tori so that it is no longer perfectly circular. The resultant force on each torus is no longer guaranteed to go through the shear center (centroid) of the torus and could therefore impart some torque. In the case of the T4, this rotation corresponds to significant displacement of the outside of the cross section (i.e. the PONTOS dots). A rotation of 2 degrees, which is roughly the maximum the T4 experienced, corresponds to a tangential displacement around the minor circumference of 0.23 inches.

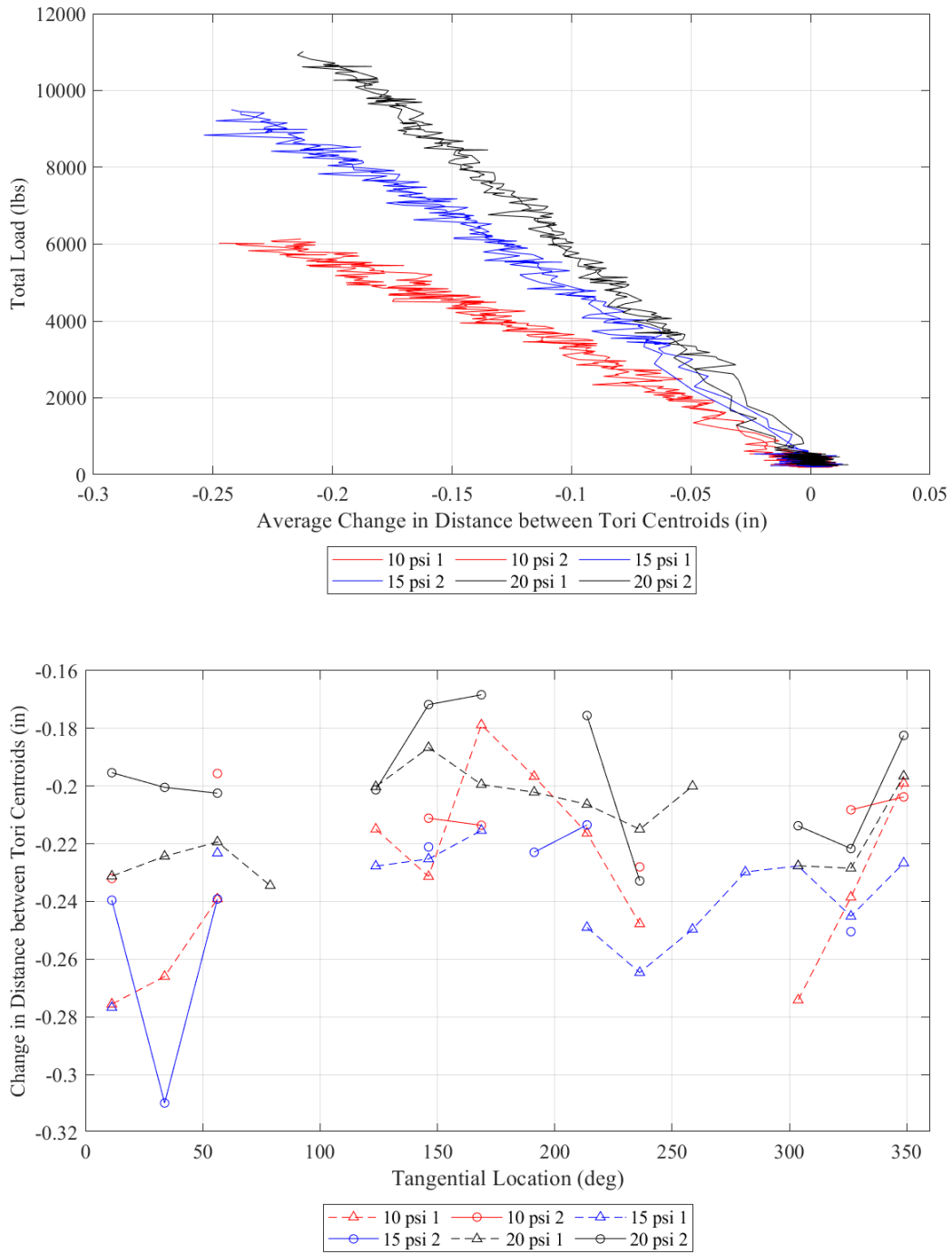


Figure 56. Change in distance between tori centroids

As shown in Figure 56, the tori were compressed together during testing, and the amount of compression decreased with increasing inflation pressure as expected.

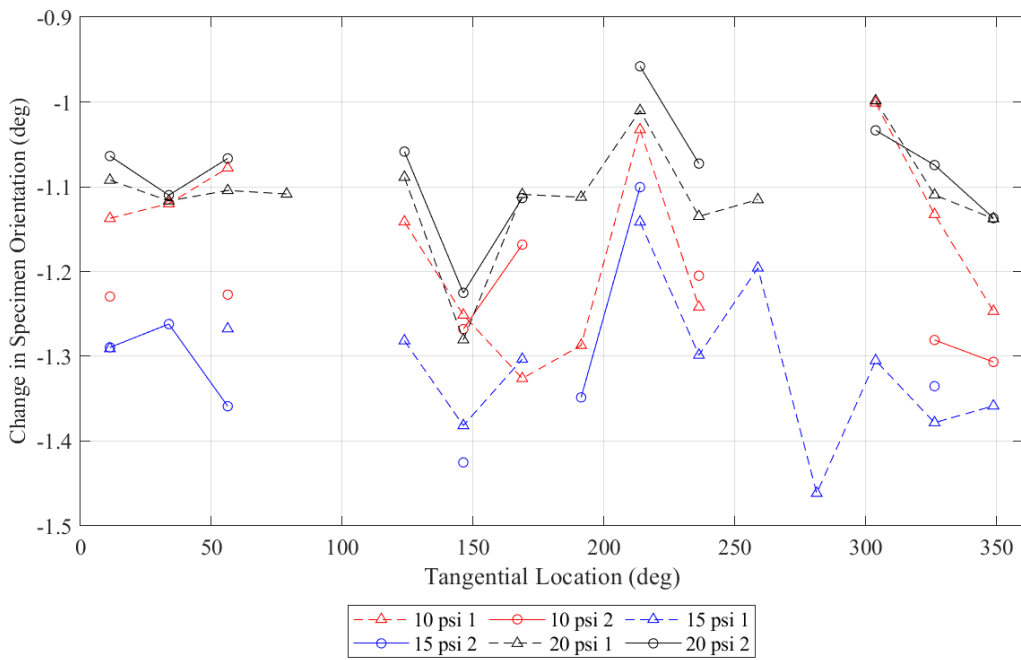
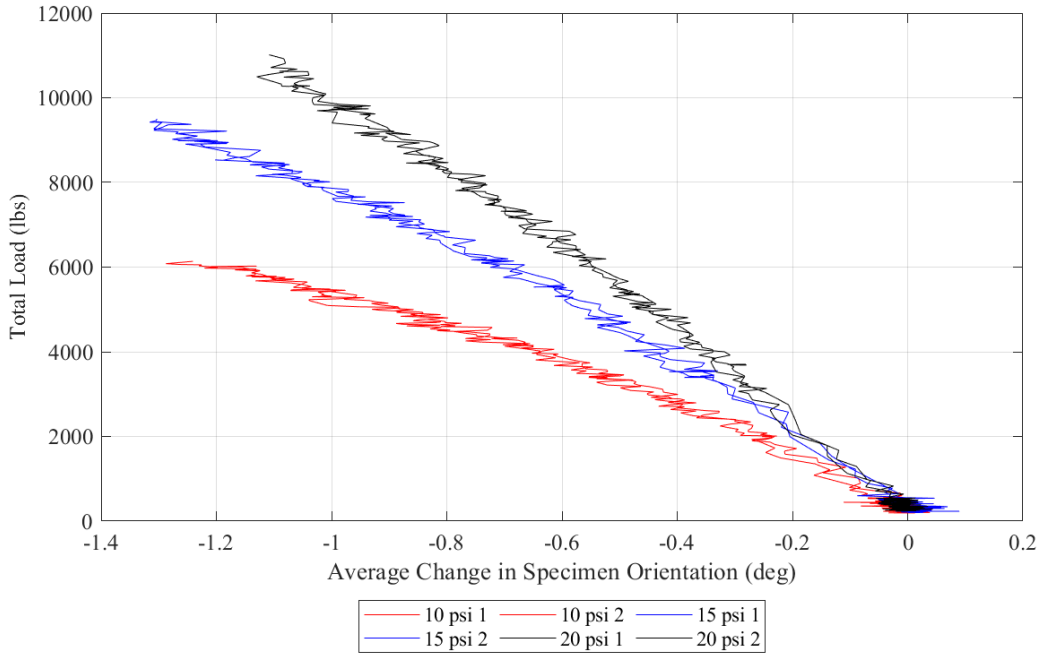


Figure 57. Change in specimen orientation

Most of the displacement of the specimen comes from the T4 translating downwards and rotating inwards. The net effect of this movement was the tori were compressed together and the angle of specimen orientation was slightly reduced. This deformation mode was not anticipated, and the

original aim of the testing was to displace both tori radially inward. However, because of space constraints of the test setup, the loading method had to change from a strap with a spreader beam to just a strap, which made downwards force on the T4 unavoidable.

Also looking at Figure 50 through Figure 57, average section displacements varied with respect to tangential location. This is most likely due to the variation in cable loads; however, the imperfections of the torus geometry and variations in orientation of load cables could also have an impact. One important observation, however, is that increasing pressure increased the load the specimen could withstand at a given displacement. Further, the results show that the pair of tori are significantly stiffer than the sum of the stiffness of an individual T4 and T5.

4.4 Summary

A specimen consisting of two tori strapped together was tested using similar methods as those discussed in Chapter 3. Both the collection of quality photogrammetry data and the control of the test was more difficult for the paired specimen compared to the singles. The testing resulted in an unexpected mode of deformation where the upper torus rotated up and over the lower torus, while both tori were compressed together. Chapter 5 details the modeling of the paired specimen tests discussed here.

CHAPTER 5 MODELING OF PAIRED TORUS TESTING

This chapter details the modeling performed of the paired torus testing discussed in Chapter 4. This was done using a modified version of the beam-based finite element model discussed by Young, (2017, 2017a, 2017b, 2018). The tori are modeled with “flexibility-based fiber beam elements” that capture both pressure and shear effects (Young, 2017b). The model is constrained using linear and bilinear springs (Young, 2017b). The straps were modeled using test data and connected to the tori via rigid links (Young, 2018).

For the current research, the properties of some of the elements were modified. Three analyses were run corresponding to the three internal specimen pressures of 10, 15 and 20 psi. Like during testing, there was a load-controlled preload phase and a displacement controlled second phase. The results were then compared to those collected during testing. These modeling results are preliminary, as the scope of the modeling in this project was very limited. Please see Figure 10 and Figure 43 for information on terminology and the cylindrical coordinate system referred to throughout this chapter.

5.1 Element Properties

The model consists of five types of elements torus, strap (both pairing loops and load straps), link (strap to torus), interaction (torus to torus) and boundary. See Figure 58 for a plot of the model.

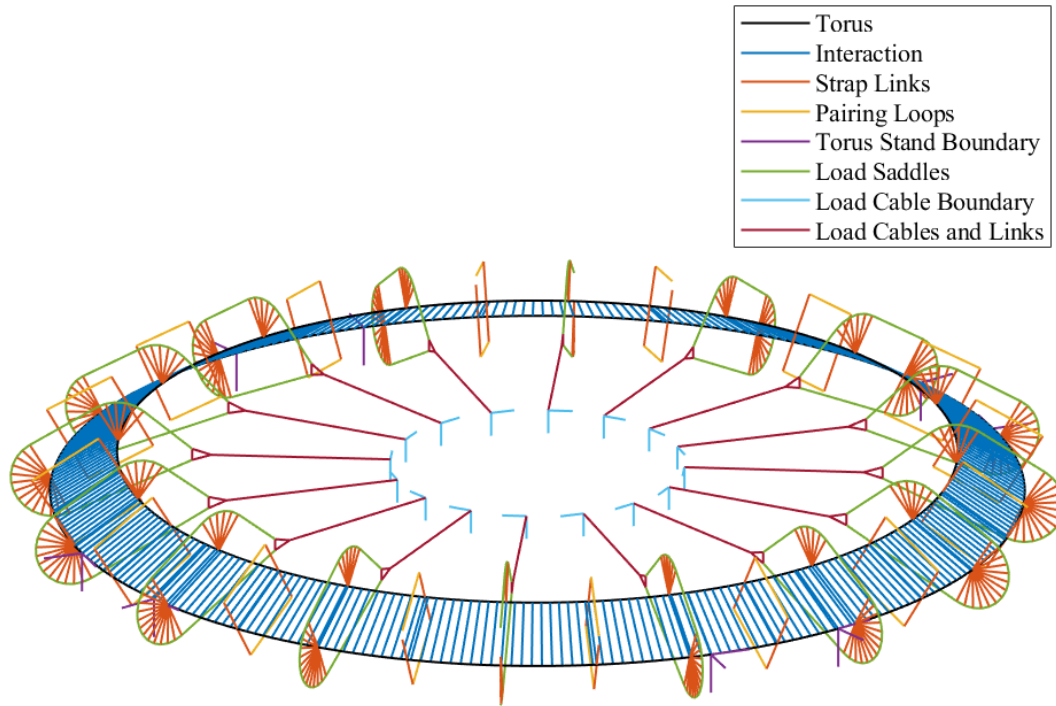


Figure 58. Model

5.1.1 Torus elements

The torus elements were “three-dimensional, corotational, flexibility-based beam elements” detailed in Young, (2017, 2017a, 2017b and 2018). These are straight beam elements located at the centroidal axes of both tori. 300 elements were used to approximate the circular shape of each torus and the nodes lay on a horizontal perfect circle of the specimen’s nominal radius. Like the real specimens, they had a 71 degree braid angle and two reinforcing cords on the inner half of the cross section at +/- 60 degrees from horizontal. The gross axial stiffness of the shell and the shear stiffness of the shell are all pressure dependent. The properties used are the same as those used for Technora in Young, (2017a and 2017b) and are derived from netting theory and testing detailed by Clapp (2016a and 2016b). They are shown in Table 3 below.

Table 3. Properties of torus shell

Pressure (psi)	E_{gross} (lb/in)	G_{LH} (lb/in)
10	103	1830
15	114	2400
20	131	2670

The cords integrated into the shell were nonlinear in tension and hysteretic, meaning they have different loading and unloading curves. The force-strain relationship is preprogrammed for each cord depending on where it is on the cross section, i.e. whether it will be loading or unloading during the analysis (Young, 2017a).

5.1.2 Interaction Elements

The interaction elements connect T4 to T5 nodes at the same tangential location and simulate the contact between tori. The axial stiffness of the interaction elements was determined from testing performed at Fort Lewis College led by Dr. Andrew Young. He found the stiffness, K_{ax} , varied linearly with specimen pressure, p , by the relationship shown in Equation 2.

$$K_{ax} = 1.97 * p + 8.16 \quad \text{Equation 2}$$

The bending stiffness of the interaction elements in the global radial direction was kept the same as in (Young, 2017). The bending stiffness in the global tangential direction was estimated by Dr. Young by considering a new model of a straight tube of length l , fixed at the bottom as shown in Figure 59.

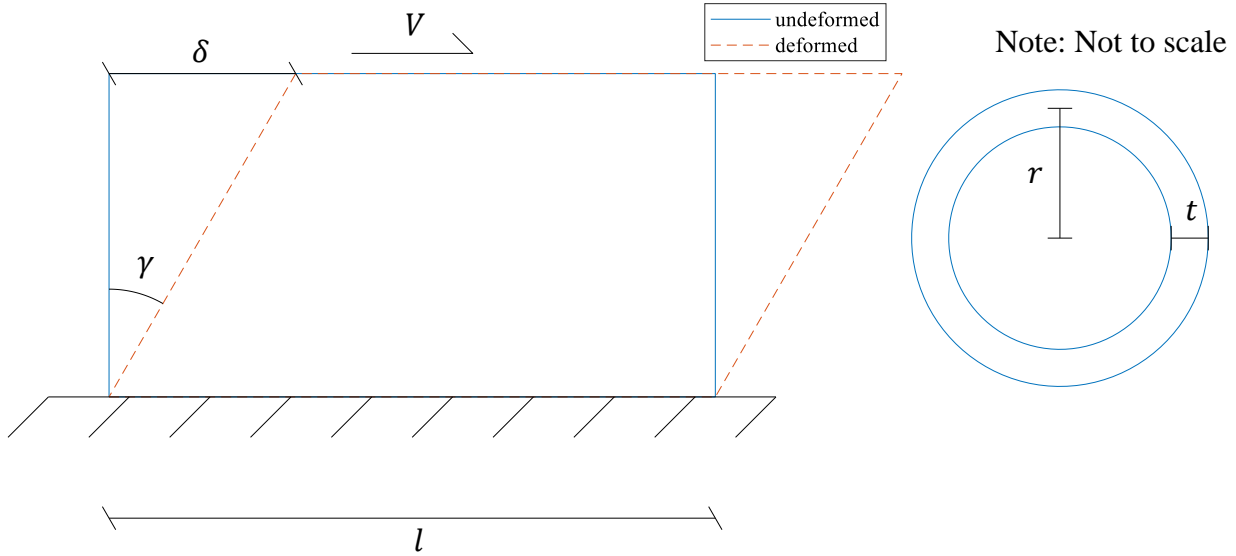


Figure 59. Illustration of interaction element bending stiffness problem

Assuming the shell is linear elastic the shear stress, τ , is given in Equation 3.

$$\tau = G * \gamma \quad \text{Equation 3}$$

G is shear modulus and γ is shear strain. Equation 4 is obtained by substituting the membrane shear modulus $G_{LH} = G * t$ in Equation 3 and using the fact that pure shear stress is shear force, V , divided by cross sectional area, which is approximated as $2lt$.

$$\tau = \frac{G_{LH} * \gamma}{t} = \frac{V}{2lt} \quad \text{Equation 4}$$

Equation 5 is obtained by solving Equation 4 for γ .

$$\gamma = \frac{V}{2lG_{LH}} \quad \text{Equation 5}$$

Assuming the length of tube in shear is half the circumference of the cross section, shear strain can be expressed as in Equation 6.

$$\tan \gamma = \frac{\delta}{\pi r} \quad \text{Equation 6}$$

Using the small angle approximation and substituting Equation 5 for γ , δ can be calculated by Equation 7.

$$\delta = \pi r * \frac{V}{2lG_{LH}} \quad \text{Equation 7}$$

The shear stiffness is given in Equation 8. The length l , was taken as a unit length such that the stiffness could be scaled depending of torus element length.

$$k = \frac{V}{\delta} = \frac{2lG_{LH}}{\pi r} \quad \text{Equation 8}$$

The moment of inertia of the interaction elements in the tangential directions was calculated from the stiffness by examining a cantilever beam in series, as described in (Young, 2017).

5.1.3 Strap Elements

Two types of strap elements were used. The first simulated the pairing loops and had identical properties to the straps discussed in Chapter 5 of Young, 2017. The second type of straps were the loading saddles. Their orientation could not be calculated directly from the nominal geometry, so it was found using PONTOS data from targets on the load cables.

The load saddles could not be tested to determine their stiffness properties, so these values were estimated. Their bending and compression stiffnesses were set to be very small. The effective strap tension stiffness was determined by a minimization process that captured the cumulative effects of saddle stiffness and local indentation of the torus. During testing, both cable end displacements and loads were measured. Since the model was run in displacement control, the measured cable end displacements were enforced. The sum of the squares of the errors between

measured and modeled cable loads were minimized using the MATLAB built-in function `fminbnd`. The minimization was performed a total of three times for the three different specimen pressures of 10, 15 and 20 psi.

5.1.4 Link elements

In the real specimen, straps wrapped around its minor circumference. Because the torus elements are beam elements, they do not have a cross section and the straps must be connected to the nodes of the torus elements with a third type of element called a link. Two types of link elements were used in the current model. The first type connected the pairing loops to both torus centroids. These links were linear and rigid, which meant they were very stiff relative to the strap and torus elements. This is the same as the link elements used in (Young, 2017b and 2018). The second type of link element connected the load straps to the tori. During testing, parts of the load strap could lift off a torus as the straps slid while the load cables reached their equilibrium height. To simulate this behavior, many link elements with a very low bending stiffness and a bilinear axial force displacement relationship were employed. The links were rigid in compression but had almost zero stiffness in tension and bending. This allowed the straps in the model to slide around the outside of the specimen cross section.

5.1.5 Boundary Elements

The torus stands that supported the specimen were modeled with linear springs in three orientations, radial, tangential, and vertical. Only the two nodes at the edges of each stand were restrained. The vertical springs were stiff, representing the stands supporting the torus. During the test set up, release film was put in between the torus and the stands to make the interface between them as close to frictionless as possible. To simulate this, while also keeping the model stable, radial and tangential springs with low stiffnesses were added.

To ensure stability of the model, the load straps also had to be constrained. Axially stiff elements representing the load cables were connected to the ends of the load straps via rigid triangular links and extended to where the top of the pulleys would be in the test fixture. The free ends of the load cable elements were connected to tangential and vertical springs. The tangential springs were soft and only for stability. During the load controlled preload phase, the vertical springs were stiff, to keep the ends of the load cables at the correct height. Before the displacement controlled phase, the stiffness of the vertical elements was reduced to a very small number because otherwise there was unreasonably high loads in these elements at the end of the simulation. Furthermore, the cable ends were controlled by the prescribed displacements during the second phase and so the stiff vertical springs were unnecessary.

5.2 Comparison to Paired Tori Testing

What follows is a discussion of the results of the modeling compared to the paired torus testing. Figure 60 - Figure 67 show centroid displacements versus tangential location at final load for both the test and the model. Since both tests at each pressure were similar, only the first test at each pressure is shown.

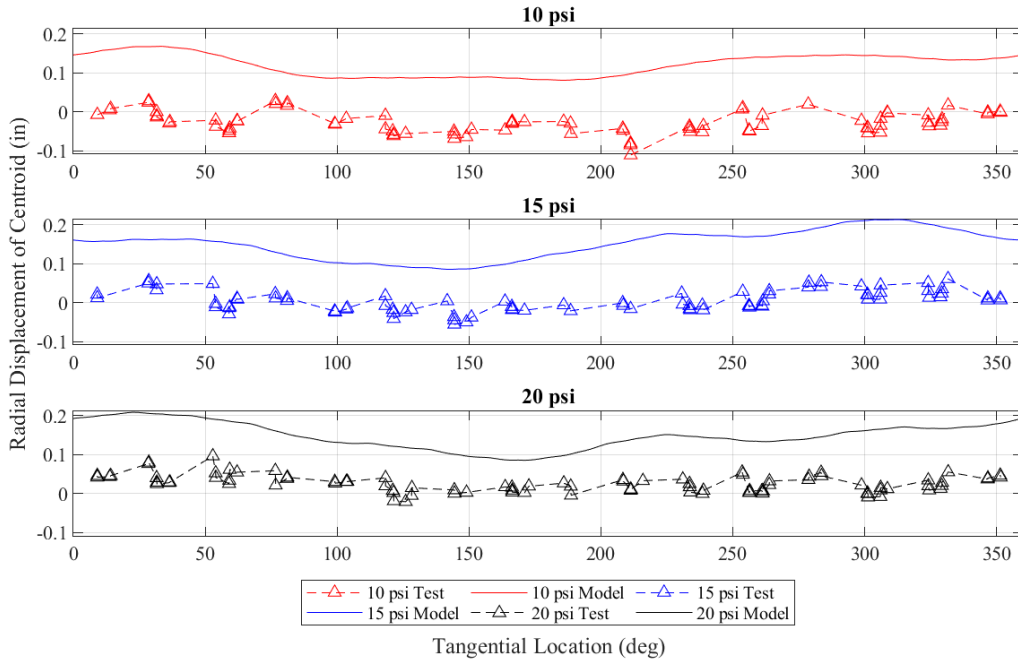


Figure 60. Radial displacement of T4, test and model

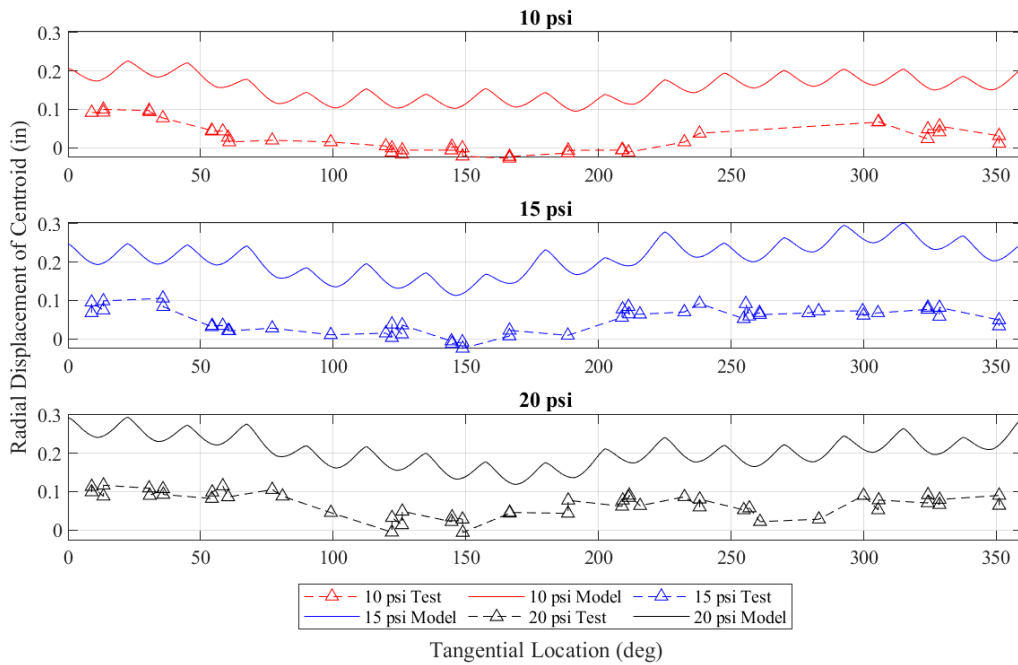


Figure 61. Radial displacement of T5, test and model

The model predicted that both tori displaced radially inwards, with the T5 moving more than the T4 as shown in Figure 60 and Figure 61. This makes sense because the T5 is more flexible than

the T4 and because the load straps transmit more radial force to the T5 than the T4. However, the model-predicted radial displacement much greater than that measured during testing.

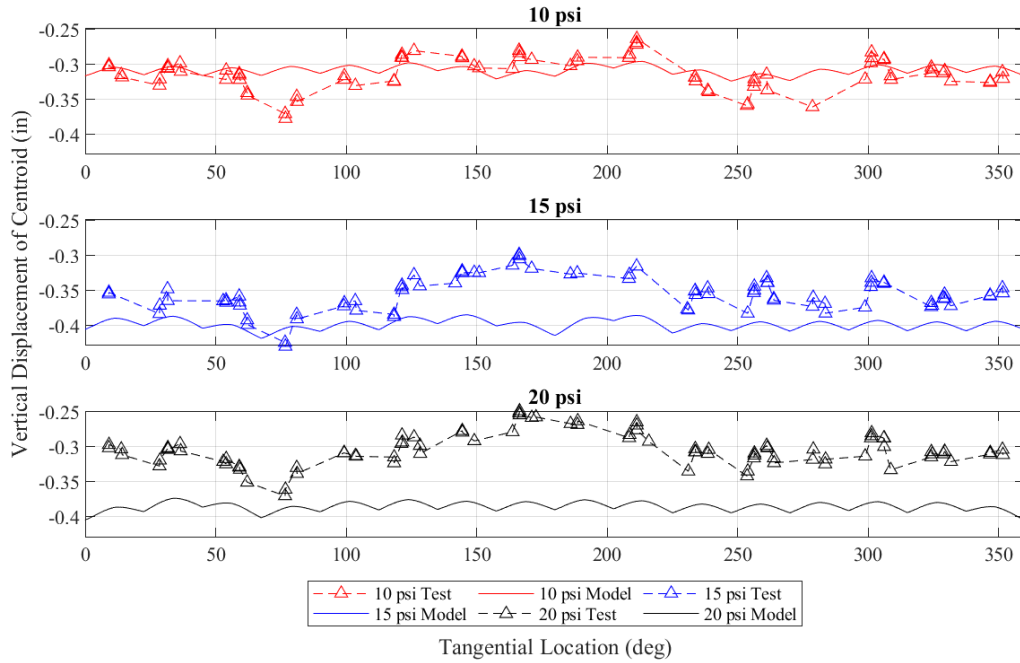


Figure 62. Vertical displacement of T4, test and model

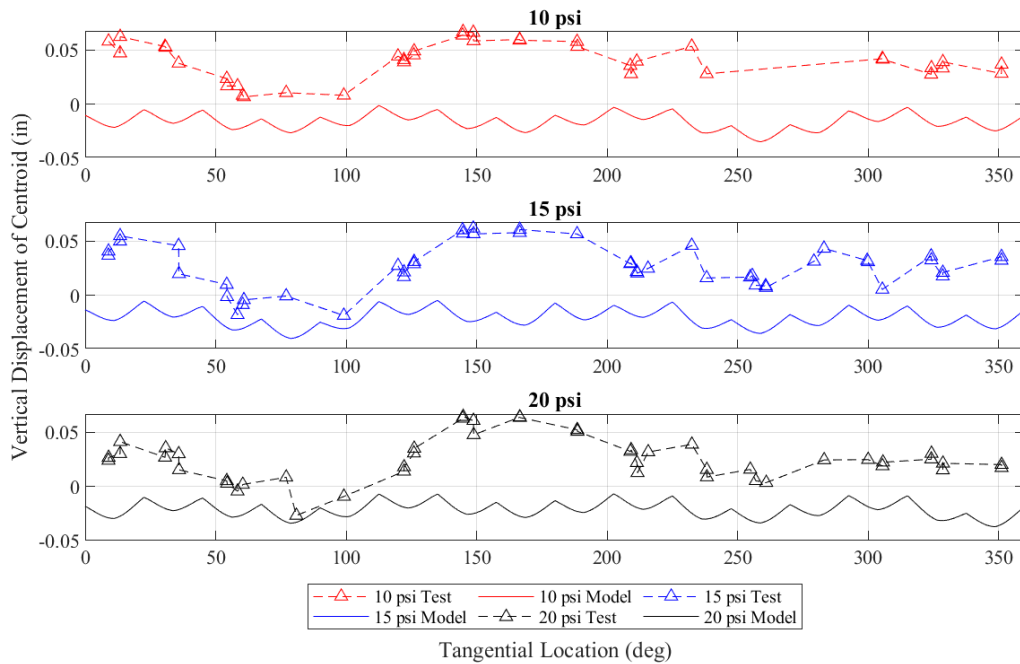


Figure 63. Vertical displacement of T5, test and model

As shown in Figure 62, the model predicts the downward displacement of the T4 at 10 psi well at most locations, but over predicts the downward displacement at 15 and 20 psi. As shown in Figure 63, the model predicts that the T5 moves slightly downwards, whereas during testing the data show it moving slightly upwards. However, it is difficult to draw a definitive conclusion because the vertical displacement of the T5 is so small that the error in the PONTOS data could play a significant role.

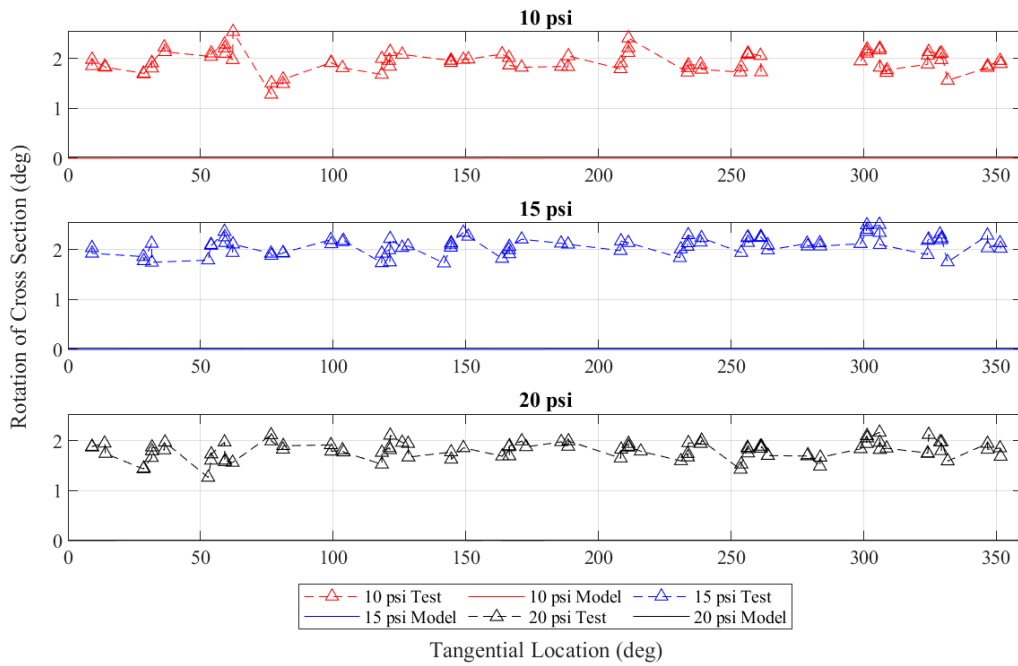


Figure 64. Rotation of T4 cross section, test and model

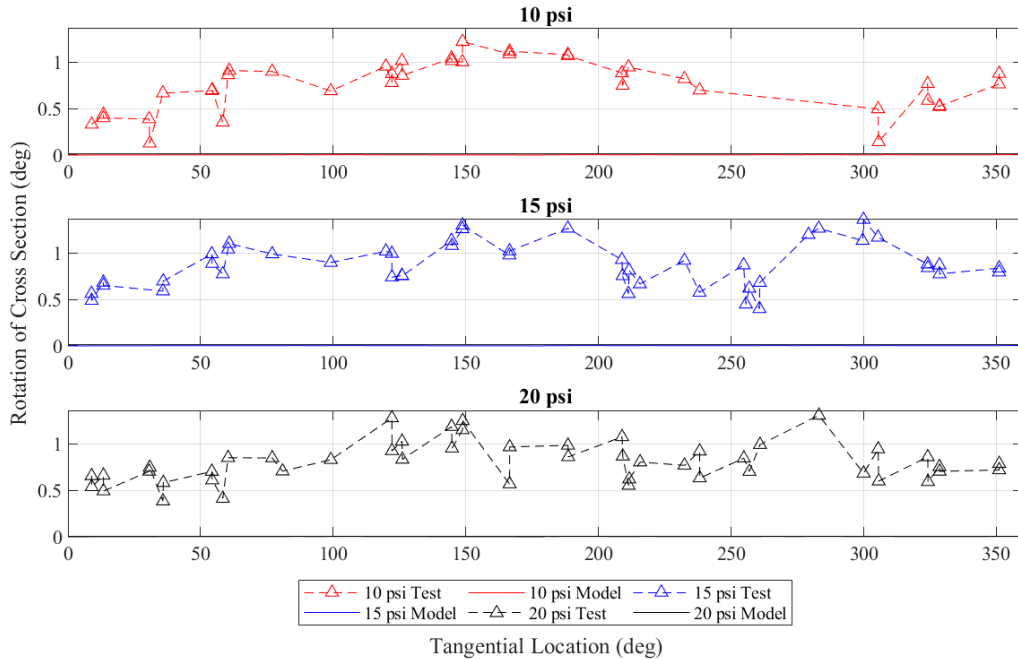


Figure 65. Rotation of T5 cross section, test and model

As shown in Figure 64 and Figure 65, the tori cross sections do not rotate in the model but do rotate significantly during the test. The rotation from testing could be a result of local deformation of the cross section at the load straps either where the straps contact the tori or where the tori contact each other. If the cross section is no longer perfectly circular, this could cause a net torque because the line of action of the force resultants no longer go through the shear center (centroid) of the torus. Currently, the model does not take into account deformation of the cross section, which means all forces on the tori are applied through their shear centers and there is no rotation. This could also help explain the discrepancies in radial and vertical displacement between the test and the model discussed above. Another potential source of torsion is friction between the load saddles and tori. While two layers of release film were sandwiched between each load saddles and torus to minimize shear transfer at the saddle-torus interface, it is possible some shear did develop during the test.

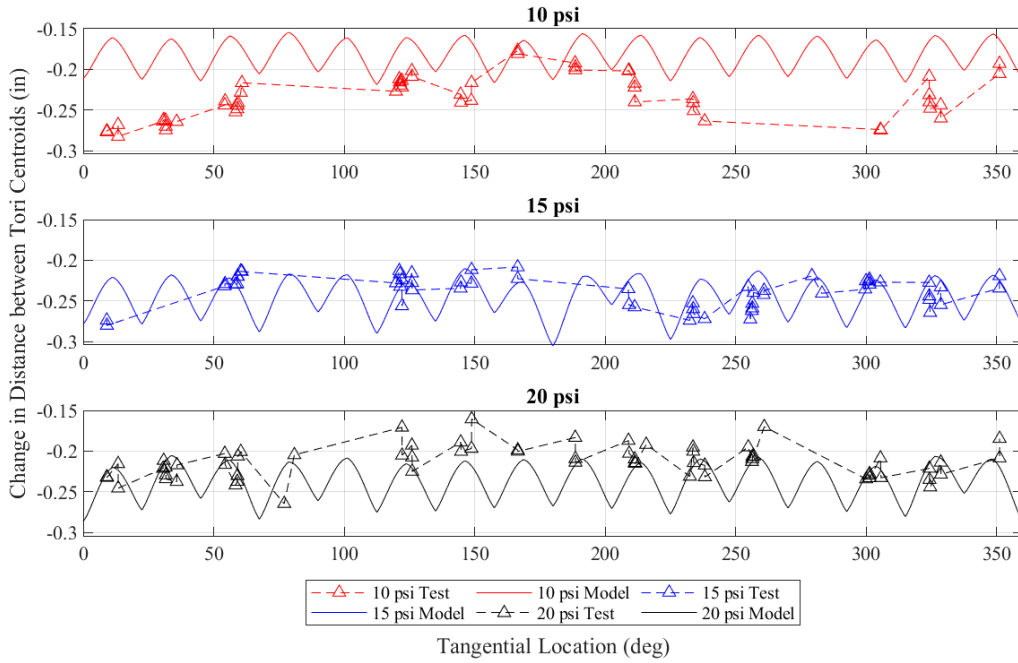


Figure 66. Change in distance between tori centroids, test and model

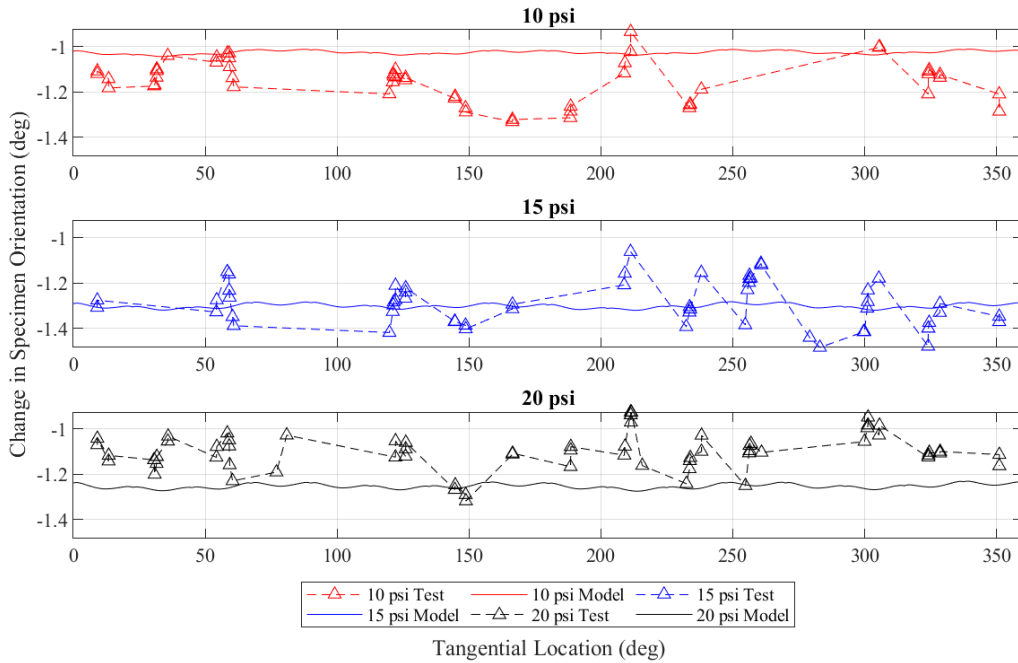


Figure 67. Change in specimen orientation, test and model

Figure 66 and Figure 67 show the change in distance between tori centroids (or inter-torus compression) and the change in specimen orientation (angle of the line through both tori centroids with the horizontal). Both agree quite well with model results, which suggests the axial stiffness and bending stiffness in the radial direction of the interaction elements are accurate.

Future improvements to the model would be the inclusion of local deformation of the cross section and shear transfer between the load saddles and tori. This could be achieved by modifying the axial and bending stiffnesses of the load strap to torus links. Another way agreement between the model and the test could possibly be improved would be to use the initial major radius and height data from PONTOS as the initial coordinates of the tori centroids in the model instead of a perfectly horizontal circle. The PONTOS data of the orientation of the load straps could also be used instead of nominal values.

CHAPTER 6 CONCLUSIONS

The testing fixture described by Young (2017b) was upgraded to withstand the maximum actuator force from all 16 actuators simultaneously. The pulleys and wire rope were upgraded. The outer ring of the test fixture was checked using ABAQUS. Next, tests of single torus specimens were set up and run. Load cells and string pots were attached at each load cable. A pair of cameras was set up for digital image correlation and DIC targets were glued to the specimens. The control code described in Whitney (2016) was modified for the new testing. After this, a paired specimen was set up and tested in a very similar way to the single torus tests, with a few modifications. Because of the limitations of the cameras, getting quality data from the DIC was more difficult. Controlling the test was also harder probably because the paired specimen was much stiffer than the single tori the system was originally tuned for. Finally, the beam based finite element model discussed in Young (2017a, 2017b and 2018) was applied to the paired torus testing.

With the testing of the single tori, both decreasing major radius and increasing pressure increased radial stiffness, as expected. The paired specimen was also radially stiffer with higher pressure. Changing from 10 to 15 psi, the effect on stiffness was much greater for the paired than the singles, with a 56% increase compared to 27% for the single specimens. The change of stiffness from 15 to 20 psi was similar for both kinds of tests, 15% and 14% for the singles and paired, respectively. At 20 psi, the paired specimen is almost twice as stiff as the sum of the stiffnesses of the two single tori. However, the tori in the paired specimen, especially the T4, were loaded differently during paired testing than the singles testing. There was significant unintended but also unavoidable vertical force on the T4 during testing of the paired specimen, which caused it to displace downwards very significantly. Also, both tori in the paired specimen rotated about their cross sections with the T4 rotating about 2 degrees and the T5 rotating 1 degree at final

load. Where the single specimens displaced in radially, the tori in the paired specimen compressed together and the T4 rotated over the T5.

The results of the model of the paired specimen had mixed agreement to the testing. The model did capture the compression of the tori into each other relatively well at all pressures. However, it vastly over-predicted the radial displacement of the tori and did not predict any cross section rotation. These discrepancies could come from a couple of different sources. Though there was release film between the torus and the load saddles during testing, there could have been unintended friction on the tori. The load saddles were modeled as frictionless. Secondly, the model does not explicitly take cross section deformations of the tori into account. The rotation from testing could be a result of local deformation of the cross section at the load straps either where the straps contact the tori or where the tori contact each other. If the cross section is no longer perfectly circular, this could cause a net torque because the line of action of the force resultants no longer go through the shear center (centroid) of the torus.

The behavior of the paired specimen is still not completely understood and more testing could be useful. However, if the current test fixture was to be used again it is strongly recommended that many of the components be upgraded. The cameras that are part of the DIC system should be replaced with cameras with a wider field of view so that more of the lower torus is visible. This could also be achieved by using multiple sets of cameras. The control code should be sped up, ideally fast enough to run the full test in load control. This could possibly be achieved by writing the control code in a language more optimized for speed than MATLAB or replacing the actuators. If displacement control is still used, a new way to measure displacements must be devised. This could potentially be attaching the string pots to only one torus so cross section deformations have less of an effect on the string pot readings. Alternatively, the actuators could

be replaced with ones that have integrated potentiometers and the test could be controlled using actuator displacement. Finally, the loading method should be modified so that there is less vertical force on the tori. Hopefully this could allow for the specimen to be displaced radially inwards instead of cross section and vertical deformations making up most of the displacement. It is difficult to say with any certainty how to improve the model of the paired specimen without a set of data where the paired torus specimen displaces radially inward significantly. Getting a data set like this and then revisiting the paired model could potentially be helpful. Also, the model could be further validated with completely new test cases. The bending stiffnesses of the interaction elements could be further refined through a combination of testing and/or modeling. Local deformations of the torus cross section could be incorporated more explicitly than fitting an effective stiffness of the load strap. This could possibly be achieved by modifying the stiffnesses of the links connecting the torus centroids to the straps or other objects that are compressing them.

REFERENCES

- Brune, A.J., West, T.K., Hosder, S. (2019). "Uncertainty quantification of planetary entry technologies." *Progress in Aerospace Sciences*, 111, 100574
- Clapp, J.D. (2017). *Structural Behavior of Inflatable, Reinforced, Braided Tubular Members*. The University of Maine, Orono, Maine.
- Clapp, J.D., Davids, W.G., Goupee, A.J., Young, A.C.. (2016a). "Experimental Determination of Inflatable, Braided Tube Constitutive Properties." *Strain*, 52, 148-161.
- Clapp, J.D., Young, A.C., Davids, W.G., Goupee, A.J. (2016b). "Bending response of reinforced, inflated, tubular braided fabric structural members." *Thin-Walled Structures*, 107, 415-426.
- Hollis, B.R., Berry, S.A., Hollingsworth, K.E., Wright, S.A. (2017). *Experimental Study of Convective Heating on the Back Face and Payload of a Hypersonic Inflatable Aerodynamic Decelerator (HIAD) Aeroshell*. NASA Technical Report NF1676L-20696
- NASA. (2022, Dec 7). *Low-Earth Orbit Flight Test of an Inflatable Decelerator (LOFTID)*. https://www.nasa.gov/mission_pages/tdm/loftid/index.html
- Whitney, D. J. (2016). *Experimental methods and practices for the study of toroidal inflated, braided fabric members*. University of Maine, Orono, Maine.
- Young, A.C. (2017). *Large Payload HIAD Systems: Development of Computationally Efficient Modeling Strategies and Structural Investigations*. University of Maine, Orono, Maine.
- Young, A.C., Davids, W.G., Goupee, A.J., Clapp, J.D. (2017a). "Computationally efficient finite-element modeling of braided, inflatable structural members with axial reinforcing." *Journal of Engineering Mechanics* 143(6).
- Young, A.C., Davids, W.G., Whitney, D.J., Clapp, J.D., Goupee A.J. (2017b). "Structural testing and analysis of a braided, inflatable fabric torus structure." *Acta Astronautica*, 139, 189-200
- Young, A.C., Davids, W.G., Cheatwood, F.M., Lindell, M.C. (2018). "Structural analysis of hypersonic inflatable aerodynamic decelerator pressure tub testing." *Thin-Walled Structures*, 131, 869-882

Zhao, Y., Chen, J., Liu, H. (2022). “Application of improved $k-\omega-\gamma$ model to deformed hypersonic Inflatable Aerodynamic Decelerator aeroshell.” *Applied Thermal Engineering*, 214, 118794

APPENDICES

APPENDIX A ACTUATOR CONNECTION CALCULATION

Actuator Extension Bending Calculation

Inputs

$$b := 4 \text{ in} + \frac{7}{8} \text{ in}$$

$$h := 0.5 \text{ in}$$

$$F_y := 36 \text{ ksi}$$

$$M_{max} := 5.25 \text{ in} \cdot \text{kip} \quad \text{From structurally indeterminate analysis}$$

Check bending stress

$$S := b \cdot \frac{h^2}{6} = 0.203 \text{ in}^3$$

$$f_{bmax} := \frac{M_{max}}{S} = (2.585 \cdot 10^4) \text{ psi}$$

$$n_b := \frac{F_y}{f_{bmax}} = 1.393$$

Actuator Mount Checks

Inputs

$$S_{y_pin} := 92 \text{ ksi}$$

$$P := 2000 \text{ lbf}$$

$$d_{pin} := 0.5 \text{ in}$$

$$t_{con} := 0.5 \text{ in}$$

$$F_{u_con} := 58 \text{ ksi}$$

$$F_{y_con} := 36 \text{ ksi}$$

$$l_c := 0.25 \text{ in}$$

$$F_{EXX} := 60 \text{ ksi}$$

$$l_{weld} := 4.5 \text{ in}$$

$$weld_size := \frac{1}{8} \text{ in}$$

Check shear in pin

$$S_{sys_pin} := 3^{-.5} \cdot S_{y_pin}$$

$$\tau_{pin} := 4 \cdot \frac{P}{\pi \cdot d_{pin}^2} = (1.019 \cdot 10^4) \text{ psi}$$

$$n_{sys_pin} := \frac{S_{sys_pin}}{\tau_{pin}} = 5.215$$

Check bearing/tearout in connector at pin

$$S_{bc1} := 2.4 \cdot d_{pin} \cdot 2 \cdot t_{con} \cdot F_{u_con} = (6.96 \cdot 10^4) \text{ lbf}$$

$$S_{bc2} := 1.2 \cdot l_c \cdot 2 \cdot t_{con} \cdot F_{u_con} = (1.74 \cdot 10^4) \text{ lbf}$$

$$S_{b_con} := \min(S_{bc1}, S_{bc2})$$

$$n_{b_con} := \frac{S_{b_con}}{P} = 8.7$$

Check weld strength

$$r := \frac{P}{l_{\text{weld}}} = 444.444 \frac{\text{lb}}{\text{in}}$$

$$R := .6 \cdot F_{EXX} \cdot \text{weld_size} \cdot 2^{-0.5} = (3.182 \cdot 10^3) \frac{\text{lb}}{\text{in}}$$

$$FS := \frac{R}{r} = 7.159$$

Check base metal

$$R_b := .6 \cdot F_{y_con} \cdot t_{con} = (1.08 \cdot 10^4) \frac{\text{lb}}{\text{in}}$$

$$FS := \frac{R_b}{r} = 24.3$$

APPENDIX B PULLEY MOUNT CALCULATIONS

Note: SM is steel manual, 15th ed

Loading calcs start on page 3

Pulley mount base plate bending calcs start on page 3

Weld calcs start on page 6

Pulley extension bending calcs start on page 8

1. Input Parameters

Loading

$P := 2000 \text{ lbf}$ Maximum load in cable

$\theta_{ap} := 3.7021 \text{ deg}$ Angle between actuator and pulley

Pulley Mount

$S_{y_pin} := 45000 \text{ psi}$ Tensile strength of pulley pin

$S_{y_bolt} := 92000 \text{ psi}$ Tensile strength of bolts

$d_{pin} := 0.75 \text{ in}$ Diameter of pin

$A_{bolt} := 0.0318 \text{ in}^2$ Area of bolt

$A_{bolt_s} := 0.0269 \text{ in}^2$ Shear area of bolt

$d_{bolt} := \frac{3}{8} \text{ in}$ Diameter of bolt + 1/16 clearance + 1/16 damage

$t_{con_b} := 0.125 \text{ in}$ Thickness of pulley mount sides

$t_{con_t} := 0.25 \text{ in}$ Thickness of pulley mount base

$l_c := 0.425 \text{ in}$ Minimum distance between center of pulley pin hole and edge of pulley mount side

$F_{u_con} := 58000 \text{ psi}$ Ultimate strength of mount steel

$F_{y_con} := 36000 \text{ psi}$ Yield strength of mount steel

$w_{b_con} := 1.75 \text{ in}$ Minimum width of pulley mount side

$w_{t_con} := 3 \text{ in}$ Width of pulley mount base

$w_{t_con_wb} := 4.25 \text{ in}$ Width of wide pulley mount base

$w_{slot} := 2 \cdot \frac{3}{16} \text{ in}$ Width of slots in base

$M_u := 0.078 \text{ kip}\cdot\text{ft}$	Maximum bending moment in mount baseplate, from Risa model
$M_{u_wb} := 0.117 \text{ kip}\cdot\text{ft}$	
$l_{weld} := 3.5 \text{ in} + \frac{1}{16} \text{ in}$	Length of weld
$weld_size := \frac{1}{8} \text{ in}$	
$F_{EXX} := 60000 \text{ psi}$	Strength of weld material
$e_{x_wb} := 0.57 \text{ in}$	Distance between center of weld/pulley mount sides and center of bolt pattern for wide base
$e_y := 2.6 \text{ in}$	Distance between center of pin hole and bottom surface of mount base
$d_b := 3.2 \text{ in}$	Distance between bolts of skinny base
$d_{b_wb} := 2 \text{ in}$	Distance between bolts of wide base

Pulley Extension

$w_{ext} := 3 \text{ in} - \left(0.5 + \frac{1}{16}\right) \text{ in} \cdot 2 = 1.875 \text{ in}$	Width of extension plate, minus bolt holes
$t_{ext} := 0.5 \text{ in}$	Thickness of extension plate
$M_{u_ext} := 1940 \text{ in}\cdot\text{lb}$	Maximum bending moment in extension plate, from MatLab
$S_{tb} := 3500 \text{ lbf}$	McMaster strength of turnbuckle in pulley extension tension member
$S_{hr} := 5000 \text{ lbf}$	McMaster strength of hoist ring
$d_{h_tm} := 16.963 \text{ in}$	Horizontal distance between hoist rings
$d_{v_tm} := 11.8775 \text{ in}$	Vertical distance between hoist rings

2. Geometry of Loading

Controlling case for R + V has theta for actuator to pulley = 3.70 deg. See Matlab.
Controlling case for T has T = P

$$V := (\sin(\theta_{ap}) + 1) \cdot P = (2.129 \cdot 10^3) \text{ lbf}$$

$$V_{weld} := \frac{V}{2}$$

$$T := P = (2 \cdot 10^3) \text{ lbf}$$

$$T_{weld} := \frac{T}{2}$$

$$t := \cos(\theta_{ap}) \cdot P = (1.996 \cdot 10^3) \text{ lbf}$$

$$R := (V^2 + t^2)^{\frac{1}{2}} = (2.918 \cdot 10^3) \text{ lbf}$$

3. Pulley Mount Design Checks

Check shear in pin

$$S_{sys_pin} := S_{y_pin} \cdot 3^{-0.5} = (2.598 \cdot 10^4) \text{ psi}$$

$$\tau_{pin} := 4 \cdot \frac{R}{\pi \cdot d_{pin}^2} = (6.606 \cdot 10^3) \text{ psi}$$

$$n_{sys_pin} := \frac{S_{sys_pin}}{\tau_{pin}} = 3.933$$

Check bearing/tearout in connector at pin

$$S_{bc1} := 2.4 \cdot d_{pin} \cdot 2 \cdot t_{con_b} \cdot F_{u_con} = (2.61 \cdot 10^4) \text{ lbf}$$

$$S_{bc2} := 1.2 \cdot l_c \cdot 2 \cdot t_{con_b} \cdot F_{u_con} = (7.395 \cdot 10^3) \text{ lbf}$$

$$S_{b_con} := \min(S_{bc1}, S_{bc2})$$

$$n_{b_con} := \frac{S_{b_con}}{R} = 2.534$$

Check shear in connector at pin

$$S_{cb1} := 0.6 \cdot t_{con_b} \cdot F_{u_con} \cdot (w_{b_con} - d_{pin}) = (4.35 \cdot 10^3) \text{ lbf}$$

$$S_{cb2} := 0.6 \cdot t_{con_b} \cdot F_{y_con} \cdot w_{b_con} = (4.725 \cdot 10^3) \text{ lbf}$$

$$n_{sys_con_bot} := \frac{\min(S_{cb1}, S_{cb2})}{V} = 2.043$$

Check tension in connector at bolts

$$S_{ct1} := t_{con_t} \cdot F_{u_con} \cdot (w_{t_con} - 2 \cdot d_{bolt}) = (3.263 \cdot 10^4) \text{ lbf}$$

$$S_{ct2} := t_{con_t} \cdot F_{y_con} \cdot w_{t_con} = (2.7 \cdot 10^4) \text{ lbf}$$

$$n_{y_con_top} := \frac{\min(S_{ct1}, S_{ct2})}{T} = 13.5$$

Check bending in connector (wide base)

$$Z_{wb} := \frac{(w_{t_con_wb} - w_{slot}) \cdot t_{con_t}^2}{4} = 0.061 \text{ in}^3$$

$$n_{bending_wb} := \frac{Z_{wb} \cdot F_{y_con}}{M_{u_wb}} = 1.552$$

Check bending in connector (skinny base)

$$Z := \frac{(w_{t_con} - w_{slot}) \cdot t_{con_t}^2}{4} = 0.041 \text{ in}^3$$

$$n_{bending} := \frac{Z \cdot F_{y_con}}{M_u} = 1.578$$

Bolt Shear Check

$$S_{sys_bolt} := S_{y_bolt} \cdot 3^{-0.5} = (5.312 \cdot 10^4) \text{ psi}$$

$$\tau_{bolt} := \frac{V}{4 \cdot A_{bolt_s}} = (1.979 \cdot 10^4) \text{ psi}$$

$$n_{sys_bolt} := \frac{S_{sys_bolt}}{\tau_{bolt}} = 2.684$$

Bolt Tension Check (Combined T + V)

Calculate extra tension on back bolts

Case 1: Skinny Base

$$T_{xtra_sb} := \frac{e_y \cdot V_{weld}}{d_b} = 864.962 \text{ lbf}$$

Case 2: Wide Base

$$T_{xtra_wb} := \frac{e_y \cdot V_{weld}}{d_{b_wb}} - \frac{e_{x_wb} \cdot T_{weld}}{d_{b_wb}} = (1.099 \cdot 10^3) \text{ lbf}$$

$$T_{xtra} := \max(T_{xtra_sb}, T_{xtra_wb})$$

$$\sigma_{bolt} := \frac{T}{4 \cdot A_{bolt}} = (1.572 \cdot 10^4) \text{ psi}$$

$$n_{y_bolt} := \frac{S_{y_bolt}}{\sigma_{bolt} + \frac{T_{xtra}}{A_{bolt}}} \cdot \left(1.3 - \frac{1}{n_{sys_bolt}} \right) = 1.697 \quad \text{SM Eq. J3-3}$$

Check Welds

Find required strength

$$r_{px} := \frac{V_{weld}}{l_{weld}} = 298.826 \frac{\text{lb}}{\text{in}} \quad \text{SM eq 8-5}$$

$$r_{py} := \frac{T_{weld}}{l_{weld}} = 280.702 \frac{\text{lb}}{\text{in}}$$

$$I_p := \frac{l_{weld}^3}{12} \quad \text{SM Fig 8-6}$$

$$r_{my} := \frac{V_{weld} \cdot e_y \cdot \frac{l_{weld}}{2}}{I_p} = (1.309 \cdot 10^3) \frac{\text{lb}}{\text{in}} \quad \text{SM eq 8-10}$$

$$r := \left(r_{px}^2 + (r_{py} + r_{my})^2 \right)^{\frac{1}{2}} = (1.617 \cdot 10^3) \frac{\text{lb}}{\text{in}} \quad \text{SM eq 8-11}$$

Check weld strength

$$R := .6 \cdot F_{EXX} \cdot \text{weld_size} \cdot 2^{-0.5} = (3.182 \cdot 10^3) \frac{\text{lb}}{\text{in}}$$

$$FS := \frac{R}{r} = 1.968$$

Check base metal

$$R_b := .6 \cdot F_{y_con} \cdot \min(t_{con_b}, t_{con_t}) = (2.7 \cdot 10^3) \frac{\text{lb}}{\text{in}}$$

$$FS := \frac{R_b}{r} = 1.67$$

Determine distributed load values for Risa Models

$$\text{slope} := V_{\text{weld}} \cdot \frac{e_y}{I_p} = 734.622 \text{ psi}$$

Max compression

$$m1 := 2 \cdot \left(\text{slope} \cdot \left(\frac{-l_{\text{weld}}}{2} + r_{py} \right) \right) = -2.467 \cdot 10^4 \frac{\text{lbf}}{\text{ft}}$$

Compression at bolts (skinny base)

$$m2 := 2 \cdot \left(\text{slope} \cdot \left(\frac{-l_{\text{weld}}}{2} + 0.17188 \text{ in} \right) + r_{py} \right) = -2.164 \cdot 10^4 \frac{\text{lbf}}{\text{ft}}$$

Compression at bolts (wide base)

$$m3 := 2 \cdot \left(\text{slope} \cdot \left(-2.25 \text{ in} + \frac{l_{\text{weld}}}{2} \right) + r_{py} \right) = -1.528 \cdot 10^3 \frac{\text{lbf}}{\text{ft}}$$

Max tension

$$M1 := 2 \cdot \left(\text{slope} \cdot \left(\frac{l_{\text{weld}}}{2} + r_{py} \right) \right) = (3.814 \cdot 10^4) \frac{\text{lbf}}{\text{ft}}$$

Tension at bolts

$$M2 := 2 \cdot \left(\text{slope} \cdot \left(\frac{l_{\text{weld}}}{2} - 0.17188 \text{ in} \right) + r_{py} \right) = (3.511 \cdot 10^4) \frac{\text{lbf}}{\text{ft}}$$

4. Pulley Extension Strength

Check bending in extension plate

$$S_{ext} := \frac{w_{ext} \cdot t_{ext}^2}{6} = 0.078 \text{ in}^3$$

$$n_{bending_ext} := \frac{S_{ext} \cdot F_{y_con}}{M_{u_ext}} = 1.45$$

Check tension member components

$$\theta_{tm} := \text{atan}\left(\frac{d_{v_tm}}{d_{h_tm}}\right) = 35 \text{ deg}$$

$$T_{tm} := \frac{T}{\sin(\theta_{tm})} = (3.487 \cdot 10^3) \text{ lbf}$$

Tension in tension member, assuming all tension is carried by tension member. Very conservative, MatLab model says it carries less than half.

$$n_{tb} := \frac{S_{tb}}{T_{tm}} = 1.004$$

OK, S_{tb} is working capacity, not ultimate

$$n_{hr} := \frac{S_{hr}}{T_{tm}} = 1.434$$

APPENDIX C CONTROL CODE

```
function test_driver_IH_ml_cams(inputs)

global Stop_Session im_ts im_ts_all

global time_save LCdata_save LCRaw_save SPdata_save SPRaw_save pwm_save
global GEN_save tot_error time_cell LCdata_cell LCRaw_cell SPdata_cell
global SPRaw_cell pwm_cell GEN_cell tot_error_cell rv_cell reg_vals PID_save PID_cell

% Get inputs
struct_fields = fieldnames(inputs);
for i = 1:length(struct_fields)
    eval([struct_fields{i} '= inputs.' struct_fields{i} ';' ]);
end

% Get gui handles
try
    gh = guihandles(gui_fun());
catch
    gh = [];
end
junk = onCleanup(@() write(inputs.d2,[false,false,false]));

% Get log file id
fid = DAQ_session.UserData.fid;

% Get number of tests
num_steps = length(test_mat(1,1,:));

pho_freq = freq;

% Initialize save variables
time_cell = cell(num_steps,1);
LCdata_cell = cell(num_steps,1);
LCRaw_cell = cell(num_steps,1);
SPdata_cell = cell(num_steps,1);
SPRaw_cell = cell(num_steps,1);
pwm_cell = cell(num_steps,1);
GEN_cell = cell(num_steps,1);
tot_error_cell = cell(num_steps,1);
rv_cell = cell(num_steps,1);
im_ts_all = cell(num_steps,1);
PID_cell = cell(num_steps,1);
tot_calls = zeros(num_steps,1);
times_switched = tot_error;
```



```

% Loop through tests
for k = start_test:num_steps

    % Write to log
    msg = {'Preparing for test ', num2str(k), ' at ' char(datetime('now'))};
    write2log(fid,msg,{},gh);

    % Stop if stop session has been activated
    if Stop_Session==1
        msg = {'Test stopped at ' char(datetime('now')) '.'};
        write2log(fid,msg,{},gh);
        break
    end

    % Assign matrix for current test
    TST_p = test_mat(:, :,k);

    % Update gui
    if ~isempty(gh)
        gh.test_mat_tab.Data = [cell(size(TST_p,1),1),num2cell(TST_p)];
        gh.test_mat_slider.Value = k;
        gh.slider_tb.String = num2str(k);
        gh.press_tb.String = {'Target Pressure: ' num2str(PressV(k))};
    end

    if ~isempty(p_loc) && do_press(k) && con_press

        DAQ_session.UserData.start_infl = 1;

        % Start DAQ if it isn't running
        if ~DAQ_session.Running
            start(DAQ_session,'Continuous')
        end

        % Change pressure, deflating first if requested
        [save_data] = change_press_mlc(PressV(k),deflate(k),wait_timeM(k),...
            DAQ_session,drain_val,gui_fun);

        % Set pressure variables and update gui
        DAQ_session.UserData.target_press = PressV(k);
        DAQ_session.UserData.d2 = d2;
        gh = guihandles(disp_dat);
        gh.press_txt.String{2} = ['Target Pressure: ' ...
            num2str(real(PressV(k)), '%.3f') ' psi'];

        % Save pressure data
        press_save{k} = save_data;
    else
        DAQ_session.UserData.target_press = [];
        press_save{k} = [];
    end

    if ~DAQ_session.Running
        start(DAQ_session,'continuous')
    end
end

```

```

waitfor(DAQ_session, 'NumScansAvailable')

daq_fun(DAQ_session);

% Check if session has been stopped
pause(0.002)
if Stop_Session
    msg = {'Test stopped at ' char(datetime('now')) '.'};
    write2log(fid,msg,{},gh);
    break
end
%pause(10)

if add_cam && ~isempty(cams)
    % Make test photo folder
    cur_pho_loc = [test_loc, '\Test' num2str(k)];
    if ~exist(cur_pho_loc, 'dir')
        mkdir(cur_pho_loc)
    end
    for i = 1:length(cams)
        cams(i).LoggingMode = 'disk&memory';
        % Add disklogger
        V = VideoWriter([cur_pho_loc '\c' num2str(i)], 'Grayscale AVI');
        cams(i).DiskLogger = V;

    end

    % Clear timestamp variable
    im_ts = cell(1,2);
    im_ts{1} = cell(0);
    im_ts{2} = cell(0);

    % Start cams
    start(cams)
elseif add_cam
    cams = struct('TriggerType', 'immediate');
    cam_timer = [];
else
    cam_timer = [];
end

% Run control code
multi_actuator_control_m1_cams(TST_p, PIDslopes_lc, PIDslopes_dc, ...
    Integr_L, DAQ_session, shut_down_time, PID_PD_mod, act_freq, pho_freq, ...
    cams, cam_timer, avg_ld, daq_fun, gui_fun, dc_con, dc_con_ramp);

% Save data
LCdata_cell{k} = LCdata_save;
LCRaw_cell{k} = LCRaw_save;
SPdata_cell{k} = SPdata_save;
SPRaw_cell{k} = SPRaw_save;
pwm_cell{k} = pwm_save;

```

```

GEN_cell{k} = GEN_save;
time_cell{k} = time_save;
tot_error_cell{k} = tot_error;
if add_cam && ~isempty(cams)
im_ts_all{k} = im_ts;
end

rv_cell{k} = reg_vals;
PID_cell{k} = PID_save;

% Check if session has been stopped
pause(0.1)
if Stop_Session == 1
    msg = {'Test stopped at ' char(datetime('now')) '.'};
    write2log(fid,msg,{},gh);
    break
end
end

% Save data
save_loc = [test_loc, '\test_data.mat'];
[save_loc] = get_unique_filename(save_loc);

save(save_loc, 'time_cell', 'LCdata_cell', ...
    'LCRaw_cell', 'SPdata_cell', 'SPRaw_cell', 'pwm_cell', 'GEN_cell', ...
    'tot_error_cell', 'press_save', 'im_ts_all', 'rv_cell', 'PID_cell');

```

```

function [tot_calls,times_switched] = multi_actuator_control_ml_cams(...
    TST_p,PIDslopes_lc,PIDslopes_dc,Integr_L,DAQ_session,shut_down_time,...
    PID_PD_mod,freq,pho_freq,cams,cam_timer,avg_ld,daq_fun,gui_fun,...
    dc_con,dc_con_ramp)

global StopTest Stop_Session
global time_save LCdata_save LCRaw_save SPdata_save SPRaw_save
global pwm_save GEN_save tot_error reg_vals PID_save

% Get GUI handles
try
    gh = guihandles(gui_fun());
catch
    gh = [];
end

% Initializing/setting variables
act_ind = DAQ_session.UserData.act_ind;
fid = DAQ_session.UserData.fid;
num_act = length(act_ind);
StopTest = 0;
calls = 0;
progress = 0;
Error_hist = zeros(Integr_L,num_act);
time_Cur = 0;
T_hold = 0;
PWM_old = ones(1,num_act)*0.02;
PWM = PWM_old;

% When the function ends (either normally, because of the user or
% because of an error), this will extend the actuators and stop
% the image and data acquisition
junk = onCleanup(@() SessionShutDown_ml_cams(DAQ_session,act_ind,cams));

% Compute test times
[time_switch,Tfinish]=comp_test_times(TST_p);% Computes switch times

cur_time_switch=time_switch(1);

% Initialize error variable
currerrr = zeros(round(1.1*freq*Tfinish),num_act);

% Reallocating the data storage locations
save_pre_length=freq*time_switch(length(time_switch))+1+freq*shut_down_time;
LCdata_save=zeros(save_pre_length,length(DAQ_session.UserData.lc_ind));
LCRaw_save=zeros(save_pre_length,length(DAQ_session.UserData.lc_ind));
SPdata_save=zeros(save_pre_length,length(DAQ_session.UserData.sp_ind));
SPRaw_save=zeros(save_pre_length,length(DAQ_session.UserData.sp_ind));
pwm_save=zeros(save_pre_length,num_act);
GEN_save=zeros(save_pre_length,3);
time_save = NaN(save_pre_length,1);
tot_error = zeros(save_pre_length,num_act);
reg_vals = zeros(save_pre_length,3);
if avg_ld

```

```

        PID_save = zeros(save_pre_length,3);
else
    PID_save = zeros(save_pre_length,16,3);
end
times_switched = NaN(size(TST_p,1),1);

waitfor(DAQ_session, 'NumScansAvailable')

% Gets zeros for SPs and current load
[~,LCdata,SPdata] = daq_fun(DAQ_session);

% Set camera variables, start cameras if needed
if ~isempty(cams)
    switch cams(1).TriggerType
        case 'immediate'
            if isstruct(cams)
                waitfor(msgbox('Please start cameras'))

                end
                DAQ_session.UserData.pho_start = tic;
                DAQ_session.UserData.pho_ct = 0;
                DAQ_session.UserData.pho_trig = 0;

            case 'manual'
                DAQ_session.UserData.trig_typ = 'manual';
                if ~isempty(cam_timer)
                    start(cam_timer)
                else
                    trigger(cams)
                end
            end
        end
    end
tic

% Loop through steps of test
while ~StopTest && ~Stop_Session && time_Cur < Tfinish
    % Increment loop counter
    calls=calls+1;

    % Determine if the program just entered a different test stage and set
    % up if true
    if cur_time_switch<=time_Cur
        time_old = datetime('now');
        if progress == 0 || TST_p(progress,1) ~= TST_p(progress + 1,1)
            DAQ_session.UserData.zero_graphs = 1;
        end
        zeroSP = SPdata;
        % Increment stage counter
        progress = progress + 1;
        times_switched(progress) = datetime('now');
        % Update log file and gui
        msg = {'Starting row ' num2str(progress) ' at ' char(datetime('now'))};
        fid = write2log(fid,msg,{},gh);
        if ~isempty(gh)
            gh.test_mat_tab.Data{progress,1} = '->';
        end
    end
end

```

```

        if progress > 1
            gh.test_mat_tab.Data{progress - 1,1} = '';
        end
    end

    % Set end time of stage
    cur_time_switch=time_switch(progress+1);

    % Proportional parameter
    pam = TST_p(progress,5);

    % First call of stage
    f_call = calls;

    % Set current control type and PID slopes
    cur_type = TST_p(progress,1) - 1;
    DAQ_session.UserData.cur_type = cur_type;
    PIDslopes = PIDslopes_lc.*~cur_type + PIDslopes_dc.*cur_type;

    % This step checks if this test uses load control and sets values
    if TST_p(progress,1)==1

        if TST_p(progress,2) == TST_p(progress,3)
            Start_D = TST_p(progress,3);
            End_D=TST_p(progress,3);
        else
            Start_D = mean(LCdata);
            End_D=TST_p(progress,3);
        end

        %This step checks if this test uses displacement control
    elseif TST_p(progress,1)==2

        % Sets the zero for the string pots

        DAQ_session.UserData.sp0 = zeros(16,1);

        if TST_p(progress,2) == TST_p(progress,3)
            Start_D = TST_p(progress,3);
            End_D=TST_p(progress,3);
        else
            Start_D=0;
            End_D=TST_p(progress,3);
        end

    end

    Error_hist=zeros(Integr_L,num_act);
    PID_vals=TST_p(progress,5:7);
    time_diff = zeros(Integr_L,1);

end
cur_dur = time_Cur-time_switch(progress);

```

```

pwm_con = min(cur_dur/dc_con_ramp,1)*dc_con*cur_type;

% Control target value
desired=(End_D-Start_D).*(cur_dur)/...
    (cur_time_switch-time_switch(progress))+Start_D;

DAQ_session.UserData.desired = desired;

% Read Data from Hardware
[time_t,LCdata,SPdata,Pressure,SPRaw,LCRaw,rv] = daq_fun(DAQ_session);

% Add length of current time step
time_diff = [seconds(time_t - time_old);time_diff(1:end - 1)];
time_old = time_t;

% Set load cells reading compression to 0 (significant compression isn't
physically
% possible)
LCdata_act = LCdata;
LCdata(LCdata < 0) = 0;

% Evaluates the error
curerrr(calls,.)=(-SPdata + zeroSP)*cur_type + LCdata*~cur_type - desired;

Error_hist=[curerrr(calls,.);Error_hist(1:Integr_L-1,:)];

% Gives the P value a large boost for the beginning of displacement
% controlled tests
PID_vals(1) = pam+cur_type*pam*PID_PD_mod/(calls-f_call+1);

% Set the Actuators to the desired Voltage
PWM_old = PWM;

if ~StopTest && ~Stop_Session && cur_type < 2
    [ PWM,PID_use ] = PID_IH(
PID_vals,Error_hist,time_diff,LCdata,PIDslopes,avg_ld,pwm_con);
    ch_ind = PWM ~= PWM_old;
elseif ~StopTest && ~Stop_Session && cur_type == 2
    PWM = zeros(1,num_act) + 0.02;
    ch_ind = PWM ~= PWM_old;
else
    ch_ind = ones(num_act,1);
    PWM = ones(num_act,1).*0.02;
end

if sum(ch_ind)
    PWM_OUT_write_IH(PWM(ch_ind),act_ind(ch_ind),DAQ_session);
end

% Data Saved to Variables
time_save(calls,1:length(time_t))=time_t;
LCdata_save(calls,1:length(LCdata))=LCdata_act;
LCRaw_save(calls,1:length(LCraw))=LCraw;
SPdata_save(calls,1:length(SPdata))=SPdata;
SPRaw_save(calls,1:length(SPRaw))=SPRaw;

```

```

pwm_save(calls,1:length(PWM))=PWM;
GEN_save(calls,1:length([desired(1) Pressure cur_type]))=...
    [desired(1) Pressure cur_type];% fill camSpeed ];
tot_error(calls,:) = curerrr(calls,:);
reg_vals(calls,:) = rv;
if avg_ld
    PID_save(calls,:) = PID_use';
else
    PID_save(calls,:,1:3) = reshape(PID_use',1,[],3);
end

% Pause to check if a stop command has been issued
pause(0.0000000001)% also allows matlab to clear queue

% Synchronization of execution to achieve desired frequency
while toc-calls/freq < 1/freq
end
time_Cur = toc-T_hold;
end
%_____ %
% The Test had been Completed or Aborted
% The following section shuts down the system and saves the recorded data
% Puts the actuators at full extend

msg = {'Test ramping down at ' char(datetime('now'))};
write2log(fid,msg,{},gh);
PWM_OUT_write_IH(zeros(1,num_act) + 0.02,act_ind,DAQ_session)

if StopTest==1
    msg = {'Current test skipped.'};
    write2log(fid,msg,{},gh);
end
tot_calls = calls;

% Ramp down test (Unloading for 10 seconds)
for p=1:shut_down_time*freq
    calls=calls+1;

    % Read Data from LV
    [time_t,LCdata,SPdata,Pressure,SPRaw,LCRaw] = daq_fun(DAQ_session);
    % Save Data
    time_save(calls,1:length(time_t))=time_t;
    LCdata_save(calls,1:length(LCdata))=LCdata;
    LCRaw_save(calls,1:length(LCRaw))=LCRaw;
    SPdata_save(calls,1:length(SPdata))=SPdata;
    SPRaw_save(calls,1:length(SPRaw))=SPRaw;
    pwm_save(calls,1:length(PWM))=PWM;
    GEN_save(calls,1:length([desired(1) Pressure cur_type]))=...
        [desired(1) Pressure cur_type];
    if avg_ld
        PID_save(calls,:) = PID_use';
    else
        PID_save(calls,:,1:3) = reshape(PID_use',1,[],3);
    end
end

```



```

% Stops Image Aquasition
if p==(shut_down_time-2)*freq && ~isempty(cams)
    if ~isstruct(cams)
        stop(cams);
    end
    if strcmp(cams(1).TriggerType,'immediate')
        DAQ_session.UserData.pho_start = [];
    end
end

% Synchronization of excecution to achieve desired frequency
while toc - calls/freq < 1/freq
end

end

time_save(calls + 1:save_pre_length,:) = [];
LCdata_save(calls + 1:save_pre_length,:) = [];
LCRaw_save(calls + 1:save_pre_length,:) = [];
SPdata_save(calls + 1:save_pre_length,:) = [];
SPRaw_save(calls + 1:save_pre_length,:) = [];
pwm_save(calls + 1:save_pre_length,:) = [];
GEN_save(calls + 1:save_pre_length,:) = [];
tot_error(calls + 1:save_pre_length,:) = [];
PID_save(calls + 1:save_pre_length,,:,) = [];

if ~isempty(gh)
    gh.test_mat_tab.Data{progress,1} = '';
end

```

```

function [time,LCdata,SPdata,Pres_data,SPRaw,LCRaw,reg_vals]=DAQ_read_2comp...
    (DAQ_session)
time = [];
LCdata =[];
SPdata =[];
Pres_data = [];
SPRaw = [];
LCRaw = [];
reg_vals = [];

global StopTest Stop_Session

% Read data
if DAQ_session.NumScansAvailable < round(.1*DAQ_session.Rate)
    dat = [];
    while size(dat,1) < 2
        pause(0)
        [dat,ts,st] =
read(DAQ_session,round(.1*DAQ_session.Rate),'OutputFormat','Matrix');
    end
else
    [dat,ts,st] = read(DAQ_session,'all','OutputFormat','Matrix');
end

daq_data = mean(dat,1);

% Get log file id
fid = DAQ_session.UserData.fid;

% If test hasn't been stopped
if ~Stop_Session

    % Get inputs
    P_Cal = DAQ_session.UserData.P_Cal;
    SP_Cal = DAQ_session.UserData.SP_Cal;
    LC_Cal = DAQ_session.UserData.LC_Cal;
    SP_triang = DAQ_session.UserData.SP_triang;
    lc_ind = DAQ_session.UserData.lc_ind;
    sp_ind = DAQ_session.UserData.sp_ind;
    p_ind = DAQ_session.UserData.p_ind;
    max_load = DAQ_session.UserData.max_load;
    scale_SP = DAQ_session.UserData.scale_SP;

    lc_uz = DAQ_session.UserData.lcs_unzeroed;
    lc_des = DAQ_session.UserData.lc_des;

    sp0 = DAQ_session.UserData.sp0;

    tol = 0.02;
    target_press = DAQ_session.UserData.target_press;
    press_tol = DAQ_session.UserData.press_tol;
    test_loc = DAQ_session.UserData.test_loc;

```

```

d2 = DAQ_session.UserData.d2;
do_table = DAQ_session.UserData.do_table;

if do_table
    try
        gh = guihandles(disp_dat);
    catch
        gh = [];
    end
end

SP_min=SP_triang(1,:);
SP_max=SP_triang(2,:);

% Min + tol*range
SP_min_tol = (1 - tol).*SP_min + tol.*SP_max;

% Max - tol*range
SP_max_tol = (1 - tol).*SP_max - tol.*SP_min;

% Pressure transducer calibration
p_slope=P_Cal(2);
p_int=P_Cal(1);

% Process pressure and get pressure regulator value
if ~isempty(p_ind)
    Pressure_raw = daq_data(:,p_ind);
    Pres_data = Pressure_raw*p_slope + p_int;
    if ~isempty(target_press)
        press_diff = Pres_data - target_press;
        old_press = d2.UserData.old_reg(1:2);
        if ~sum(old_press)
            reg_value = logical(([1,0].*(press_diff > 0) + [0,1].*...
                (press_diff < 0)).*(abs(press_diff) > press_tol));
        else
            reg_value = old_press.*((press_diff > 0) == old_press(1));
        end

        d2.UserData.old_press = reg_value;
    else
        reg_value = [false,false];
    end
end

else
    reg_value = [false,false];
    Pres_data = 0;
end

% Check if cameras need to be triggered
if ~isempty(DAQ_session.UserData.pho_start) && ~DAQ_session.UserData.pho_trig...
    && toc(DAQ_session.UserData.pho_start) > ...
    DAQ_session.UserData.pho_ct/DAQ_session.UserData.pho_freq
    pho_trig = true;

```

```

        DAQ_session.UserData.pho_ct = DAQ_session.UserData.pho_ct + 1;
    else
        pho_trig = false;
    end
    DAQ_session.UserData.pho_trig = pho_trig;

    % Write to digital output card
    reg_vals = [reg_value, pho_trig];
    if sum(reg_vals == d2.UserData.old_reg) ~= length(reg_vals)
        write(d2, reg_vals)
        d2.UserData.old_reg = reg_vals;
    end

    % Read time
    try
        time = datetime(st, 'ConvertFrom', 'datenum') + seconds(ts(end));
    catch ex
        size(dat)
        rethrow(ex)
    end

    % Process lc data
    if ~ isempty(lc_ind)
        LCRaw = daq_data(:, lc_ind);
        LCdata = LCRaw.*(LC_Cal(2,:)) + (LC_Cal(1,:));
        % Zero load cells if this is the first run of the function
        if lc_uz
            DAQ_session.UserData.lcs_unzeroed = 0;
            if isempty(lc_des)
                lc_des = zeros(size(LCdata));
            end
            if min(size(lc_des)) == 2
                DAQ_session.UserData.LC_Cal(1,:) = lc_des(1,:);
            else
                lc_offset = lc_des' - LCdata;
                LC_Cal(1,:) = LC_Cal(1,:) + lc_offset;
                DAQ_session.UserData.LC_Cal = LC_Cal;
                DAQ_session.UserData.LC_Offsets = lc_offset;
                cal_folder = [test_loc, '\Load Cell Calibrations'];
                if ~exist(cal_folder, 'dir')
                    mkdir(cal_folder)
                end
                lc_file = [cal_folder '\lc_cal_'
                    datestr(datetime('today'), 'yyyy_mm_dd')];
                [lc_file] = get_unique_filename(lc_file);
                save(lc_file, 'LC_Cal')
            end
            LCdata = LCRaw.*(LC_Cal(2,:)) + (LC_Cal(1,:));
        end

        if ~DAQ_session.UserData.disable_daq_errors
            if any(abs(LCdata) > max_load)

```

```

        StopTest = 1;
        ind = find(LCdata > max_load);
        msg(end + 1) = {'Error! The following load cells have exceeded ',...
            num2str(max_load), ' lbf: '};
        dat(end + 1) = {ind};

        end
    end
    DAQ_session.UserData.cur_load = LCdata;
else
    LCdata = zeros(1,16);
    LCRaw = LCdata;
end

% Process string pot data
if ~isempty(sp_ind)

    SPRaw = daq_data(:,sp_ind);
    SPdata_unscaled = SPRaw.*(SP_Cal(2,:)) + (SP_Cal(1,:));

    if scale_SP

        SPdata = SPdata_unscaled;
        if ~sum(sp0)
            sp0 = SPdata;
            DAQ_session.UserData.sp0 = sp0;
        end
        SPdisp = sp0' - SPdata';
    else
        SPdata = SPdata_unscaled;
        SPdisp = SPdata';
    end

    % Check string pots
    if ~DAQ_session.UserData.disable_daq_errors
        % This logic checks if the stringpots are about to extend past the max,
to
        % prevent damage to the string pots the test will be ended (if the SP
were
        % past 99% of their maximum values.
        max_ch_sp = SPdata_unscaled > SP_max_tol;
        msg = {};
        dat = {};
        if any(max_ch_sp)
            StopTest = 1;
            ind = find(max_ch_sp);
            msg(end + 1) = {'Error! The following string pots have exceeded'...
                'their maximum:'};
            dat(end + 1) = {ind};
        end

        min_ch_sp = SPdata_unscaled < SP_min_tol;
        if any(min_ch_sp)
            StopTest = 1;
            ind = find(min_ch_sp);

```

```

                msg(end + 1) = {'Error! The following string pots have bottomed
out: '};
                dat(end + 1) = {ind};
            end
        end
    else
        SPdata = zeros(1,16);
        SPRaw = SPdata;
        SPdisp = SPdata';
    end

% Update live plots
if DAQ_session.UserData.do_graphs && ~isempty(sp_ind) && ~isempty(lc_ind)

    % Create plots if they dont exist
    if ~isfield(DAQ_session.UserData, 'load_plot')
        time_plot = repmat([time;NaT],length(LCdata),1);
        figure('Position',[1100,10,800,1070]);
        subplot(3,1,1)
        load_plot = [LCdata;nan(size(LCdata))];
        DAQ_session.UserData.load_plot = plot(time_plot,load_plot(:));
        title('Load')
        subplot(3,1,2)
        sp_plot = [SPdisp';nan(size(SPdisp'))];
        DAQ_session.UserData.disp_plot = plot(time_plot,sp_plot(:));
        title('SP Disp')
        subplot(3,1,3)
        err_plot = [zeros(size(LCdata));nan(size(LCdata))];
        DAQ_session.UserData.err_plot = plot(time_plot,err_plot(:));
        title('Error')

    % Zero sp plot and reset
    elseif DAQ_session.UserData.zero_graphs
        time_plot = repmat([time;NaT],length(LCdata),1);
        load_plot = [LCdata;nan(size(LCdata))];
        sp_plot = [SPdisp';nan(size(SPdisp'))];
        DAQ_session.UserData.load_plot.XData = time_plot;
        DAQ_session.UserData.load_plot.YData =load_plot(:);
        DAQ_session.UserData.disp_plot.XData = time_plot;
        DAQ_session.UserData.disp_plot.YData = sp_plot(:);

        % If control is running, plot error
        if ~isempty(DAQ_session.UserData.desired)
            err_plot = [DAQ_session.UserData.cur_type.*SPdisp' + ...
                ~DAQ_session.UserData.cur_type.*LCdata - ...
                DAQ_session.UserData.desired;nan(size(LCdata))];
            DAQ_session.UserData.err_plot.XData = time_plot;
            DAQ_session.UserData.err_plot.YData = err_plot(:);
        end
        DAQ_session.UserData.zero_graphs = 0;

    else % Add data point to stringpot and load cell graphs
        num_act = length(LCdata);
        all_time = DAQ_session.UserData.load_plot.XData;
        end_dat = find(isnat(all_time),1) - 1;

```

```

time_dat = repmat([all_time(1:end_dat),time,NaT],1,num_act);
DAQ_session.UserData.load_plot.XData = time_dat;
DAQ_session.UserData.disp_plot.XData = time_dat;
load_plot = reshape([DAQ_session.UserData.load_plot.YData],[],num_act);
lp = [load_plot(1:end - 1,:);LCdata;nan(1,num_act)];
DAQ_session.UserData.load_plot.YData = lp(:);
sp_plot = reshape([DAQ_session.UserData.disp_plot.YData],[],num_act);
sp = [sp_plot(1:end - 1,:);SPdisp';nan(1,num_act)];
DAQ_session.UserData.disp_plot.YData = sp(:);

% If control is running, plot error
if ~isempty(DAQ_session.UserData.desired)
    DAQ_session.UserData.err_plot.XData = time_dat;
    err_plot = reshape([DAQ_session.UserData.err_plot.YData],[],num_act);
    ep = [err_plot(1:end - 1,:);DAQ_session.UserData.cur_type...
        .*SPdisp' + ~DAQ_session.UserData.cur_type.*LCdata - ...
        DAQ_session.UserData.desired;nan(1,num_act)];
    DAQ_session.UserData.err_plot.YData = ep(:);
end

end

end

% Update gui
if ~StopTest && do_table && ~isempty(gh)
    gh.inst_tab.Data = round(real([LCdata',SPdisp]),3);
    gh.press_txt.String{1} = ['Pressure: ' num2str(real(Pres_data),'%.3f') '
psi'];
    guidata(gh.press_txt,gh)
end

else
    % Stop data acquisition if test is stopped
    if ~ischar(DAQ_session.ScansAvailableFcnCount)
        msg = {'Session stopped!'};
        dat = {};
        write(DAQ_session.UserData.d2,[false,false,false])
        stop(DAQ_session)
        flush(DAQ_session)
    end
end

% Write errors to log if there are any
if StopTest == 1 || Stop_Session == 1
    write2log(fid,msg,dat,gh);
end

```

```

function [ PWM,PID_use ] = PID_IH(
parms,Error_hist,del_t,LC_data,PIDslopes,avg_ld,pwm_con)
% PID - This function calculates the output for the pwm output
% parms-is a row vector of the pid values [ 0 0 0 ]
% del_t is the time step per value
% LC_error_hist - is a matrix of the LC error history.
%      LC1 LC2 LC3 .....  LCn   @t
%      LC1 LC2 LC3 .....  LCn   @t-1
%      .
%      .
%      .
%      LC1 LC2 LC3 .....  LCn   @t-p
%      Where p - is the number of timesteps to integrate
%            n - is the number of loadcells averages
if avg_ld
    load = mean(LC_data(1,:));
else
    load = LC_data(1,:);
end
PID_use=[abs(parms(1)+PIDslopes(1).*parms(1).*load)
         abs(parms(2)+PIDslopes(2).*parms(2).*load)
         abs(parms(3)+PIDslopes(3).*parms(3).*load)];

% During displacement control, reduce reaction of control to 80% for string
% pots that have displaced too much
neg_ch = ones(size(Error_hist));
if parms(1) > .1
neg_ch(Error_hist > 0) = .8;
end

P=-PID_use(1,:).*Error_hist(1,:).*neg_ch(1,:);
I=-PID_use(2,:).*(sum(Error_hist.*neg_ch.*del_t));

D=-PID_use(3,:).*(-Error_hist(1,:)+Error_hist(2,:))./2;

PID_cal=P+I-D.*sign(P+I);

% Determine the PWM output
PWM=PID_cal+0.5 + pwm_con;
PWM(PWM > 0.98) = 0.98;
PWM(PWM < 0.02) = 0.02;
end

function PWM_OUT_write_IH(data,act_ind,DAQ_session)
% Change duty cycle of each actuator

for i = 1:length(act_ind)
    DAQ_session.Channels(act_ind(i)).DutyCycle=data(i);
end

```



```

function test_inputfile_ml_cams
fclose('all');

addpath('G:\My Drive\1728\1728.2\Final Control Code\Controler_4',...
        'G:\My Drive\1728\1728.2\Final Control Code\Controler_4\Controler_Code',...
        'G:\My Drive\1728\1728.2\Final Control Code\GUIs',...
        'G:\My Drive\1728\1728.2',...
        'G:\My Drive\1728\1728.2\Final Control Code\Camera Control',...
        'G:\My Drive\1728\1728.2\Final Control Code\Camera Control\MatLab')

% General test info
if exist('E:\000_New Data','dir')
    inputs.test_loc = 'E:\000_New Data'; %
else
    un = getenv('USERNAME');
    inputs.test_loc = ['C:\Users\'',un, '\Desktop\1728 Test Data'];
end

inputs.use2comp = 1;
inputs.driver_fun = @test_driver_IH_ml_cams;
inputs.gui_fun = @new_gui_mlc_2comp1;
inputs.daq_fun = @DAQ_read_2comp;
inputs.start_test = 1;
inputs.inputfile_path = mfilename('fullpath');

%% Actuator/PID info
inputs.add_act = 1;
inputs.PIDslopes_lc = [-1/600 1/400 1/8000];
inputs.PIDslopes_dc = [1/10000 1/400 1/8000];
inputs.Integr_L = 80;
inputs.shut_down_time = 20;
inputs.PID_PD_mod = 10;
inputs.act_freq = 10;
inputs.avg_ld = 0;
inputs.act_loc = [ones(8,1).*2,[0:7]';ones(8,1).*4,[0:7]'];
inputs.act_loc([5,3],:) = inputs.act_loc([3,5],:);
inputs.act_loc = [ones(size(inputs.act_loc,1),1),inputs.act_loc];
inputs.dc_con = 0;
inputs.dc_con_ramp = 1;

%% Camera stuff
inputs.add_cam = 0;
inputs.temp_freq = 1/2; % Photos/s
inputs.freq = 1;

%% DAQ
% General DAQ
inputs.daq_rate= 1000; % Hz
inputs.disable_daq_errors_setup = 1;
inputs.disable_daq_errors_testing = 1;
inputs.daq_update_rate = 1; % Every x seconds

```

```

inputs.active_daq = [1:16];
inputs.daq_update_rate_cams = 1/3;

% Stringpots
inputs.scale_SP = 0;
inputs.SP_loc = [5 7;6 1;6 2;6 3;6 4;6 7;5 0;5 6;6 6;5 6;5 1;5
                2;5 3;5 4;5 5;6 5;6 0];
inputs.SP_loc = [ones(size(inputs.SP_loc,1),1),inputs.SP_loc];
%inputs.SP_loc(5,:) = [];

% Load cells
inputs.LC_loc = [9 0
7 3
9 5
6 0
9 3
9 6
9 7
9 4
7 2
7 5
7 7
7 0
7 6
7 4
9 1
5 1];
inputs.LC_loc = [ones(size(inputs.LC_loc(:,1))).*2,inputs.LC_loc];
inputs.max_load = ones(1,16).*1800;
inputs.max_load(16) = 1000;
inputs.lc_des = [-0.637111773376890,0.258999359916682,0.551132077331543,...
-13.0481780087501,-10.7248518157188,-2.85109457438926,...
41.5337172046160 - 4.9 - 4.45,-13.8829708961365,-17.5560365488912,...
-8.81533780003131,-18.2795342813920,-18.9364568464148,...
-24.7389437531464,-14.9886758230087,-4.87685742869501,...
-18.9371261223289 + 107;1171857.18000000,1171971.71700000,1165501.01400000,...
1159354.65500000,1162708.40900000,1164674.91800000,1172570.95900000,...
1166968.73900000,1163081.53800000,1165102.82800000,1164123.51300000,...
1166624.32400000,1168441.64800000,1174229.36300000,1160264.76300000,...
1159410.81600000];

% Graphing in gui
inputs.do_graphs_setup = 0;
inputs.do_graphs_testing = 1;

% Table in GUI
inputs.do_table_setup = 1;
inputs.do_table_testing = 0;

% Calibration info
inputs.LC_cal_file = 'G:\My Drive\1728\1728.2\Instrumentation\lc_cals.mat'; %'G:\My
Drive\1728\1728.1\Control\Dans_Code_edited\Controler_4\Insturmentation_Info\lc_cals.m
at';

```

```

inputs.SP_cal_file = 'G:\My
Drive\1728\1728.1\Control\Dans_Code_edited\Controler_4\Insturmentation_Info\sp_cal.s.m
at';
inputs.SP_loc_file = 'G:\My
Drive\1728\1728.1\Control\Dans_Code_edited\Controler_4\Insturmentation_Info\sp_loc_20
21_07_15.mat';
inputs.P_cal_file = 'G:\My
Drive\1728\1728.1\Control\Dans_Code_edited\Controler_4\Insturmentation_Info\press_cal
.mat';

%% Pressure

pn = 20;
% Setup pressure info
inputs.p_loc = [1,8,5];
inputs.target_press_setup = pn;
inputs.press_tol_setup = .1; % psi
inputs.end_press = 5; % psi

% Inflation pressure info
inputs.save_infl_pho = 0;
inputs.infl_press = 5;
inputs.wait_time_infl = 0;

% Testing pressure info
inputs.press_tol = .1;
inputs.drain_val = 1;

% The following 5 vectors must have length = size(test_mat,3)
n = 1;
inputs.do_press = ones(n,1);
inputs.save_press_pho = zeros(n,1);
inputs.wait_timeM = ones(n,1).*0;
inputs.PressV = pn;%[10,15,15,20,20];%ones(n,1).*pn;
inputs.deflate = zeros(n,1);
inputs.con_press = 1;

%% Test matrix
inputs.test_mat = [1, 0, 25, 60, 0.0203558, 0.00208759, 0.000170923
    1, 0, 35, 60, 0.0203558, 0.00208759, 0.000170923
    2, 0, .375, 3*60, 1.5, .2, 0.03];

%% Check lengths of variables
ch_vars = {inputs.PressV;inputs.do_press;inputs.save_press_pho;...
    inputs.deflate;inputs.wait_timeM};

len_vars = cellfun(@length,ch_vars);
len_ch = len_vars ~= size(inputs.test_mat,3);
if sum(len_ch)
    lc = find(len_ch);
    var_names = {'pressV';'do_press';'save_press_pho';'deflate';'wait_timeM'};
    bad_vars = '';
    for i = 1:sum(len_ch)
        bad_vars = [bad_vars,var_names{lc(i)}, ', '];
    end
end

```

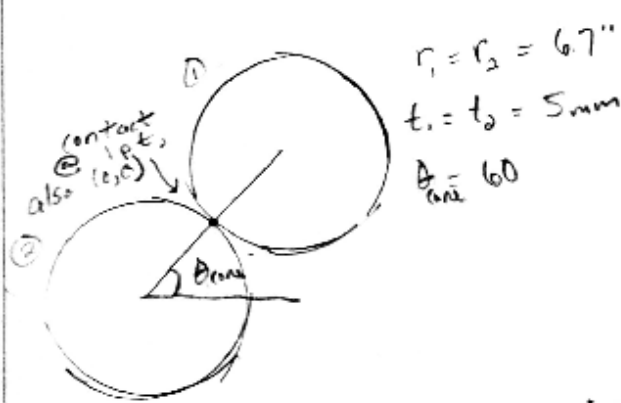
```
    end
    bad_vars = bad_vars(1:end - 2);
    error_str = ['The following variables are not the correct lengths: ' bad_vars];
    error(error_str)
end

%% Run gui
st = dbstack;

if length(st) == 1
    inputs.gui_fun(inputs);
end
```

APPENDIX D SHEAR CENTER CALCULATION
 Following (Megson 2010).

$\sum M_{ext} = \sum M_{int}$
 $y_{sc} \cdot S_x = \int p q_s ds$
 $q_s = q_1 + q_2$
 $q_s = \left(\frac{S_x I_{xx} - S_y I_{xy}}{I_{xx} I_{yy} - I_{xy}^2} \right) \int t x ds - \left(\frac{S_y I_{yy} - S_x I_{xy}}{I_{xx} I_{yy} - I_{xy}^2} \right) \int t y ds$
 $S_y = 0$ and I_{xy} negligible (see MC sheet)
 t is constant
 $q_1 = \frac{S_x \cdot t}{I_{yy}} \int x ds$



$r_1 = r_2 = 6.7''$
 $t_1 = t_2 = 5 \text{ mm}$
 $A = 60$

Convert to polar coordinates + do each circle separately

Upper:

$x = r \cos \theta + r \cos \theta_{con}$
 $ds = r d\theta$
 $q_1 = \frac{S_x \cdot t}{I_{yy}} \int_0^{\theta} (r \cos \theta + \frac{r}{2}) r d\theta = \frac{S_x \cdot t \cdot r^2}{I_{yy}} (\sin \theta + \frac{\theta}{2})$

Lower:

$$x = r \cos \theta = r \cos \theta_{\text{lower}}$$

$$ds = r d\theta$$

$$q_{s, \text{lower}} = \int_0^{2\pi} (r \cos \theta - \frac{t}{2}) r d\theta \cdot \frac{S_x \cdot t}{I_{yy}} = \frac{S_x \cdot t \cdot r^2}{I_{yy}} (\sin \theta - \frac{\theta}{2})$$

$$q_{s,0} = - \frac{\int q_s ds}{\int ds}$$

$$\int ds = \int_0^{2\pi} r d\theta = 2\pi r : \text{circumference}$$

$$\text{Upper: } q_{s, \text{upper}} = - \frac{\int_0^{2\pi} \frac{S_x \cdot t \cdot r^2}{I_{yy}} (\sin \theta + \frac{\theta}{2}) r d\theta}{2\pi r} = - \frac{S_x \cdot t \cdot r^2}{I_{yy}} \left(\frac{\pi}{2} \right)$$

$$\text{Lower: } q_{s, \text{lower}} = - \frac{\int_0^{2\pi} \frac{S_x \cdot t \cdot r^2}{I_{yy}} (\sin \theta - \frac{\theta}{2}) r d\theta}{2\pi r} = \frac{S_x \cdot t \cdot r^2}{I_{yy}} \left(\frac{\pi}{2} \right)$$

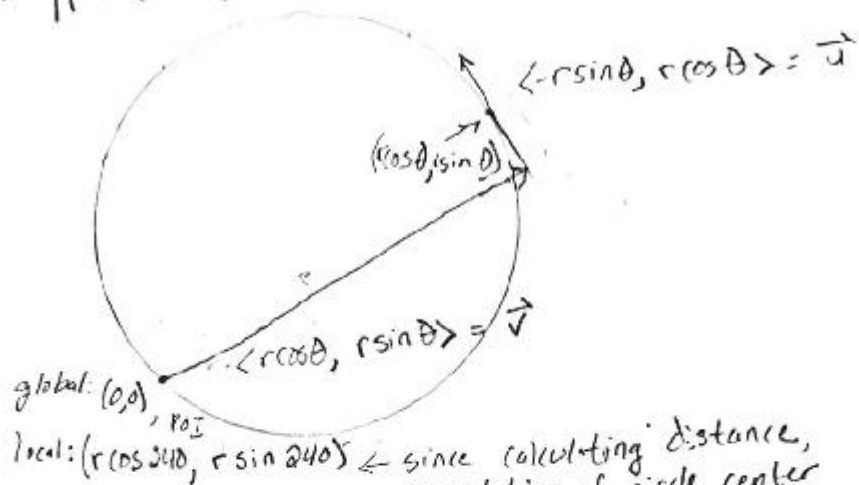
$$\int p q_s ds = \int p q_s ds + 2A q_{s,0}$$

p : \perp distance from line of action of shear flow to point of interest \rightarrow where moments are summed

choose $(0,0)$ as POI

Will find p on next page

For upper circle, using polar coordinates



local: $(r \cos 240, r \sin 240)$ ← since calculating distance, translation of circle center doesn't matter (in all terms, will cancel out)

At an arbitrary point on X-Y $(r \cos \theta, r \sin \theta)$, the direction of g_s is $\vec{u} = \langle -r \sin \theta, r \cos \theta \rangle$

A vector \perp to \vec{u} is $\vec{v} = \langle r \cos \theta, r \sin \theta \rangle$, and it must go thru $(r \cos 240, r \sin 240)$.

To find P , solve for b :

$$a \cdot \vec{u} + (r \cos \theta, r \sin \theta) = b \cdot \vec{v} + (r \cos 240, r \sin 240)$$

$$p = \|b \cdot \vec{v}\| = |b \cdot r|$$

where a, b are scalars

Repeat for bottom circle except:

$$POI = (r \cos \theta, r \sin \theta)$$

From matlab:

$$P_{upper} = |r (\cos(\theta - \frac{\pi}{2}) + 1)|$$

$$P_{lower} = |r (\cos(\theta - \frac{\pi}{2}) - 1)| \quad P_{upper} \cdot q_{b-upper}$$

$$S_x \cdot y_{sc} = \frac{S_x t r^2}{I_{yy}} \left(\int_0^{2\pi} |r (\cos(\theta - \frac{\pi}{2}) + 1)| \cdot (\sin \theta + \frac{\theta}{2}) + \dots \right)$$

$$\underbrace{|r (\cos(\theta - \frac{\pi}{2}) - 1)| \cdot (\sin \theta - \frac{\theta}{2})}_{P_{lower} \cdot q_{b-lower}} \underbrace{r \delta \theta}_{ds} + 2\pi r^2 \cdot \left(\frac{\pi}{2} - \frac{\pi}{2} \right)$$

$$P_{lower} \cdot q_{b-lower}$$

S_x cancels, plug into Matlab

$$y_{sc} \approx 0$$

Inputs and preliminary calculations

$$\theta_{cone} := 60 \text{ deg}$$

$$\theta_{cord} := 60 \text{ deg}$$

$$t := 0.5 \text{ mm}$$

$$r := 170 \text{ mm}$$

$$r_0 := r - t = 6.673 \text{ in}$$

$$R_1 := 1.779 \text{ m}$$

$$R_2 := R_1 + r \cdot \cos(\theta_{cone}) = 73.386 \text{ in}$$

$$a := \frac{1}{4} \text{ in}$$

+

$$b := a$$

$$A_{tor} := \pi \cdot (r^2 - r_0^2) = 0.827 \text{ in}^2$$

Calculate E's and transform section

$$E_{tor} := \frac{13 \frac{N}{mm}}{t}$$

$$E_{cord} := \frac{\frac{6000 N}{\frac{\pi \cdot a^2}{4}}}{.02 - .01}$$

$$n := \frac{E_{cord}}{E_{tor}} = 728.686$$

$$b := n \cdot b = 182.172 \text{ in}$$

$$A_{cord} := \frac{\pi}{4} \cdot a \cdot b = 35.769 \text{ in}^2$$

Centroid of full cross section (see hand calc)

$$x_{bar} := \frac{r \cdot (2 \cdot A_{tor} \cdot (1 + \cos(\theta_{cone})) + 4 \cdot A_{cord} \cdot (1 + \cos(\theta_{cone}) + \cos(\theta_{cord})))}{2 \cdot A_{tor} + 4 \cdot A_{cord}} = 13.348 \text{ in}$$

$$y_{bar} := r + r \cdot \sin(\theta_{cone}) = 12.489 \text{ in}$$

MOI about each shape's centroid

$$I_{c_tor} := \pi \cdot r^3 \cdot t = 18.541 \text{ in}^4$$

$$I_{c_cord_x} := \frac{\pi}{4} \cdot a \cdot b^3 = (1.187 \cdot 10^6) \text{ in}^4$$

Calculate Ix (it ended up being unneeded because Ixy is negligible)

$$I_x := 2 \cdot I_{c_tor} + 4 \cdot I_{c_cord_x} + 2 \cdot A_{tor} \cdot (r \cdot \sin(\theta_{cone}))^2 = (4.748 \cdot 10^6) \text{ in}^4$$

$$I_x := I_x + A_{cord} \cdot 2 \cdot r^2 \cdot ((\sin(\theta_{cone}) - \sin(\theta_{cord}))^2 + (\sin(\theta_{cone}) + \sin(\theta_{cord}))^2) = (4.758 \cdot 10^6) \text{ in}^4$$

Calculate Iy

$$I_y := 2 \cdot I_{c_tor} + 4 \cdot I_{c_cord_x} + A_{tor} \cdot ((x_{bar} - r)^2 + (x_{bar} - r - r \cdot 2 \cdot \cos(\theta_{cone}))^2)$$

$$I_y := I_y + 2 \cdot A_{cord} \cdot ((x_{bar} - r - r \cdot \cos(\theta_{cord}))^2 + (x_{bar} - r - r \cdot 2 \cdot \cos(\theta_{cone}) - r \cdot \cos(\theta_{cord}))^2)$$

$$I_y = (4.75 \cdot 10^6) \text{ in}^4$$

Calculate Ixy (because the shapes are symmetric, it is just sum(Axy))

$$I_{xy} := A_{tor} \cdot r \cdot (-\sin(\theta_{cone}) \cdot (r - x_{bar}) + \sin(\theta_{cone}) \cdot (r + 2 \cdot r \cdot \cos(\theta_{cone}) - x_{bar}))$$

$$I_{xy} := I_{xy} + A_{cord} \cdot r \cdot (\sin(\theta_{cone}) + \sin(\theta_{cord})) \cdot (r + 2 \cdot r \cdot \cos(\theta_{cone}) + r \cdot \cos(\theta_{cord}) - x_{bar})$$

$$I_{xy} := I_{xy} + A_{cord} \cdot r \cdot (\sin(\theta_{cone}) - \sin(\theta_{cord})) \cdot (r + 2 \cdot r \cdot \cos(\theta_{cone}) + r \cdot \cos(\theta_{cord}) - x_{bar})$$

$$I_{xy} := I_{xy} + A_{cord} \cdot r \cdot (-\sin(\theta_{cone}) + \sin(\theta_{cord})) \cdot (r + r \cdot \cos(\theta_{cord}) - x_{bar})$$

$$I_{xy} := I_{xy} + A_{cord} \cdot r \cdot (-\sin(\theta_{cone}) - \sin(\theta_{cord})) \cdot (r + r \cdot \cos(\theta_{cord}) - x_{bar}) = (2.807 \cdot 10^3) \text{ in}^4$$

Check the term of the shear center equation that includes Ixy

$$ch := I_x \cdot I_y - I_{xy}^2 = (2.26 \cdot 10^{13}) \text{ in}^8$$

$$ch2 := \frac{(ch - I_x \cdot I_y)}{I_x \cdot I_y} = -3.487 \cdot 10^{-7} \quad \text{Ixy is negligible}$$

APPENDIX E LOADING CALCULATION

It was determined that the specimen could not be loaded horizontally through the shear center.

This meant that there would be a net vertical reaction on the specimen and/or applied torque due to not loading through the shear center. To choose a height for the torus stands, angle of twist of the specimen cross section and the vertical reaction on the torus stands were desired. This meant the applied forces on the torus needed to be determined. To do this, a system of three equations was developed and then solved using MATLAB. Refer to Figure 68 for more information.

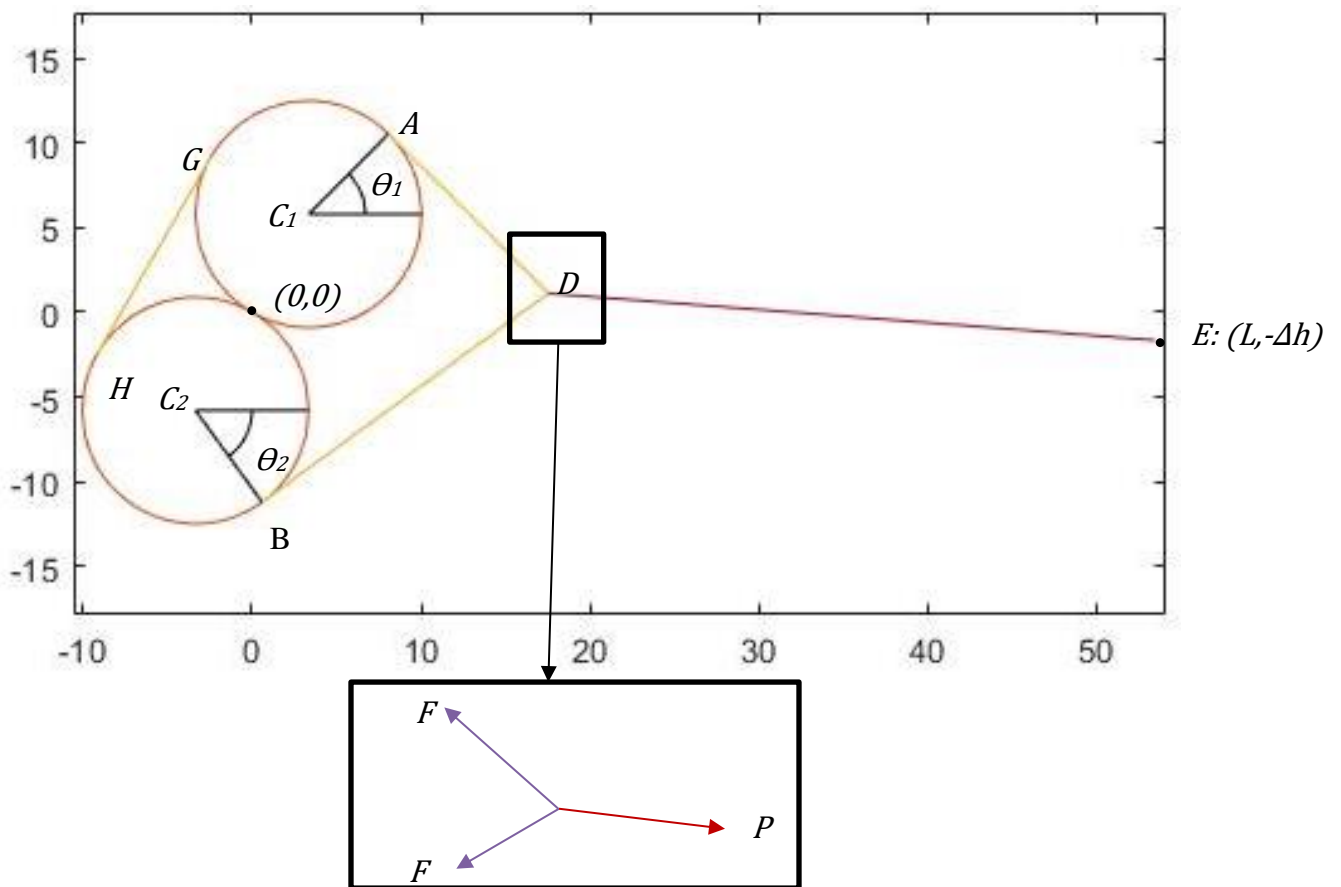


Figure 68. Symbol definitions

The first two equations were the sum of forces in the x and y directions at point *D* are equal to zero. The self-weight of all components was ignored. The third equation was the length of the strap was equal to six and a half feet. The strap consisted of the yellow line segments *AD*, *BD*, *GH*

and arcs AG and BH . The three unknowns were θ_1 , θ_2 and the strap force, F . The angles are positive in the counter-clockwise direction and range from $-\pi$ to π radians. The strap only carried axial tension, and was both in contact and tangent with the tori at points A and B. The origin was set as the tangent point of the two tori. The force in the load cable, P , the radius of the tori, r_{tor} , the centers of the tori C_1 and C_2 , and the location of point E were all known. P can be set to any reasonable value of cable force that is expected to be occur during a load test, since it has no effect on the locations of points A , B or D . The radius and centers of the tori were constants. The coordinates of Point E are defined below in Eq. 1.

$$(E_x, E_y) = (L, -\Delta h) \quad \text{Equation 9}$$

L is the horizontal distance between the tangent point of the tori and the top of the pulley. It was a constant obtained from the Solidworks model of the test fixture. Δh was the vertical distance from the top of the pulley to the tangent point of the tori and is therefore defined by the stand height.

To write the equations for sum of the forces, the coordinates of points A , B and D must be found as functions of θ_1 and θ_2 . The locations of points A and B are given in Equation 10 and Equation 11 below.

$$(A_x, A_y) = (r_{tor} * \cos(\theta_1) + C_{1x}, r_{tor} * \sin(\theta_1) + C_{1y}) \quad \text{Equation 10}$$

$$(B_x, B_y) = (r_{tor} * \cos(\theta_2) + C_{2x}, r_{tor} * \sin(\theta_2) + C_{2y}) \quad \text{Equation 11}$$

The slopes of line segments AD and BD are perpendicular to the slopes of line segments C_1A and C_2B and are therefore the negative of the cotangent of θ_1 and θ_2 , respectively. The equations for the lines through AD and BD are then given by Equation 12 and Equation 13.

$$\overline{AD}: y = -\cot(\theta_1) * (x - A_x) + A_y \quad \text{Equation 12}$$

$$\overline{BD}: y = -\cot(\theta_2) * (x - B_x) + B_y \quad \text{Equation 13}$$

Substituting D_x and D_y for x and y in equations Equation 12 and Equation 13 and then solving the resulting system gives Equation 14 and Equation 15.

$$D_x = \frac{A_x * \cot(\theta_1) + A_y - B_x * \cot(\theta_2) - B_y}{\cot(\theta_1) - \cot(\theta_2)} \quad \text{Equation 14}$$

$$D_y = -\cot(\theta_1) * (D_x - A_x) + A_y \quad \text{Equation 15}$$

Now the forces at point D can be summed resulting in Equation 16 and Equation 17.

$$\sum f_x = \left(\frac{A_x - D_x}{\sqrt{(A_x - D_x)^2 + (A_y - D_y)^2}} + \frac{B_x - D_x}{\sqrt{(B_x - D_x)^2 + (B_y - D_y)^2}} \right) \dots \quad \text{Equation 16}$$

$$* F + \frac{L - D_x}{\sqrt{(L - D_x)^2 + (-\Delta h - D_y)^2}} * P = 0$$

$$\sum f_y = \left(\frac{A_y - D_y}{\sqrt{(A_x - D_x)^2 + (A_y - D_y)^2}} + \frac{B_y - D_y}{\sqrt{(B_x - D_x)^2 + (B_y - D_y)^2}} \right) \dots \quad \text{Equation 17}$$

$$* F + \frac{-\Delta h - D_y}{\sqrt{(L - D_x)^2 + (-\Delta h - D_y)^2}} * P = 0$$

To write the third equation, the lengths of line segments AD , BD , GH and arcs AG and BH are required. The lengths of AD and BD can be calculated from the coordinates of their respective endpoints but to find the remaining lengths the coordinates of G and H must be obtained. Please refer to Figure 69 below.

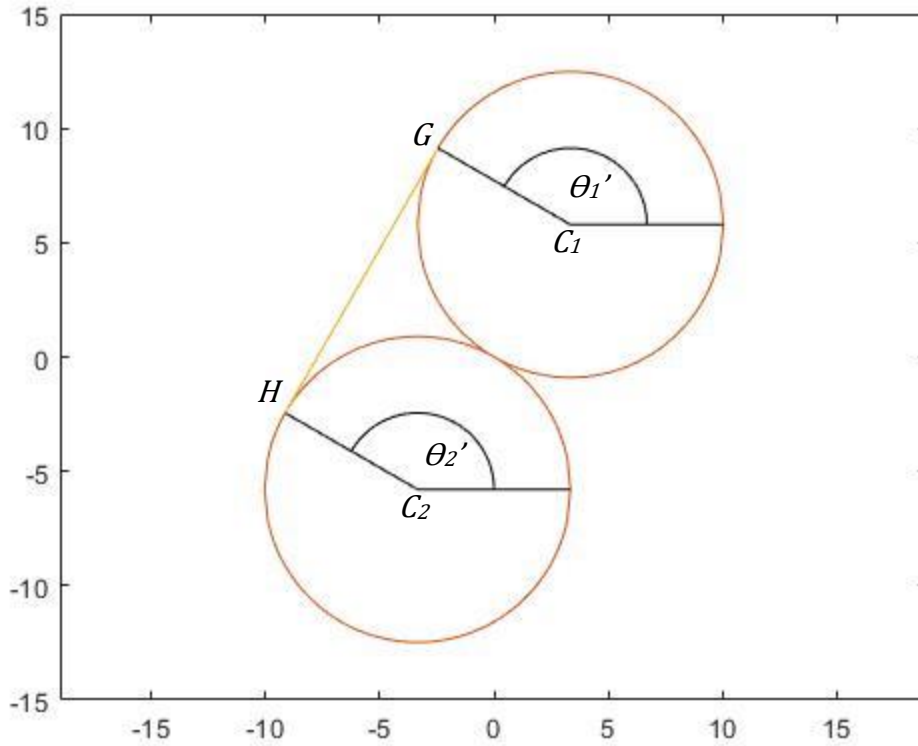


Figure 69. Symbol definitions for the determination of G and H

The strap must be in contact and tangent to the tori at G and H . Since the slope of GH is constant, this means $\theta_1' = \theta_2' = \theta$. The coordinates of G and H are given by Equation 18 and Equation 19.

$$(G_x, G_y) = (r_{tor} * \cos(\theta) + C_{1x}, r_{tor} * \sin(\theta) + C_{1y}) \quad \text{Equation 18}$$

$$(H_x, H_y) = (r_{tor} * \cos(\theta) + C_{2x}, r_{tor} * \sin(\theta) + C_{2y}) \quad \text{Equation 19}$$

The slope of GH , m , is given by Equation 20-a.

$$m = \frac{r_{tor} * \sin(\theta) + C_{1y} - r_{tor} * \sin(\theta) - C_{2y}}{r_{tor} * \cos(\theta) + C_{1x} - r_{tor} * \cos(\theta) - C_{2x}} \quad \text{Equation 20-a}$$

This simplifies to Equation 20-b.

$$m = \frac{C_{1y} - C_{2y}}{C_{1x} - C_{2x}} \quad \text{Equation 20-b}$$

The slope of GH is equal to the slope of C_1C_2 , which is constant at $\pi/3$ rad. This means $\theta = \pi/3 + \pi/2 = 5\pi/6$ rad. The length of GH is equal to the distance between the centers of the tori which is $2*r_{tor}$.

The last lengths needed for the length of the strap is the lengths of the arcs AG and BH . These are equal to the change in angle multiplied by the radius of the torus. This means the length is given by Equation 21.

$$L_{arcs} = r_{tor} * (\theta - \theta_1 + (2\pi + \theta_2) - \theta) = r_{tor} * (2\pi + \theta_2 - \theta_1) \quad \text{Equation 21}$$

Note the 2π is added because θ_2 varies from $-\pi$ to π instead of 0 to 2π .

The total length of the strap is then given by Equation 22.

$$L_{strap} = \sqrt{(A_x - D_x)^2 + (A_y - D_y)^2} + \sqrt{(B_x - D_x)^2 + (B_y - D_y)^2} \dots \quad \text{Equation 22}$$

$$+ 2 * r_{tor} + r_{tor} * (2\pi + \theta_2 - \theta_1) = 78 \text{ in}$$

The equations for the sums of the forces and the length of the strap can be solved simultaneously using the built-in function `vpasolve` in MATLAB. θ_1 , θ_2 , and F were limited to the intervals $[-\pi/4, \pi/2]$, $[-\pi/2, \pi/4]$, and $[0, P]$, respectively.

With the solutions for θ_1 and θ_2 , the components of P in the horizontal and vertical directions can be calculated using Equation 23 and Equation 24.

$$P_x = \frac{L - D_x}{\sqrt{(L - D_x)^2 + (-\Delta h - D_y)^2}} * P \quad \text{Equation 23}$$

$$P_y = \frac{-\Delta h - D_y}{\sqrt{(L - D_x)^2 + (-\Delta h - D_y)^2}} * P \quad \text{Equation 24}$$

The reaction on a torus stand, which is four times the vertical component of the load cable force P , can be calculated using Equation 25.

$$R = 4 * P_y \quad \text{Equation 25}$$

The multiplier of 4 is due to the test setup of 16 load cables and 4 evenly spaced torus stands.

The applied moment on the specimen cross section at a load cable is the horizontal component of P multiplied by the vertical distance of the line of action of P to the shear center, e_y , as shown in Equation 26.

$$M_z = P_x * e_y \quad \text{Equation 26}$$

The shear center of the paired tori cross section is at the tangent point of the two tori as derived in the previous progress report. Since the origin was set at the tangent point, the vertical distance of the line of action of P to the shear center is the y-intercept of the line through points D and E . This is given by Equation 27.

$$e_y = D_y - \frac{D_y + \Delta h}{D_x - L} * D_x \quad \text{Equation 27}$$

The next step is to calculate the angle of twist, ϕ , using Equation 28 which is from basic mechanics of materials.

$$\phi' = \frac{M_z}{G * K_T} \quad \text{Equation 28}$$

Here G is the shear modulus and K_T is the torsional constant of the cross section.

The shear modulus is dependent on the internal pressure of the specimen and was determined through previous testing (Clapp, 2016a). It was reported as a membrane resultant, G_{mem} which is related to G as shown in Equation 29. t is the thickness of the torus wall.

$$G_{mem} = \frac{G}{t} \quad \text{Equation 29}$$

Assuming the cross section is thin walled and consists of two separated continuous cells, the torsion constant is the sum of the torsion constants of each torus (Heins, 1975). This is twice the torsion constant of a thin-walled tube and is given by Equation 30.

$$K_T = 4\pi * r_{tor}^3 * t \quad \text{Equation 30}$$

The 16 cable loads were simplified into a uniformly distributed load by dividing by the tributary length, L_{trib} , which is a sixteenth of the circumference of the circle passing through the shear center or as given in Equation 31.

$$L_{trib} = \frac{R_{tp} * \pi}{8} \quad \text{Equation 31}$$

Here R_{tp} is the major radius of the specimen to the tangent point of the two tori.

This means that rate of angle of twist and the angle of twist are given by Equation 32 and Equation 33, respectively.

$$\phi' = \frac{\phi}{L_{trib}} \quad \text{Equation 32}$$

$$\phi = \frac{M_z * L_{trib}}{G_{mem} * \frac{K_T}{t}} \quad \text{Equation 33}$$

```

syms th1 th2 F tx1 tx2 ty1 ty2

% Inputs
P = 1;

R_pulley = 26-2.1;

r_tor = 6.7;

strapL0 = 72 + 3.125*2;

R_T5 = 80.7;

% Shear modulus and torsion constant
G = [320,420,468].*25.4.*.225;

KT = 4*pi*r_tor^3;

% Torus centers
C1x = r_tor*cosd(60);
C1y = r_tor*sind(60);

C2x = -r_tor*cosd(60);
C2y = -r_tor*sind(60);

% Radius of circle through tangent points
R_tp = R_T5 + C2x;

% X location of top of pulley
L = R_tp - R_pulley;

% Coordinates of where strap comes off tori (A and B)
Ax = r_tor*cos(th1) + C1x;
Ay = r_tor*sin(th1) + C1y;

Bx = r_tor*cos(th2) + C2x;
By = r_tor*sin(th2) + C2y;

% Coordinates of strap intersection point (D)
Dx = (Ax*cot(th1) - Bx*cot(th2) + Ay - By)/(cot(th1) - cot(th2));

Dy = -cot(th1)*(Dx - Ax) + Ay;

% Lengths of AD and BD
dist1 = norm([Ax - Dx,Ay - Dy]);

dist2 = norm([Bx - Dx,By - Dy]);

% Length of arcs
L_arcs = (th2 + 2*pi - th1).*r_tor;

% Eqn for length of strap
L_strap = dist1 + dist2 + L_arcs + 2.*r_tor == strapL0;

```

```

% Delta h vector
dha = linspace(-3,9,50);

for i = 1:length(dha)

    % Current delta h
    delta_h = dha(i);

    % Length of DE
    dist3 = norm([L - Dx,-delta_h - Dy]);

    % Sum of the forces
    fx = (Ax - Dx)./dist1.*F + (Bx - Dx)./dist2.*F + P.*(L - Dx)./dist3 == 0;

    fy = (Ay - Dy)./dist1.*F + (By - Dy)./dist2.*F + P.*(-delta_h - ...
        Dy)./dist3 == 0;

    % Create and solve system
    eqns = [fx,fy,L_strap];

    sol = vpasolve(eqns,[th1,th2,F],[-pi/4,pi/2;-pi/2,pi/4;0,P]);

    % Evaluate variables needed for further calculations
    plot_var = [Ax,Ay,Bx,By,Dx,Dy];

    pv = subs(plot_var,sol);

    % Calculate eccentricity for torque
    ey = double(pv(6) - (pv(6) + delta_h)/(pv(5) - L)*pv(5));

    % Calculate components of P
    Px = double(subs(P.*(L - Dx)./dist3,sol));
    Py = double(subs(P.*(-delta_h - Dy)./dist3,sol));

    % Calculate applied torque and angle of twist
    Mz = Px*ey;
    phi(i,:) = R_tp*pi/8*Mz./G./KT;

    % Calculate reaction on the stand
    R(i,1) = -4*Py;

    % Plot
    if i == 20

        % Create and plot tori
        eqn_t1 = (tx1 - C1x).^2 + (ty1 - C1y).^2;
        eqn_t2 = (tx2 - C2x).^2 + (ty2 - C2y).^2;

        t1 = solve(eqn_t1 == r_tor^2,ty1);
        x_plot = linspace(C1x - r_tor,C1x + r_tor);
        y_plot = double(subs(t1,tx1,x_plot));
        figure(2)
    end
end

```

```

clf
plot(x_plot,y_plot,'Color',[0.8500 0.3250 0.0980])
t2 = solve(eqn_t2 == r_tor^2,ty2);
x_plot2 = linspace(C2x - r_tor,C2x + r_tor);
y_plot2 = double(subs(t2,tx2,x_plot2));
hold on
plot(x_plot2,y_plot2,'Color',[0.8500 0.3250 0.0980])

% Plot AD and BD
plot([pv(3),pv(5)], [pv(4),pv(6)], 'Color',[0.9290 0.6940 0.1250])
plot([pv(1),pv(5)], [pv(2),pv(6)], 'Color',[0.9290 0.6940 0.1250])

% Plot load cable (DE)
x_lc = [L,double(pv(5))];
y_lc = [-delta_h,double(pv(6))];
plot(x_lc,y_lc)

% Plot GH
strap_pts = [cosd(150)*r_tor + [C1x;C2x],sind(150)*r_tor + ...
            [C1y;C2y]];

plot(strap_pts(:,1),strap_pts(:,2),'Color',[0.9290 0.6940 0.1250])

% Plot lines and arcs to define thetas
th1x = [pv(1),C1x,x_plot(end)];
th2x = [pv(3),C2x,x_plot2(end)];
th1y = [pv(2),C1y,y_plot(end)];
th2y = [pv(4),C2y,y_plot2(end)];

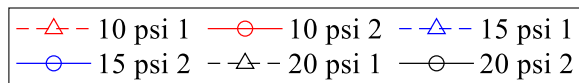
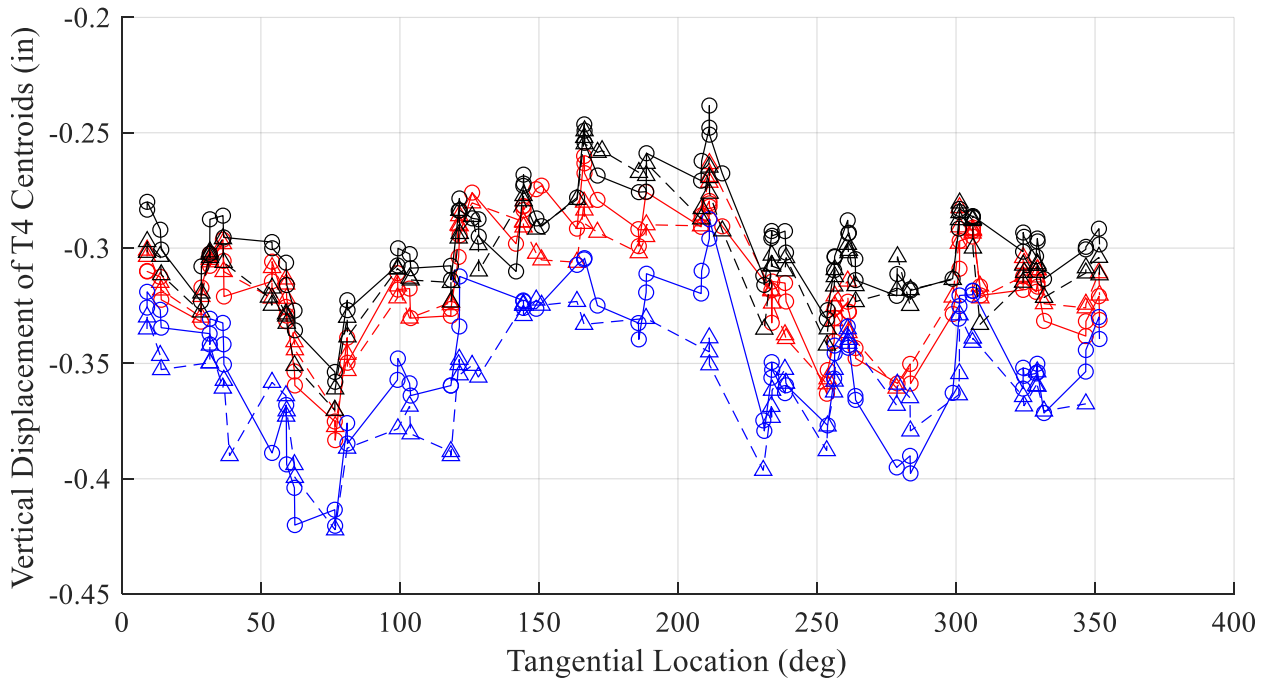
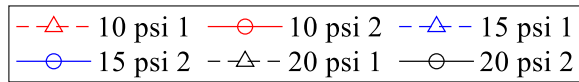
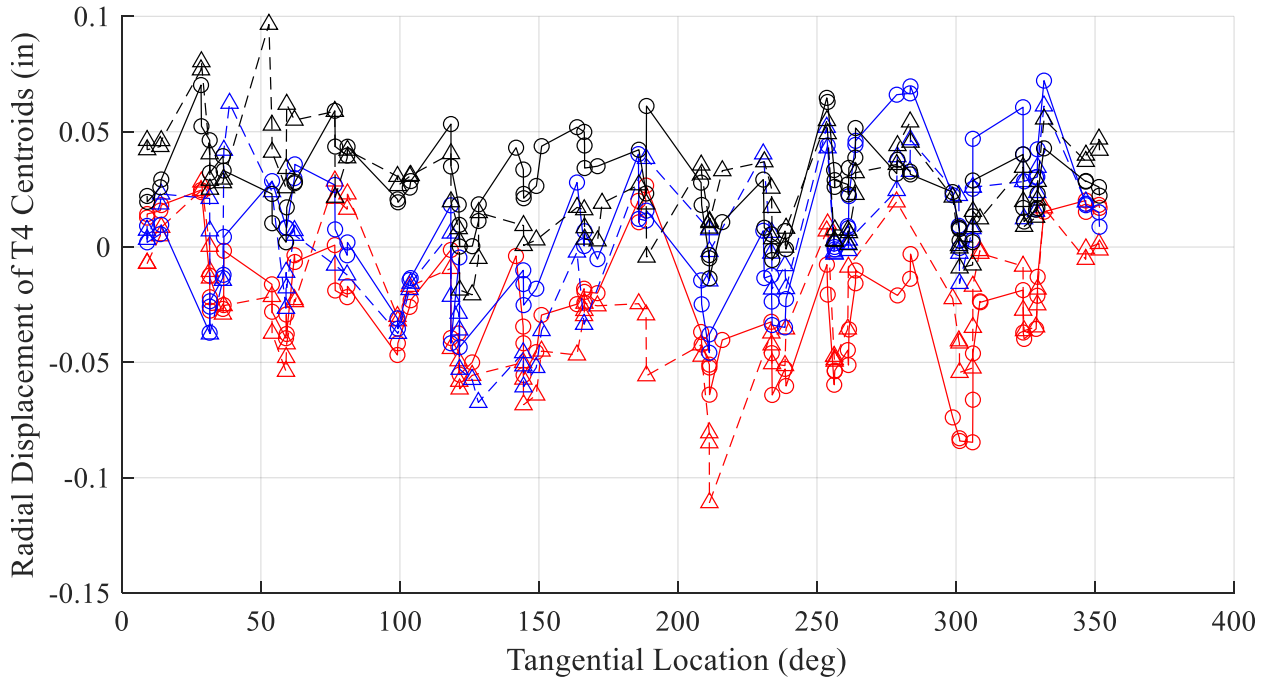
plot(th1x,th1y,'k')
plot(th2x,th2y,'k')

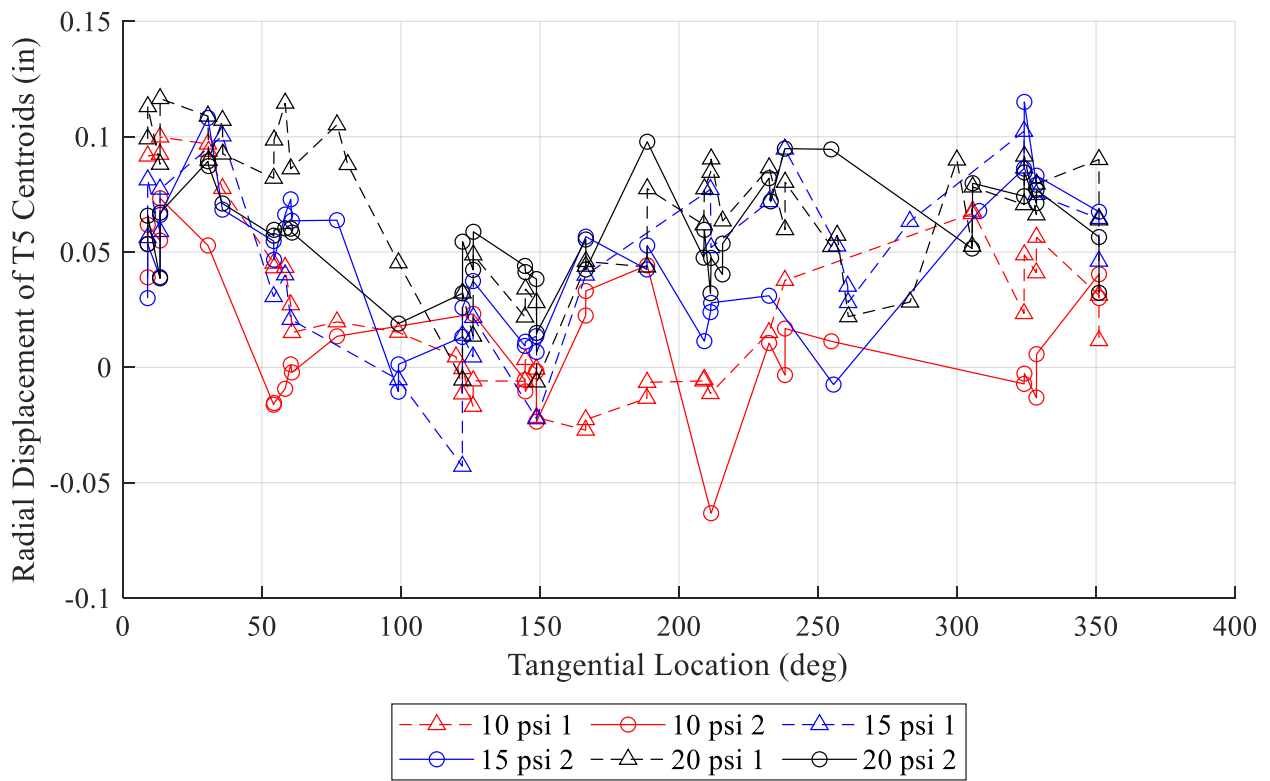
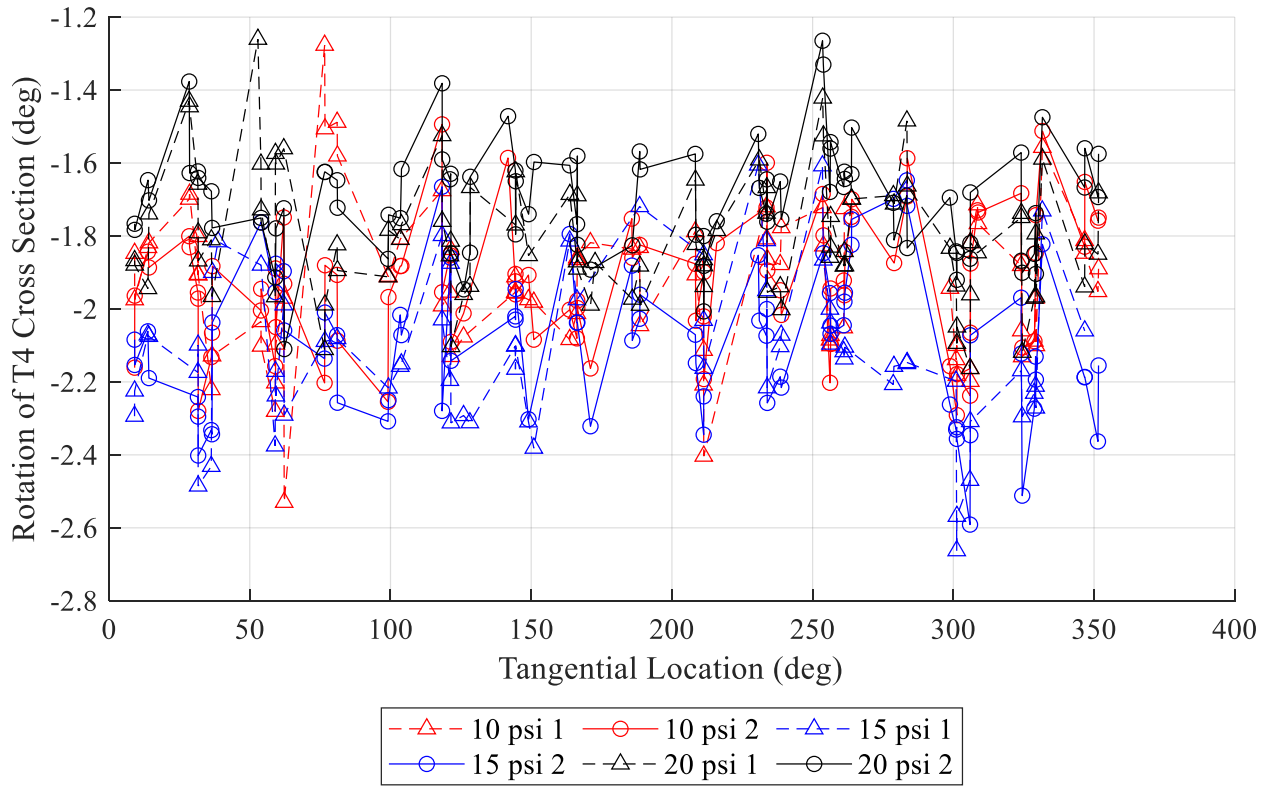
th1_plot = linspace(0,double(sol.th1));
x_th1 = r_tor/2*cos(th1_plot) + C1x;
y_th1 = r_tor/2*sin(th1_plot) + C1y;

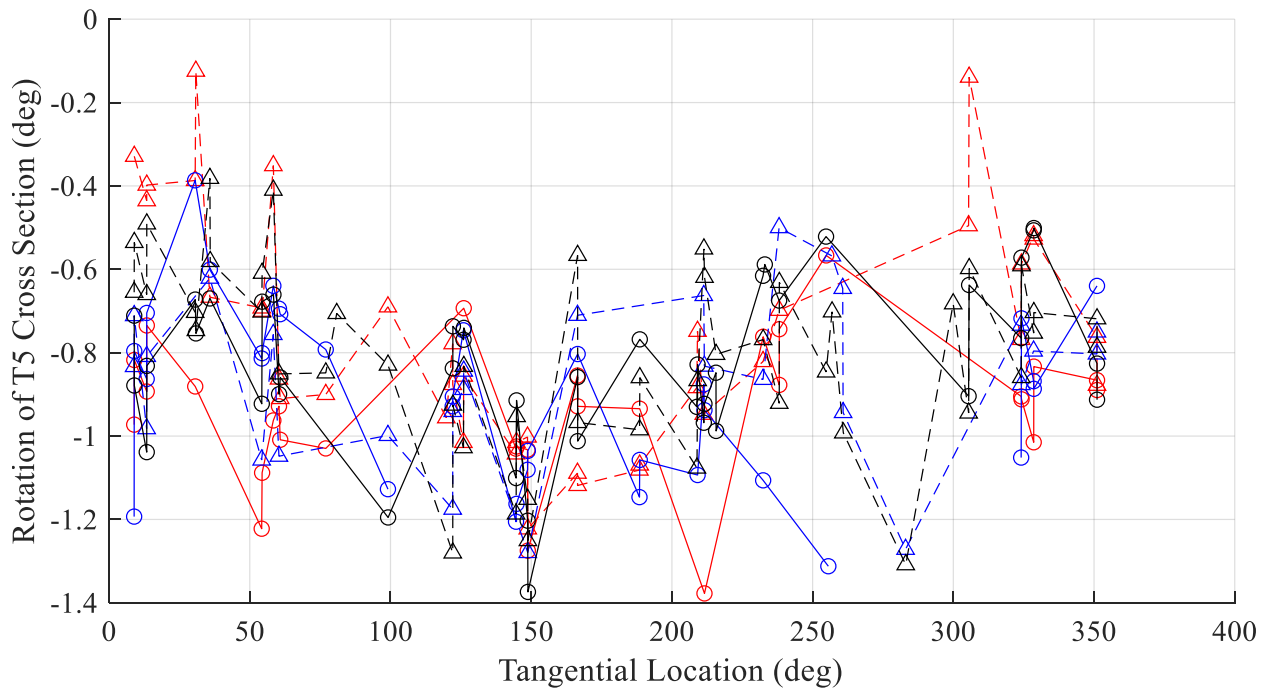
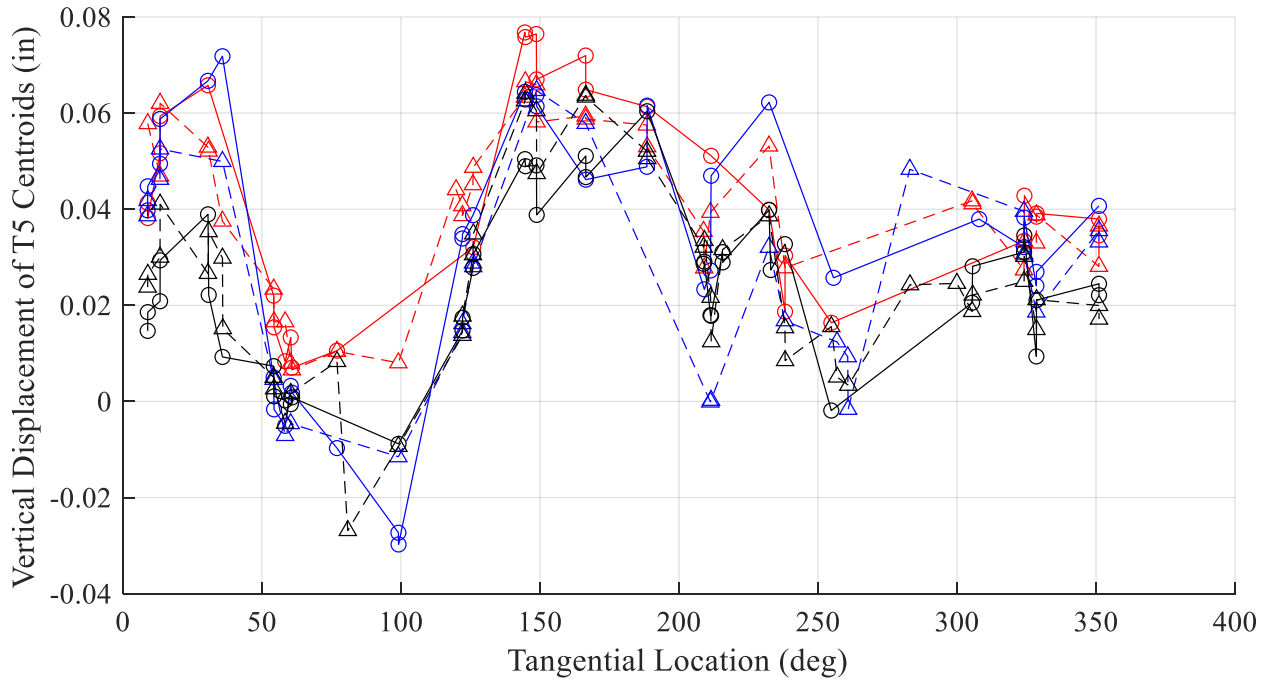
th2_plot = linspace(double(sol.th2),0);
x_th2 = r_tor/2*cos(th2_plot) + C2x;
y_th2 = r_tor/2*sin(th2_plot) + C2y;
plot(x_th1,y_th1,'k')
plot(x_th2,y_th2,'k')
axis equal
end
end
% Plot results
figure(1)
clf
plot(R,phi)
xlabel('R/P')
ylabel('\phi/P (/lbf)')
legend('10 psi','15 psi','20 psi')

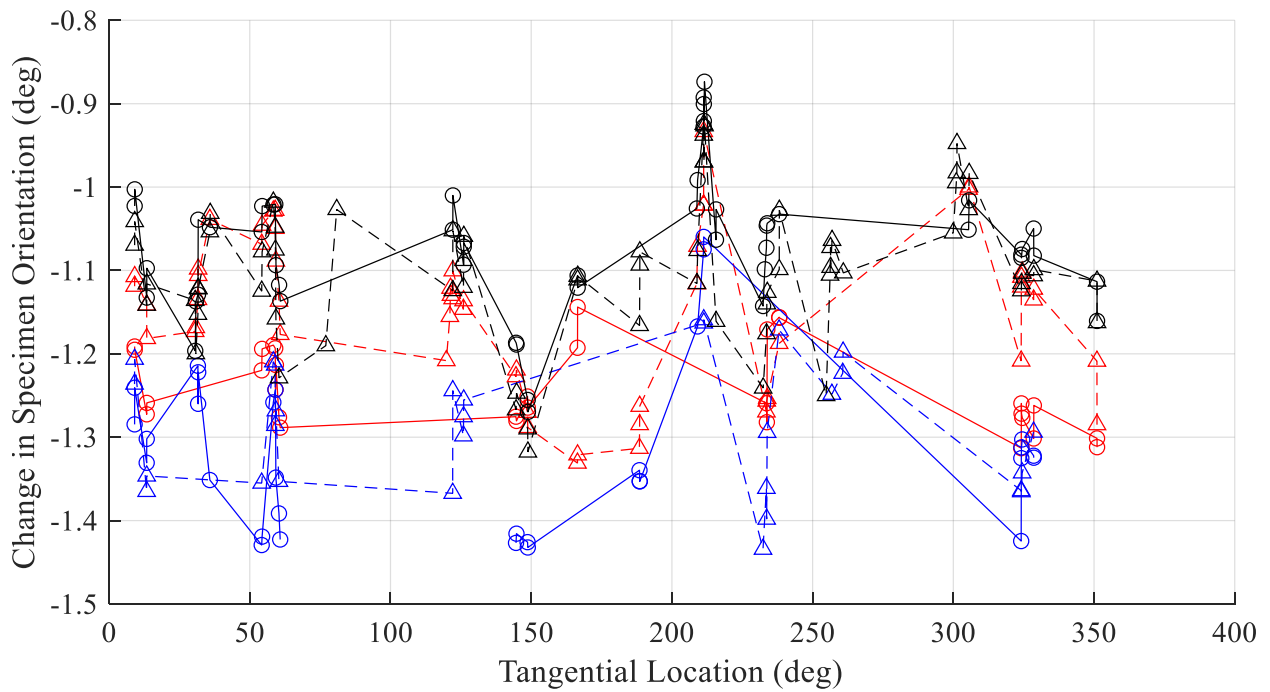
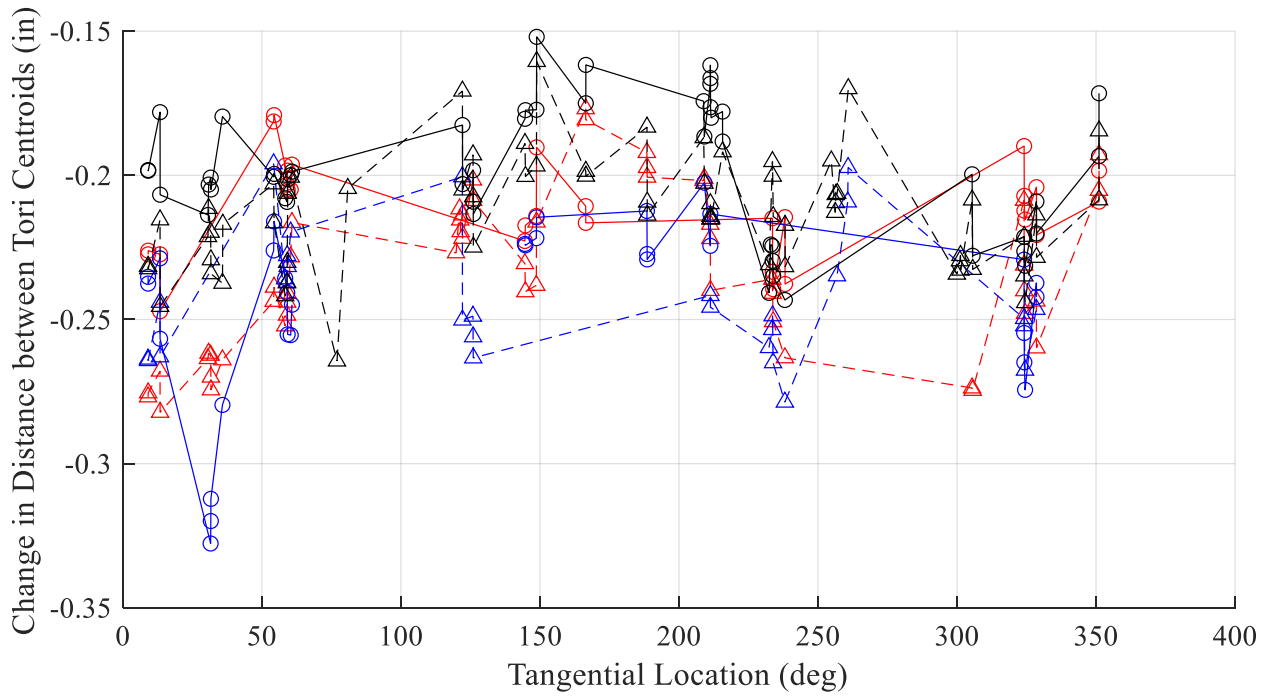
```

APPENDIX F PAIRED SPECIMEN DATA









BIOGRAPHY OF THE AUTHOR

Irja Hepler was born in Bangor, Maine to Kirsten and Allen Hepler. She was raised in Stetson, Maine and graduated from the Maine School of Science and Mathematics in 2017. She went to the University of Maine and received her Bachelor of Science in Civil Engineering in May 2020.

Irja enjoys spending time with family and friends, especially at her family's camps on Stetson Pond and Moosehead Lake or otherwise outside in the State of Maine. She also likes swimming, camping, and skiing.

After receiving her degree, Irja will continue at the Advanced Structures and Composites Center, working towards her PhD on modeling of the prints from the large-scale 3D printer. She is a candidate for the Master of Science degree in Civil and Environmental Engineering from the University of Maine in December 2022.